Resource Management in Delay Tolerant Networks and Smart Grid

by

Hao Liang

A thesis
presented to the University of Waterloo
in fulfillment of the
thesis requirement for the degree of
Doctor of Philosophy
in
Electrical and Computer Engineering

Waterloo, Ontario, Canada, 2013

I hereby declare that I am the sole author of this thesis. This is a true copy of the thesis, including any required final revisions, as accepted by my examiners.

I understand that my thesis may be made electronically available to the public.

Abstract

In recent years, significant advances have been achieved in communication networks and electric power systems. Communication networks are developed to provide services within not only well-connected network environments such as wireless local area networks, but also challenged network environments where continuous end-to-end connections can hardly be established between information sources and destinations. Delay tolerant network (DTN) is proposed to achieve this objective by utilizing a store-carry-and-forward routing scheme. However, as the network connections in DTNs are intermittent in nature, the management of network resources such as communication bandwidth and buffer storage becomes a challenging issue. On the other hand, the smart grid is to explore information and communication technologies in electric power grids to achieve electricity delivery in a more efficient and reliable way. A high penetration level of electric vehicles and renewable power generation is expected in the future smart grid. However, the randomness of electric vehicle mobility and the intermittency of renewable power generation bring new challenges to the resources management in the smart grid, such as electric power, energy storage, and communication bandwidth management.

This thesis consists of two parts. In part I, we focus on the resource management in DTNs. Specifically, we investigate data dissemination and on-demand data delivery which are two of the major data services in DTNs. Two kinds of mobile nodes are considered for the two types of services which correspond to the pedestrians and high-speed train passengers, respectively. For pedestrian nodes, the roadside wireless local area networks are used as an auxiliary communication infrastructure for data service delivery. We consider a cooperative data dissemination approach with a packet pre-downloading mechanism and propose a double-loop receiver-initiated medium access control scheme to resolve the channel contention among multiple direct/relay links and exploit the predictable traffic characteristics as a result of packet pre-downloading. For high-speed train

nodes, we investigate on-demand data service delivery via a cellular/infostation integrated network. The optimal resource allocation problem is formulated by taking account of the intermittent network connectivity and multi-service demands. In order to achieve efficient resource allocation with low computational complexity, the original problem is transformed into a single-machine preemptive scheduling problem and an online resource allocation algorithm is proposed. If the link from the backbone network to an infostation is a bottleneck, a service pre-downloading algorithm is also proposed to facilitate the resource allocation.

In part II, we focus on resource management in the smart grid. We first investigate the optimal energy delivery for plug-in hybrid electric vehicles via vehicle-to-grid systems. A dynamic programming formulation is established by considering the bidirectional energy flow, non-stationary energy demand, battery characteristics, and time-of-use electricity price. We prove the optimality of a state-dependent double-threshold policy based on the stochastic inventory theory. A modified backward iteration algorithm is devised for practical applications, where an exponentially weighted moving average algorithm is used to estimate the statistics of vehicle mobility and energy demand. Then, we propose a decentralized economic dispatch approach for microgrids such that the optimal decision on power generation is made by each distributed generation unit locally via multiagent coordination. To avoid a slow convergence speed of multiagent coordination, we propose a heterogeneous wireless network architecture for microgrids. Two multiagent coordination schemes are proposed for the single-stage and hierarchical operation modes, respectively. The optimal number of activated cellular communication devices is obtained based on the tradeoff between communication and generation costs.

Acknowledgements

I would like to express my deepest and sincerest gratitude to my supervisor, Professor Weihua Zhuang. It was Professor Zhuang's invaluable guidance and continuous encouragement that brought me from a graduate student with basic knowledge to a researcher who can tackle the real and challenging problems. Professor Zhuang has a very high standard on research quality. My weekly meetings with her are always enlightening and rewarding. The strictness, carefulness, and strong commitment that Professor Zhuang conveyed to me are exactly the essential qualities of an excellent researcher. Professor Zhuang is and will always be the role model of mine.

Furthermore, I wish to thank my thesis examining committee members: Professor Zhu Han, Professor Xinzhi Liu, Professor Kankar Bhattacharya, Professor Sagar Naik, and Professor Liangliang Xie. Their precious time and efforts devoted to this thesis are highly appreciated.

I would like to thank Professor Xuemin Shen and Professor Jon W. Mark. Their invaluable suggestions had significantly improved the quality of my collaborative research with their students and visiting scholars. The weekly group meetings coordinated by Professor Shen provided me an excellent opportunity to broaden my knowledge and improve my presentation skills.

I am grateful to the Broadband Communications Research (BBCR) Lab members. My deep appreciation goes to Dr. Bong Jun Choi and Dr. Atef Abdrabou for the fruitful collaborations on smart grid related research, especially for their help in the simulation studies. I am also very grateful to other BBCR Lab members: Dr. Rongxing Lu, Dr. Tom (Hao) Luan, Dr. Sandra Cespedes, Xiaohui Liang, Yongkang Liu, Muhammad Ismail, Hassan Omar, Khadige Abboud, Subodha Gunawardena, Qinghua Shen, Yong Zhou, Kuan Zhang, and visiting scholars Bin Cao, Dr. Chia-Ho Ou, Dr. Hongwei Li,

To my dear parents

Contents

List of Figures

List of Tables

List of Abbreviations

ADC-MAC Adaptive distributed cooperative medium access control

AODV Ad hoc on-demand distance vector

AP Access point

CDF Cumulative density function

CTS Clear-to-send

DC Direct current

DFMAC DTN-friendly medium access control

DFT-MSN Delay/fault-tolerant mobile sensor network

DG Distributed generation

DRMAC Double-loop receiver-initiated medium access control

DSR Dynamic source routing

DTN Delay tolerant network

DTNRG Delay-tolerant networking research group

EDD Earliest due date

EV Electric vehicle

EWMA Exponentially weighted moving average

FIFO First-in-first-out

GPS	Global positioning system
GPRS	General packet radio service
IP	Internet protocol
IRTF	Internet research task force
ISM	Industrial, scientific and medical
MAC	Medium access control
MANET	Mobile ad hoc network
PDF	Probability density function
PMF	Probability mass function
QoS	Quality of service
RSU	Roadside unit
RS-WLAN	Roadside wireless local area network
RTR	Ready-to-receive
RTS	Request-to-send
RWP	Random waypoint
TOU	Time-of-use
UPS	Uninterrupted power supply
V2G	Vehicle-to-grid
VANET	Vehicular ad hoc network
WLAN	Wireless local area network
WMSN	Wireless metropolitan area sharing network
WSN	Wireless sensor network

List of Mathematical Symbols

$A_{h,k}$ — The capacity of the kth frame within the hth infostation

B — The size of each data block, bits

$\mathcal{B}$ — The set of dual-mode nodes

B_0 — The number of packets in data dissemination service

$\mathbf{c}$ — The set of all possible costs in economic dispatch

c_n — The partitioning point of virtual period

$C_{n,s_n,x_n}(U)$ — The expected energy cost during periods $\{n, n+1, \cdots, N\}$ given state s_n, energy level x_n, and decision variable U, dollars

$c_n^{rc}(z)$ — The cost to increase the energy level of battery by z in period n, dollars

D_s — The deadline of service s

$f(\cdot)$ — A bijective function which maps each CG member to its rank in the CG notification message

G — The number of types of DG units

$g(\cdot)$ — A bijective function which maps each potential CG member to its rank in the deterministic backoff

G_s — The request time of service s

H — The number of trackside infostations

i_{Tx}	The ID of the previous transmitter node
K_h	The number of frames within the hth infostation
L	The group of local nodes
L_C	The group of CG members
L_{CP}	The group of potential CG members
L_N	The group of non-storage local nodes
L_S	The group of storage local nodes
M	The number of activated cellular communication devices
$\mathcal{M}$	The set of activated cellular communication devices
M_R	The number of transmission rates
$M_{h,s}$	The number of blocks to be pre-downloaded at the hth infostation for service s
$M_{h,s}^d$	The number of blocks already pre-downloaded at the hth infostation for service s
m_{Tx}	The rate index of the previous transmission piggybacked in the ACK message
N	The number of virtual periods
N_C	The number of CG members
$\mathcal{N}_v$	The set of neighboring nodes of node v
$\mathcal{Q}_m$	The set of cluster members with respect to node m
Q_s	The size of service s
$Q_{h,k,s}^r$	The numbers of remaining blocks of service s before the resource allocation for the kth frame within the hth infostation
$\tilde{Q}_{h,k,s}^r$	The numbers of remaining blocks of service s after the resource allocation for the kth frame within the hth infostation

$Q_{\hat{s},s}^r$	The numbers of remaining blocks of service s when service $\hat{s}$ is requested
$\overline{R}_i^e$	The estimated average transmission rate of local node i, packet/s
$R'_{i,R_{Tx}}$	The one-step higher transmission rate of the potential CG member i with respect to R_{Tx}, packet/s
S	The set of on-demand data services
s_n	The state of PHEV in period n
$S_{\mathcal{Q}_m}$	The number of time slots for deterministic ad hoc communication link scheduling with respect to the nodes in $\mathcal{Q}_m$
T	The duration of information exchange period, s
T_A	The duration of information exchange via ad hoc network for hierarchical multiagent coordination, s
T_B	The duration of one broadcast, s
T_C	The duration of a beacon period, ms
T_D	The duration of economic dispatch period, h
T_E	The duration of a dedicated phase, ms
T_F	Frame duration, μs
T_{SU}	Superframe duration, ms
T_I	The starting time of a trip
T_h^i	The time for a train to come into the transmission range of the hth infostation
T_O	The ending time of a trip
T_h^o	The time for a train to go out of the transmission range of the hth infostation
T_S	The duration of a slot in deterministic backoff, ms
u_n	The energy level of the battery at the end of period n, kWh

$u_{\max}^{rc}$	The maximum energy that can be recharged into the battery in a period, kWh
$u_{\max}^{dc}$	The maximum energy that can be discharged from the battery in a period, kWh
$\mathcal{V}$	The set of all nodes in the microgrid
W_h	The bandwidth of the link from the backbone network to the hth infostation, bit/s
X_g	The cumulative generation of type g DG units, kW
$\bar{X}_g$	The average cumulative generation of type g DG units, kW
$x_{h,k,s}$	The number of blocks delivered to the vehicle station during the kth frame within the hth infostation for service s
x_n	The energy level of the battery at the beginning of period n, kWh
Y	The aggregated loads, kW
$\bar{Y}$	The average aggregated loads, kW
$\tilde{Y}$	Resource allocation variable of capacity-based formulation
$\tilde{y}_{n,s}$	The number of blocks delivered to the vehicle station within the nth virtual period for service s
β	Percentage of self-discharge effect in a period
γ_m^{th}	The SNR threshold of the mth transmission rate
ω_s	The reward of service s
ξ_n	The household energy demand in period n, kWh
$\zeta_i(m)$	The packet transmission rate of local node i under rate index m, packet/s
ζ_n	The transport demand in period n, kWh

Chapter 1

Introduction

1.1 Background

As named by the National Academy of Engineering (NAE), the Internet and electrification are two of the greatest engineering achievements of the 20th century. Although they have significantly improved human life, both of them are facing new challenges as we enter the 21th century.

1.1.1 DTN and Data Service Provisioning

The TCP/IP based Internet service model is capable of supporting various applications (e.g., web browsing, online chatting, and content sharing) based on several key assumptions on the underlying communication links: an end-to-end connection exists between the information source and destination, the round-trip delay between the source and destination is not excessive, and the end-to-end message dropping probability is considerably small. However, some challenged communication environments may violate one or more of these assumptions, and thus the TCP/IP based Internet service model cannot

perform well. In order to establish efficient and reliable information exchange in these environments, a delay tolerant network (DTN) architecture with store-carry-and-forward routing is proposed [1].

The DTN is a network architecture much different from the existing Internet which operates on a principle of providing end-to-end communications. In a DTN, continuous end-to-end connections can hardly be established between the information sources and destinations. The DTN architecture is originally proposed to combat an extremely long round-trip delay in interplanetary communications [2]. But it is soon recognized that this architecture can be directly extended to terrestrial communication environments. As defined by the Internet research task force (IRTF) delay-tolerant networking research group (DTNRG), the main concern of DTN research is "how to address the architectural and protocol design principles arising from the need to provide interoperable communications with and among extreme and performance-challenged environments where continuous end-to-end connectivity cannot be assumed", or in other words, "interconnecting highly heterogeneous networks together even if end-to-end connectivity may never be available" [3]. Some typical application scenarios of DTNs include: a mobile ad hoc network (MANET) with human-carried short-range communication devices [4], a vehicular ad hoc network (VANET) with low vehicle density or low market penetration rate of communication devices [5], and a wireless sensor network (WSN) where sensors are scheduled to be on/off periodically for power saving [6]. Since continuous end-to-end connections may not exist between information sources and destinations in a DTN, most ad hoc routing algorithms such as dynamic source routing (DSR) [7] and ad hoc on-demand distance vector (AODV) routing [8] cannot be applied. For efficient and reliable message delivery, the store-carry-and-forward based DTN routing can be implemented, where messages can be stored and carried by a relay node for a considerably long period of time until a communication opportunity arises [9].

The DTN is mainly designed to provide data services which are delay tolerant in nature. The data dissemination services and on-demand data services are two of the most important ones. Nowadays, data dissemination services are becoming more and more important as numerous telematic applications require the distribution of a certain amount of information in the network. Data packets are generated from a remote server in the Internet and destined to mobile users such as pedestrians. Typical applications of data dissemination services include traffic information downloading, entertainment content distribution, and commercial advertising. On the other hand, the mass transportation in terms of high-speed rail is fast developing all over the world [10]. Besides significantly shortened journey times as compared with the traditional trains, the passenger comforts can be largely improved by providing high-speed Internet services over the high-speed rail [11]. On demand data services such as audio/video clip downloading and bulk data retrieval can be provided for the passengers on the way via the APs deployed in close vicinity to the rail lines.

1.1.2 Smart Grid and Electricity Delivery

Most of the world's existing electricity grids are decades-old. Their monitoring and control facilities gradually become out-of-date and may cause low energy efficiency/reliability as more and more uncertainties are introduced in the power systems. The uncertainties are mainly caused by the integration of electric vehicles (EVs) with highly dynamic vehicle mobility, as well as the adoption of renewable energy sources (such as wind and solar) with intermittent and climate-dependent power generation. The next generation power grid, also known as the smart grid, aims at combining the existing power systems with the state-of-art information and communication technology to address the uncertainties and achieve electricity delivery in a more efficient, reliable, economic, and sustainable way.

Despite the high mobility of EVs, the battery storage can be better utilized to po-

tentially improve the efficient and reliable of electricity delivery. As nearly 90% of power outages and disturbances are related to the distribution network, distributed energy storage has become one of the key technologies to improve the efficiency and reliability of a smart grid [12]. At the same time, with the fast developing plug-in electric vehicles, the vehicle-to-grid (V2G) system is emerging as an auxiliary distributed storage, which exploits the capacity of vehicle batteries [13]. A key feature of the V2G system is a bidirectional energy delivery mechanism which enables the electric vehicle to either draw energy from or feed energy back to the grid. Aided by communication technologies, the energy delivery can be controlled in a smart way to reduce the transport cost while improving the grid stability. Two major applications of a V2G system are load shaving and frequency regulation [14]. Load shaving aims at using the energy stored in electric vehicles to compensate for the peak load of the grid. From the vehicle owners' point of view, since electricity price is determined by demand, the transport cost can be relatively reduced by drawing "cheap" energy from the grid, and vice versa. Frequency regulation is an ancillary mechanism to fine-tune the frequency of the grid in a small time scale, e.g., a few minutes. Frequency regulation may not necessarily involve energy delivery but simply the use of the capacity of vehicle batteries. Therefore, a small number of vehicles can saturate the demand of frequency regulation [13].

To better utilize the renewable energy sources, the concept of microgrid is proposed [15]. Operating at a distribution voltage level, the microgrids are small-scale power systems designed to utilize the distributed generation (DG) units to supply the electrical loads in local areas such as a residential community, a university, and an industrial site. Low-cost short-range wireless communication devices such as WiFi and ZigBee devices are typically used to establish the network infrastructure in microgrids mainly because the power distribution system is cost-sensitive in nature [12]. In addition to the environmental benefit in terms of using more renewable energy sources, the microgrids

can reduce the transmission and distribution losses based on the physical proximity of DG units and loads. Since various types of DG units such as wind turbines, photovoltaic (PV) panels, and fuel cells may coexist, one pivotal problem in microgrid management is the economic dispatch which balances the power generation and loads at a minimum monetary cost. Different from traditional power systems with thermal energy power generators, the economic dispatch in microgrids is challenging because of the intermittent and climate-dependent nature of renewable energy sources. As the accuracy of estimating the generation of DG units and loads is limited, the economic dispatch is performed in a relatively small time scale, e.g., every five minutes for California Independent System Operator (CAISO) with wind/solar integration [16], and a communications/control delay within 2-10 seconds [17].

1.1.3   Resource Management

The communications in a DTN can only be established with a proper management of network resources. The primary resource to be managed is the communication bandwidth resource shared by nodes in the network coverage area. However, in a DTN scenario where nodes operate cooperatively with each other for data buffering, the buffer storage of each node can also be viewed as shared resources. Therefore, the resource management in a DTN should incorporate the functionalities of buffer management. Different from the network-layer store-carry-and-forward based DTN routing which aims at providing end-to-end message delivery, the focus of resource management is on how to distribute various resources at the link layer to different nodes when they meet each other. Note that in a DTN scenario where the network is likely partitioned, the resource management and DTN routing are closely related to each other since the meetings of nodes are expected to be very brief. For instance, the times for a pedestrian and a high-speed train to pass through the coverage area of an AP are only a few minutes and a few seconds, respectively.

The electric load demand in the smart grid can only be satisfied by consuming a certain amount of electric power generated by power generators and transmitted through power transmission lines. In order to coordinate the power generators such that all load demand can be satisfied at a minimum cost, communication links should be established among the power generators and/or loads which further requires the management of communication bandwidth resources. For instance, in a microgrids where low-cost short-range communication devices (such as WiFi and ZigBee devices) are typically used, the communication bandwidth management and electric power delivery are tightly coupled with each other. The main reason is that the balance between power generation and demand depends on the accuracy of the information collected from the communication network, while the efficiency of communication bandwidth management can be potentially improve by taking into account the characteristics of power generation and demand information. Further, the battery storage resource management such as the management of EV batteries can be facilitated by utilizing the information provided by communication networks. However, the information is likely to be stochastic since the vehicle mobility is highly dynamic, which further complicates the battery management.

Although DTN and smart grid are proposed for different purposes (i.e., data service provisioning and electricity delivery, respectively), they share some common characteristics in terms of resource management. Specifically, the packet store-carry-and-forward concept in a DTN is analogous to the energy store-carry-and-deliver mechanism in a V2G system. The techniques used for buffer management in DTNs can shed a light on the battery management in V2G systems, given the unique characteristics of batteries such as energy losses in recharging/discharging are well addressed. On the other hand, as low-cost short-range wireless communication devices are widely used in DTNs and microgrids, the communication bandwidth management at the link layer is pivotal for both systems. Some critical problems such as wireless channel contentions should be ad-

dressed by taking account the uniqueness of the node mobility in DTNs and microgrids, i.e., mobile and stationary, respectively. Cellular networks can potentially be used to improve the resource management of both systems, at an extra monetary cost.

1.2   Motivation and Research Contributions

In this thesis, we study the resource management issues in DTNs and smart grid. For the resource management in DTNs, we have investigated the cooperative data dissemination via roadside WLANs and on-demand data service delivery to high-speed trains. Although packet pre-downloading (or pre-fetching) has been investigated in literature [18, 19, 20], the packet pre-downloading mechanism poses new technical challenges/opportunities in medium access control (MAC). Specifically, a packet may have multiple copies at different storage local nodes and can be cooperatively relayed by multiple non-storage local nodes. In order to transmit a packet, high wireless channel contention should be resolved among multiple direct/relay links. On the other hand, the MAC scheme can take advantage of the packet pre-downloading mechanism. The traffic characteristics at the storage local nodes can be predicted (i.e., saturated) as the packets are already pre-downloaded before the visit of a nomadic node. The efficiency of MAC can be potentially improved by reducing the signalling overhead. The MAC schemes [21, 22, 23] are transmitter-initiated for communications among multiple pairs of traffic sources and destinations, and the exchange of RTS/CTS messages is required for the channel estimation and reservation before data transmission which results in extra MAC overhead. The receiver initiated MAC scheme [24, 25] can potentially reduce MAC overhead. However, when directly applied to RS-WLANs with pre-downloaded packets, these schemes do not exploit the potential diversity gain among multiple direct/relay links. On the other hand, in order to delivery on-demand data services to a high-speed train with a large number of passengers

onboard, the resource contention among multiple services should be resolved. Moreover, the coverage provided by the infostations may not be seamless for a low deployment cost. As a high-speed train travels along a rail line, the wireless link from an infostation to a vehicle station is highly dynamic and subject to periodic disconnections, which makes the resource management challenging. The on-demand broadcast scheduling approaches [26, 27] based on a constant rate broadcast link are not applicable to data delivery via infostations. The existing resource management schemes [18, 20, 28, 29] deal with single service for each vehicle or offline resource allocation based on service popularity, which cannot be directly applied to on-demand data delivery to mass transportation vehicles such as high-speed trains.

The objective of our research on resource management in DTNs is to address the above limitations and develop effective and efficient link layer resource allocation schemes for cooperative data dissemination via roadside WLANs and on-demand data service delivery to high-speed trains, respectively. Firstly, a double-loop receiver-initiated MAC (DRMA-C) scheme is proposed for cooperative data dissemination via roadside WLANs [30, 31]. The MAC scheme can achieve spatial and temporal diversity via the outer-loop and inner-loop MAC, respectively. A receiver initiated mechanism is used to reduce the signalling overhead, where the ACK message is used as an invitation of channel contention. Secondly, the optimal resource allocation problem for on-demand data service delivery to high-speed trains via cellular/infostation integrated networks is formulated by taking account of the intermittent network connectivity and multi-service demands [32, 33]. The original problem is transformed into a single-machine preemptive scheduling problem based on a time-capacity mapping. As the service demands are not known *a priori*, an online resource allocation algorithm based on Smith ratio and exponential capacity is proposed. If the link from the backbone network to an infostation is a bottleneck, a service pre-downloading algorithm is also proposed to facilitate the resource allocation.
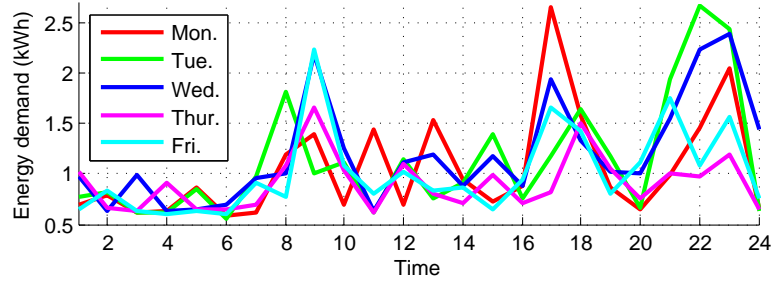
Figure 1.1: Hourly energy demand of a household in Waterloo during a week of June.
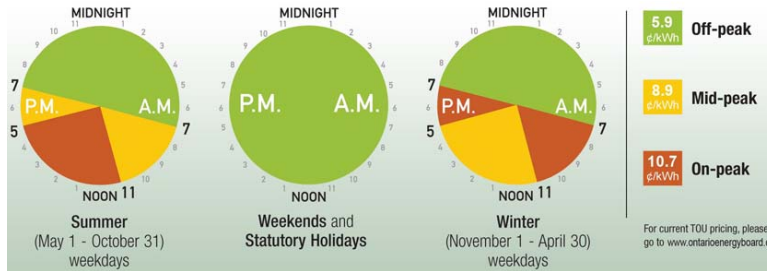
Figure 1.2: Ontario electricity time-of-use (TOU) price.

For resource management in the smart grid, we have studied the optimal energy delivery via V2G systems and decentralized economic dispatch in microgrids. For a V2G system with bidirectional energy delivery, the peak period with high electricity price should be considered. As shown in Fig. 1.1, the household demand mainly occurs during the off-peak and mid-peak hours (see Fig. 1.2) because of appliance usage such as heating/cooling, cooking, and washing[1]. Optimal energy delivery can hardly be achieved if the on-peak hours (see Fig. 1.2), during which the vehicles are likely to be parked at the work places, are ignored. Therefore, the traditional energy store-and-deliver approach [13, 35, 36, 37, 38] should be transformed into an energy store-carry-and-deliver mechanism to facilitate V2G applications. On the other hand, the existing works on

---

[1]The data is collected from the smart meter readings of a household subscribed to Waterloo North Hydro [34], to be discussed in Section 4.6.

economic dispatch [39, 40, 41, 42] are established based on the assumption that an efficient communication network can be used to obtain the power generation and demand information in a timely manner. However, this assumption can hardly hold true in a microgrid with low-cost short-range communication devices such as WiFi and ZigBee devices.

The objective of our research on resource management in the smart grid is to address the above limitations and develop an optimal energy delivery scheme for the V2G system and an efficient decentralized economic dispatch scheme for microgrids. Firstly, we have formulated the optimal energy store-carry-and-deliver problem for PHEVs via the V2G system and prove the optimality of a state-dependent double-threshold policy based on the stochastic inventory theory [43]. A modified backward iteration algorithm is devised for practical applications, where an exponentially weighted moving average (EWMA) algorithm is used to estimate the statistics of PHEV mobility and energy demand. Secondly, we have proposed a heterogeneous wireless network architecture to achieve decentralized economic dispatch in microgrids [44]. Two multiagent coordination schemes are proposed for the single-stage and hierarchical operation modes, respectively. The optimal number of activated cellular communication devices is obtained based on the tradeoff between communication and generation costs.

1.3   Outline of the Thesis

This thesis consists of two parts. In Part I, we present the resource management in DTNs. Chapter 2 proposes a DRMAC scheme for cooperative data dissemination via roadside WLANs. An analytical model is derived for the proposed MAC scheme and the analytical results are verified by simulations. Chapter 3 investigates the on-demand data service delivery problem for high-speed trains in cellular/infostation integrated networks. An online resource allocation algorithm based on Smith ratio and exponential capacity

is proposed and evaluated by simulations based on real high-speed train schedule. In Part II, we present the resource management in the smart grid. Chapter 4 investigates the optimal energy store-carry-and-deliver problem for PHEVs via V2G systems. We prove the optimality of a state-dependent double-threshold policy and devise an approximation algorithm for practical applications. The performance of the proposed algorithm is evaluated by simulations based on survey and real data collected from Canadian households. Chapter 5 presents a heterogeneous wireless network architecture for microgrids. Two multiagent coordination schemes are proposed for the single-stage and hierarchical operation modes, respectively. The efficiency of the proposed schemes is evaluated by analysis and simulations based on real power generation and load data collected from the Waterloo Region in Canada. Finally, Chapter 6 concludes this research and outlines some further research topics.

Part I: Resource Management in Delay Tolerant Networks

Chapter 2

MAC for Cooperative Data Dissemination via Roadside WLANs

As discussed in Chapter 1, MAC design is critical for efficient cooperative data dissemination via RS-WLANs. In this chapter, we present a DRMAC scheme for pedestrian nomadic nodes such as the FON subscribers [45]. The main resource under consideration is communication bandwidth. The key features of the proposed MAC scheme include:

- Two MAC loops are devised. The outer-loop MAC and inner-loop MAC are performed at relatively low and high frequencies to achieve spatial and temporal diversity, respectively.

- In order to reduce the signalling overhead, a receiver-initiated MAC strategy is adopted to suppress the RTS/CTS message exchange by using the ACK message as an invitation of channel contention. The ACK message also carries the rate information of the previous transmission to reduce channel contentions among multiple storage and non-storage local nodes.

- A novel analytical model is established using a finite-state Markov chain based channel model to characterize the time correlation between two consecutive transmissions. The analytical results are verified by extensive simulations for various visiting trajectories and speeds of a nomadic node. Compared with the IEEE 802.11 MAC, transmitter-initiated cooperative MAC, and receiver-initiated MAC, our proposed scheme can significantly improve the packet delivery rate from an RS-WLAN to a nomadic node.

2.1   Literature Review

The data dissemination services can be supported by the traditional cellular networks such as general packet radio service (GPRS) and 3G. However, as cellular networks aim at offering ubiquitous network coverage, providing the data dissemination services by cellular networks can suffer from low transmission rate and high cost [18]. Extensive research has been carried out to exploit the roadside WiFi access points (APs) for data delivery. For instance, the Drive-thru Internet architecture addresses the short-term network access problem when a mobile user walks, drives, or passes (by other means) through the coverage area of an AP [46]. To improve the availability of the roadside APs, the notion of wireless metropolitan area sharing network (WMSN) is introduced, where publicly and/or privately owned wireless local area networks (WLANs) are shared [47]. Following the same concept as WMSN, FON has successfully established a business model to stimulate the sharing of the WLANs [45]. Based on two kinds of incentives, i.e., direct payment and cooperative sharing among FON subscribers, the nomadic nodes can obtain permission to access the privately owned roadside WLANs (RS-WLANs) which are typically deployed at the roadside restaurants, cafes, and residential houses. However, in a rural area and/or an urban area with a low market penetration rate, the densities

of the shared RS-WLANs as well as the nomadic nodes are low such that an end-to-end path from an AP to a nomadic node can hardly be established. Moreover, the data rate of the wireline connection between an AP and the content server may be limited[1], which further restricts the packet delivery rate from an RS-WLAN to a nomadic node.

To achieve efficient data dissemination in such a DTN (or sparse network in general [49]), a cooperative approach (also referred to as DTCoop [19]) can be used, in which not only the AP within each RS-WLAN is shared, but also the local nodes connected to the AP can provide packet caching and relaying capabilities. Information packets are first pre-downloaded to (or cached at) a group of storage local nodes within an RS-WLAN. Upon the arrival of a nomadic node in the RS-WLAN, both direct links from storage local nodes and relay links via non-storage local nodes can be used for packet delivery.

Several MAC schemes have been proposed in literature to achieve spatial/temporal diversity in the context of cooperative communications. At the link layer, spatial diversity can be achieved by scheduling the local node with the highest average transmission rate to transmit, based on the geographic locations of local nodes [21]. On the other hand, temporal (or user) diversity corresponds to a time-varying channel condition caused by the mobility of the nomadic node, and typically requires a time-dependent scheduling based on the instantaneous transmission rates from the local nodes to the nomadic node [22, 23, 50]. The CoopMAC can achieve spatial diversity based on the historic transmission observations [21]. Each low data rate node in the network maintains a table (i.e., the CoopTable) of potential relay nodes based on the overheard transmissions from other nodes. During packet transmission, each node of a low data rate selects either direct transmission mode or relay transmission mode (through a relay node)

---

[1]For instance, the rate can be limited to a few Mbps for some residential Internet service subscribers, which is much lower than the maximum rate of the wireless connection (e.g., 54 Mbps for IEEE 802.11a based RS-WLANs) [18, 48].

based on the information provided by the CoopTable. In this way, the packet transmission time can be reduced. Without predetermined network configuration, an adaptive distributed cooperative MAC (ADC-MAC) is proposed for spatial diversity in dynamic vehicular networks [22]. A heartbeat mechanism is devised so that the ADC-MAC can self-learn the geographic location information of the relay nodes and dynamically update the CoopTable. Since the source node adaptively selects the most suitable transmission mode and/or relay node based on the latest information in the CoopTable (which may not be up-to-date in comparison with the instantaneous information), temporal diversity can be potentially achieved. The distributed cooperative MAC achieves both spatial and temporal diversity [23]. The relay selection is completed in a distributed manner and the instantaneous channel quality is estimated during the request-to-send(RTS)/clear-to-send(CTS) message exchange. As demonstrated in [24, 25], the receiver-initiated MAC schemes can reduce the signalling overhead for predictable traffic source. The RTS part of the RTS/CTS message exchange is suppressed, while the CTS part is used as an invitation by the receiver node for the transmitter node.

2.2   System Model

In this section, we first introduce the network topology. Then, the cooperative data dissemination approach is described, followed by a local information exchange mechanism to facilitate the cooperative data dissemination.

2.2.1 Network Topology

Consider a service area where a number of RS-WLANs are deployed. Local nodes reside in the coverage area of an RS-WLAN, while the nomadic nodes are roaming in the entire network region. We consider pedestrian nomadic nodes which can be disconnected for hours and walk through the coverage area of an RS-WLAN within several minutes. The densities of the RS-WLANs and nomadic nodes are low, which results in a DTN scenario [49]. Focusing on MAC, we consider a single RS-WLAN (e.g., in a residential house) with a group, L, of local nodes (including the AP), as shown in Fig. 2.1.

The RS-WLAN provides services to both local and nomadic nodes. For the resource sharing, we consider a superframe structure as shown in Fig. 2.2 [51]. Time is partitioned into superframes with constant duration T_{SU}. Each superframe begins with a beacon period with duration T_C. Following the beacon period, a dedicated phase with duration T_E ($T_E < T_{SU} - T_C$) is reserved for the data dissemination service upon the arrival of a nomadic node. The remaining period in the superframe is used to serve the local nodes. For the resource allocation among multiple nomadic nodes which are simultaneously present in an RS-WLAN, a time sharing mechanism is used, in which each dedicated phase is assigned to a nomadic node. The AP notifies the local nodes about the assignment during the beacon period. At the beginning of each dedicated phase, a dedicated phase assignment message is broadcasted by one of the local nodes to notify the nomadic node.

Suppose a data dissemination service (e.g., to distribute a flyer of a supermarket or a video clip of a commercial advertisement) is initiated and destined to a group of nomadic nodes[2]. The data file for dissemination is segmented to B_0 packets with equal size. Without loss of generality, we consider an IEEE 802.11 based RS-WLAN with M transmission rates at the physical layer [48]. The mth rate is selected for wireless transmission

---

[2]If there are multiple data dissemination services, they are served according to a first-in-first-out (FIFO) policy.
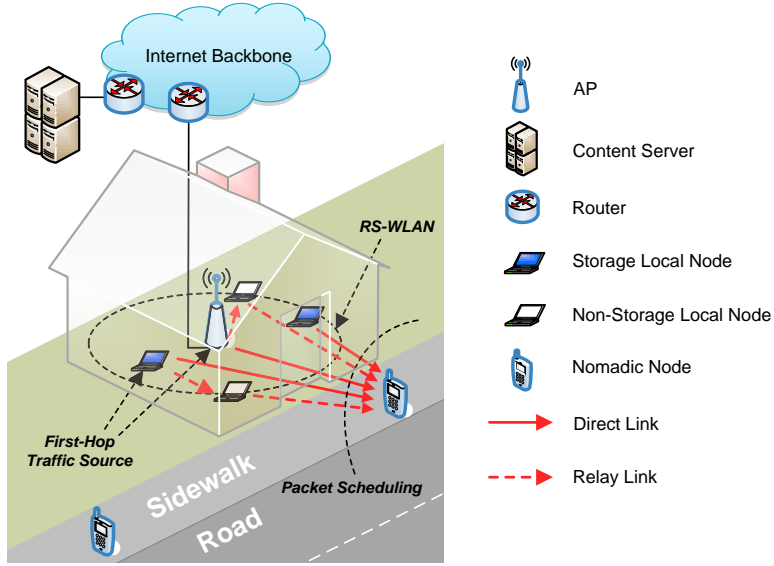
Figure 2.1: Network topology and the cooperative data dissemination approach.
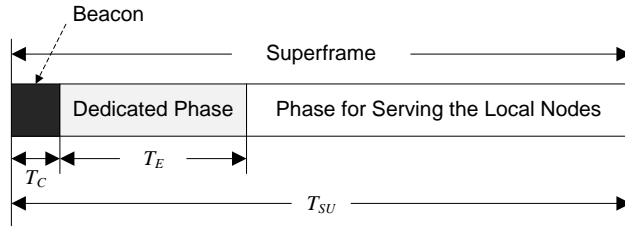
Figure 2.2: The superframe structure.

if the instantaneous received signal-to-noise ratio (SNR) is within $[\gamma_m^{th}, \gamma_{m+1}^{th})$, where γ_m^{th} $(m = 1, 2, \cdots, M_R)$ is the SNR threshold of the mth rate such that the wireless transmission can be considered as error free [52]. The M_Rth rate is selected when the SNR is above γ_M^{th} (i.e., $\gamma_{M+1}^{th} = \infty$), while no wireless transmission is established when the SNR is below γ_1^{th}. The RS-WLAN under consideration is fully connected. In order to efficiently utilize the radio resources, we assume that a neighbor discovery mechanism is in place, which admits a nomadic node to the RS-WLAN when a non-zero transmission rate can be supported with a high probability.

2.2.2 The Cooperative Data Dissemination Scheme

The cooperative data dissemination scheme consists of two phases, i.e., packet pre-downloading and packet scheduling. Because of the buffer space limitation, the packets of the data dissemination service is pre-downloaded to a group L_S of storage local nodes, while another group L_N ($L_N \cap L_S = \emptyset$) of non-storage local nodes can provide relaying capabilities. Assuming that the packet pre-downloading procedure is completed based on an existing approach[3], we focus on the scheduling of packet transmission to a visiting nomadic node. The buffer space of the AP is sufficiently large, so that the AP can also serve as a storage local node, i.e., $\{AP\} \subset L_S$. In order to achieve a high packet transmission rate, an opportunistic scheduling scheme is applied by considering both direct links from the storage local nodes and the relay links from the non-storage local nodes. Among these links, the one with the highest transmission rate is selected.

2.2.3 Local Information Exchange

Each non-storage local node is paired with a storage local node for the highest link transmission rate. The storage local node is the first-hop traffic source for the non-storage local node. As shown in Fig. 2.1, the two non-storage local nodes select one of the storage local nodes and the AP as their first-hop traffic sources, respectively. For a non-storage local node i ($i \in L_N$), denote the rate index of the first-hop transmission from the traffic source as m_i^1. The local information, in terms of the IDs of the storage/non-storage local nodes (in L_S/L_N) and the source selection results of the non-storage local

---

[3]For instance, on-demand packet pre-downloading exploits the instantaneous mobility information (which is delivered via a cellular network) to pre-download data packets to the RS-WLANs on the movement trajectory of a nomadic node [18], while stochastic packet pre-downloading uses the historic mobility information to pre-download data packets to the RS-WLANs to be visited by a nomadic node with a high probability [20].

nodes (with respect to $m_i^1, i \in L_N$), is stored at all local nodes and is transmitted to a visiting nomadic node during its neighbor discovery procedure. With low mobility of local nodes (e.g., laptops or normal users of the RS-WLANs), we assume that the local information does not change during the visiting period of a nomadic node.

When a nomadic node comes into the RS-WLAN, let m denote the index of the direct transmission rate if the source node is a storage local node or the second-hop transmission rate otherwise. Then the packet transmission rate from local node i (including the transmission of the ACK message and cooperative relaying overhead) to the visiting nomadic node is a function of m, denoted by $\zeta_i(m)$ (in packet/s) and given by [21]

$$
\zeta_i(m) = \begin{cases} \frac{1}{T_P(m)+T_{ACK}+2T_{SIFS}}, & \text{if } i \in L_S \\ \frac{1}{T_{HR}+T_P(m_i^1)+T_P(m)+T_{ACK}+4T_{SIFS}}, & \text{if } i \in L_N \end{cases} \tag{2.1}
$$

where $T_P(m)$ is the packet transmission time at the mth transmission rate, while T_{SIFS}, T_{HR}, and T_{ACK} are the time durations of short interframe space (SIFS), helping request message, and ACK message, respectively. The helping request message is sent by a non-storage local node to request a packet from the selected first-hop traffic source. All signalling messages (other than the data packet) are transmitted at the basic rate to ensure the transmission accuracy. Without loss of generality, we denote the case that the wireless transmission cannot be established by $m = 0$ with $\zeta_i(0) = 0$. Since $T_P(m)$ is monotonic with respective to m according to the transmission rate definition, $\zeta_i(m)$ is a bijective function. Therefore, if the packet transmission rate of local node i is denoted by R, we can obtain its rate index m as $m = \zeta_i^{-1}(R)$ based on the local information L_S, L_N, and m_i^1 for $i \in L_N$. For notation clarity, we use the symbols in $\{i, j, n\}$ and $\{m, l, h\}$ to denote the local nodes and the rate indices, respectively, in the following sections.

2.3 The Double-Loop Receiver-Initiated MAC Scheme

To provide high quality data dissemination services, our main objective is to minimize the service delivery delay which is mainly caused by the intermittent network connectivity. For instance, the flyer of a supermarket should be delivered to a pedestrian walking towards the supermarket as soon as possible. From the link layer point of view, this objective can be achieved by increasing the number of data packets (or data volume [46]) delivered to the nomadic node upon its visit to each RS-WLAN, or equivalently, improving the packet transmission rate from the local nodes to the nomadic node during the dedicated phase of each superframe. Towards the goal, a DRMAC scheme is proposed. In this section, we first give an overview of the proposed MAC scheme, and then present the details of its operation.

2.3.1 Overview of the MAC Scheme

A function diagram of the DRMAC scheme is shown in Fig. 2.3, where the contention group (CG) is defined as a group of local nodes which can participate in the wireless channel contention for packet transmission to the nomadic node. The DRMAC scheme consists of two MAC loops. The outer-loop MAC is performed at a low frequency to determine the CG membership for spatial diversity based on the average transmission rate, while the inner-loop MAC is performed at a high frequency to select the transmitter for temporal diversity based on the instantaneous transmission rate.

Several new messages are introduced for our proposed MAC scheme. The dedicated phase assignment message is defined in Subsection 2.2.1. Correspondingly, a receiving request message is introduced as a response to the dedicated assignment message by a nomadic node. Similar to the existing cooperative MAC schemes [21, 22, 23], we introduce a helping request message which is used by a non-storage local node (or equivalently, a
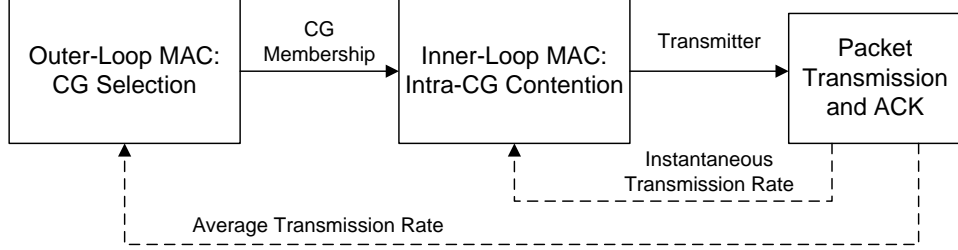
Figure 2.3: A function diagram of the DRMAC scheme.

relay node) to request a packet from the first-hop traffic source. Since the first-hop traffic source is already determined based on local information exchange, only the non-storage local node address is included in the helping request message. The storage local nodes which are selected as the first-hop traffic sources are required to decode all helping request messages for potential first-hop transmissions. By definition, the formats of dedicated phase assignment message, receiving request message, and helping request message are the same as that of the CTS message, with their RA fields being given by the addresses of the nomadic node, the local node sending the dedicated phase assignment message, and the non-storage local node requesting the packet, respectively. The ACK message sent by the nomadic node piggybacks the instantaneous transmission rate index, m_{Tx}, estimated based on the previous transmission and the packet sequence number [48]. Note that the sequence number is used to identify the packet for the next transmission, taking into account that identical packets may be stored at multiple storage local nodes in packet pre-downloading. Similar message format is used by a rate notification message for a local node to indicate its instantaneous transmission rate.

Taking account of the superframe structure as shown in Fig. 2.2, the critical operation steps of the proposed MAC scheme can be briefly summaries as follows. Here, we consider a single nomadic node which is admitted by the RS-WLAN.

1. A standard beacon mechanism [48] is used with an additional information being

broadcasted by the AP to notify the local nodes about the CG membership (which is determined based on the outer-loop MAC for spatial diversity, to be discussed in Subsection 2.3.2);

2. At the beginning of a dedicated phase, a CG attachment procedure is performed to initiate the inner-loop MAC. The procedure begins with one of the CG member sending a dedicated phase assignment message to notify the nomadic node. After the CG attachment, a CG member with the highest instantaneous transmission rate to the nomadic node is identified as the transmitter node for temporal diversity;

3. A contention-by-invitation procedure is performed for the remaining period of the dedicated phase after the CG attachment. The side information provided by the ACK message is used to reduce the MAC overhead while achieving temporal diversity.

Step 2 and Step 3 constitute the inner-loop MAC, to be discussed in Subsection 2.3.3.

2.3.2 The Outer-Loop MAC

Each local node, $i \in L$, estimates its instantaneous transmission rate (R_i^e) to the nomadic node based on the SNR of each ACK message it received. From the received SNR, if the corresponding rate index is m_i^e, we have $R_i^e = \zeta_i(m_i^e)$. The average transmission rate $\overline{R}_i^e$ can be calculated based on the previous estimates of R_i^e.

From the periodic reports of $\overline{R}_i^e$ by all local nodes, the AP selects a group L_C of local nodes with the highest average transmission rates as the CG members, and then broadcasts a CG notification message (during the beacon period) to inform all local nodes about the IDs of the CG members in a descending order of the average transmission rate. When two or more local nodes have the same average transmission rate to the nomadic

node, the ordering among them is in accordance with their IDs. For a clear presentation, we define a bijective function $f : L_C \rightarrow \{1, 2, \cdots, N_c\}$, which maps each CG member ID to its rank in the CG notification message, where $N_C = |L_C|$ is the number of CG members. Obviously, for $i, j \in L_C$, if $f(i) < f(j)$, we have $\overline{R}_i^e \geq \overline{R}_j^e$. For a larger N_C, more local nodes can participate in the channel contention for a higher temporal diversity gain.

2.3.3 The Inner-Loop MAC

The two components of the inner-loop MAC are presented as follows.

Contention-by-Invitation

If a CG member i ($i \in L_C$) can correctly decode the ACK message from the previous transmission, the value of m_{Tx} can be obtained. Then the rate of the previous transmission can be calculated as $R_{Tx} = \zeta_{i_{Tx}}(m_{Tx})$ based on the receiver address field of the ACK message (corresponding to the ID of the previous transmitter node i_{Tx} [48]). If $R_i^e > R_{Tx}$, node i is invited and will join the channel contention.

To select a transmitter node, a contention-based procedure is used based on the side information provided by the ACK message, as shown in Fig. 2.4. Each invited CG member sends a short burst, as a contention request, T_{SIFS} after the reception of the ACK message. The previous transmitter node (i_{Tx}) overhears the contention request burst and defers its transmission. Since a CG member cannot obtain the instantaneous transmission rate information of other CG members, we denote L_{CP} as the group of all potential (invited) CG members, which is a subgroup of L_C and is given by

$$L_{CP} = \{j | \max_{1 \leq l \leq M_R} \{\zeta_j(l)\} > R_{Tx}, j \in L_C \setminus i_{Tx}\}. \tag{2.2}$$
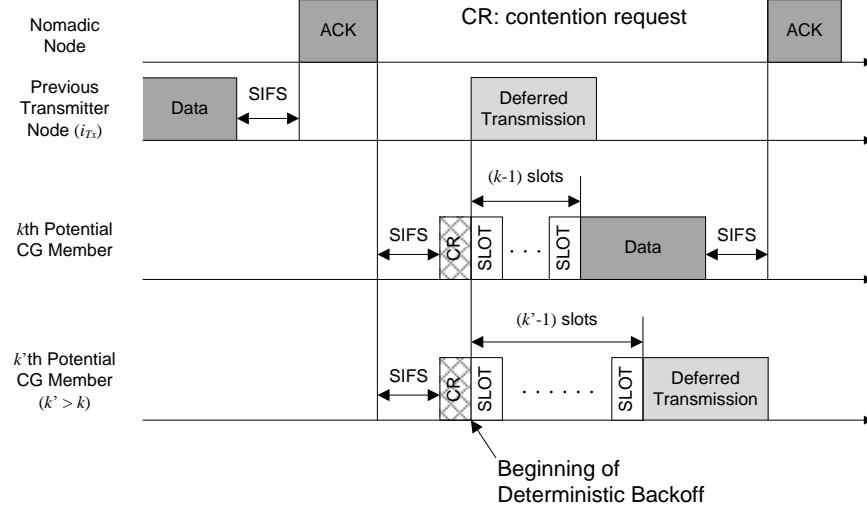
Figure 2.4: Signalling in the contention-by-invitation.

Note that a CG member is potentially invited only when it can support a transmission rate higher than R_{Tx}. Then, a deterministic backoff (with the kth potential CG member backoffs for $(k-1)$ slots before its transmission) is established by sorting all potential CG members according to the descending order of the one-step higher transmission rate, which is defined as

$$R'_{i,R_{Tx}} = \min_l\{\zeta_i(l)|\zeta_i(l) > R_{Tx}\},\ i \in L_{CP}. \tag{2.3}$$

The slot duration in the deterministic backoff is T_S [48]. The rationale behind the one-step higher transmission rate based deterministic backoff is to utilize the time correlation of a wireless channel to reduce contentions. For pedestrian mobility, the value of m_{Tx} given in the ACK message is up-to-date with a high probability and a transmission rate change to a non-adjacent index during a round of packet transmission and ACK is unlikely. Since all nodes in L_{CP} have a lower transmission rate than R_{Tx} during the previous transmission, if node i ($i \in L_{CP}$) is invited to join the channel contention, its current transmission rate equals the one-step higher transmission rate ($R'_{i,R_{Tx}}$) with a high probability. As a result, by ordering the potential CG members based on $R'_{i,R_{Tx}}$,

the CG member with the highest instantaneous transmission rate can be selected as the transmitter node with a high probability.

When two or more nodes have the same one-step higher transmission rates, the ordering among them is according to the one indicated in the CG notification message (with respect to the average transmission rate). For illustration clarity, we define a bijective function $g : L_{CP} \rightarrow \{1, 2, \cdots, |L_{CP}|\}$ which maps each CG member ID in L_{CP} to a positive integer representing its rank in the deterministic backoff. Obviously, two cases should be taken into account for any $i, j \in L_{CP}$: 1) If $R'_{i,R_{Tx}} > R'_{j,R_{Tx}}$, then $g(i) < g(j)$; 2) If $R'_{i,R_{Tx}} = R'_{j,R_{Tx}}$, then $g(i) < g(j)$ if and only if $f(i) < f(j)$. Therefore, $g(i)$ is given by

$$g(i) = 1 + \sum_{\substack{j \in L_{CP} \\ j \neq i}} \left[I \left(R'_{i,R_{Tx}} < R'_{j,R_{Tx}} \right) + I \left(R'_{i,R_{Tx}} = R'_{j,R_{Tx}} \right) I \left(f(i) > f(j) \right) \right], \ i \in L_{CP}$$

(2.4)

where $I(A)$ is an indication function which equals 1 if A is true and 0 otherwise, while the constant 1 corresponds to each potential CG member itself.

As the parameters L_C, i_{Tx}, and R_{Tx} are known by all the CG members which have correctly decoded the ACK message, the set L_{CP} can be accurately determined. Moreover, for each contending CG member i, the value of $R'_{j,R_{Tx}}$ for $j \in L_{CP} \setminus i$ can also be obtained accurately since the local information is available for all local nodes within the RS-WLAN. Therefore, contention collision is avoided in the deterministic backoff.

After the backoff is finished, the invited storage local node sends a data packet while the invited non-storage local node sends a helping request message. If any transmission is detected during the backoff procedure, an invited CG member defers its transmission since there exists another node with a higher packet transmission rate. If no contention request burst is detected, the previous transmitter node starts a new transmission immediately.

In the example shown in Fig. 2.4, the kth and k'th potential CG members participate in the channel contention. Since $k < k'$, the kth potential CG member is the first node to finish the backoff. Data transmission starts given the kth potential CG member is a storage local node, while the transmission of the k'th potential CG member is deferred.

CG Attachment

At the beginning of a new dedicated phase, the value of m_{Tx} indicated in the ACK message becomes out-of-date because of the transmission of local traffic in between the dedicated phases. Therefore, a CG attachment mechanism is needed for the first transmission in the new dedicated phase to identify a CG member with the highest instantaneous transmission rate to the nomadic node, as shown in Fig. 2.5. Each dedicated phase begins with a dedicated phase assignment message broadcasted by the CG member with the highest average transmission rate. Upon the reception, the nomadic node replies a receiving request message to the CG member. If there is no reply from the nomadic node, the dedicated phase assignment message is retransmitted. Here, we consider the retransmission continues until the end of the dedicated phase. However, a retransmission limit may be set for better utilization of the resources within an RS-WLAN.

Upon the reception of the request message, a deterministic backoff (with the kth CG member backoffs for $(k-1)$ slots before its transmission) is established. The CG members are ordered according to the CG notification message. The first CG member sends out a rate notification message to notify the other CG members about its instantaneous transmission rate which is estimated based on the receiving request message. When the backoff is finished, another CG member (except the N_Cth CG member) sends a rate notification message only if it has a higher instantaneous transmission rate than the previously indicated ones. The kth CG member starts data (or receiving request message) transmission only if no other transmission is received in the $(N_C - k)$ slots
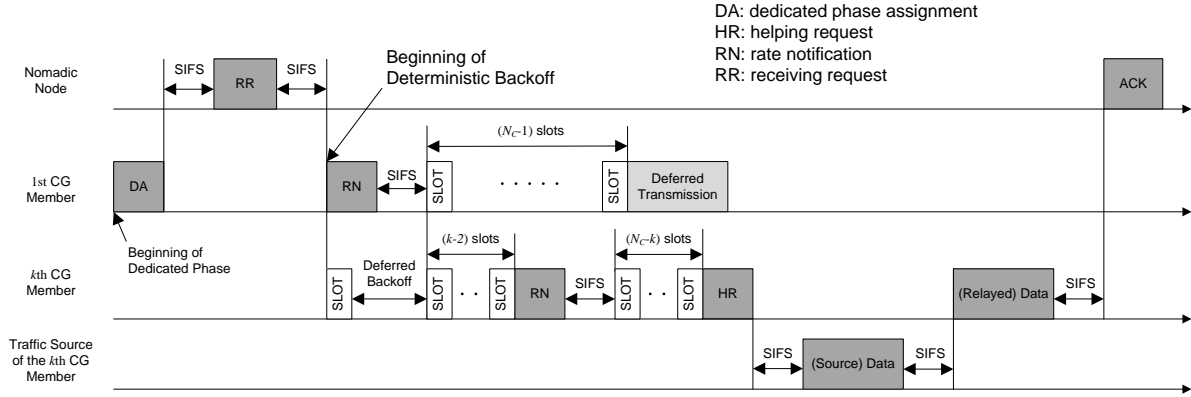
Figure 2.5: Signalling in the CG attachment.

after its rate notification. In the example shown in Fig. 2.5, the kth CG member is a non-storage local node and is the only CG member which has a higher instantaneous transmission rate than that of the first CG member. The CG attachment procedure also identifies a new transmitter node when wireless transmission cannot be established from any of the CG members, possibly caused by (temporary) deep fading or interference.

By using the receiver-initiated mechanism, no RTS/CTS message exchange is necessary before each packet transmission. Moreover, by exploiting the transmission rate indicated in the ACK message as side information, the transmitter selection (by deterministic backoff) does not need to be performed after each ACK message, which further reduces the signalling overhead.

2.4 Performance Analysis

In this section, the performance of the DRMAC scheme is analyzed. The performance metric under consideration is the number of data packets that can be delivered from an RS-WLAN to a nomadic node following a certain movement trajectory at a given speed. The existing analytical model [22, 54] can evaluate the performance of the transmitter-

initiated MAC schemes under a saturated traffic condition, similar to the cooperative data dissemination approach considered here where data packets are already pre-downloaded to the storage local nodes. However, it cannot be applied to model the receiver-initiated mechanism and the time correlation of a wireless channel utilized in the DRMAC scheme. In the following, we present a novel analytical model by using a finite-state Markov chain based channel model to characterize the wireless channel condition [55, 56].

Path loss and Rayleigh fading are considered for a typical WLAN scenario [21]. The cumulative density function (CDF) of the instantaneous SNR, $\Gamma(d)$, for a distance d between the transmitter and receiver is given by $F_{\Gamma(d)}(\gamma) = 1 - e^{-\gamma/\overline{\Gamma}(d)}$ $(0 \leq \gamma < \infty)$, where $\overline{\Gamma}(d)$ is the average SNR at d depending on the path loss effect [57]. Denote $p_{i,m,m'}^t(\tau)$ as the transition probability of the wireless transmission rate index of local node i from m to m' during τ. Based on the finite-state Markov chain channel model, we have

$$p_{i,m,m+1}^t(\tau) = \frac{\tau N_{m+1}}{P_{i,m}}, \quad m = 0, \cdots, M_R - 1 \tag{2.5}$$

$$p_{i,m,m-1}^t(\tau) = \frac{\tau N_m}{P_{i,m}}, \qquad m = 1, \cdots, M_R \tag{2.6}$$

where $N_m = f_{\max} \exp\left(-\frac{\gamma_m^{th}}{\overline{\Gamma}(d_i)}\right)\sqrt{2\pi \frac{\gamma_m^{th}}{\overline{\Gamma}(d_i)}}$ is the cross-rate of rate index m, and $f_{\max}$ is the maximum Doppler frequency which depends on the movement speed of the nomadic node. For the analysis of DRMAC scheme, τ corresponds to the duration of one packet transmission. Therefore, we have

$$p_{i,m,m}^t(\tau) = 1 - p_{i,m,m+1}^t(\tau) - p_{i,m,m-1}^t(\tau). \tag{2.7}$$

The probability of any other state transition equals zero. For analytical tractability, the following assumptions are made:

1. The RS-WLAN covers a circular region with radius r and a neighbor discovery mechanism is in place which admits a nomadic node when it comes within a distance

r_V from the AP. The value of r_V can be greater than the transmission range the AP because of the extended coverage by the local nodes;

2. The nomadic node visits the RS-WLAN along a straight line (e.g., a sidewalk as shown in Fig. 2.1). The local nodes are stationary during the visiting period, while the speed v of the visiting nomadic node is constant. The movement speed of the nomadic node (e.g., a pedestrian) is relatively low such that $p_{i,m,m+1}^t(\tau)$ and $p_{i,m,m-1}^t(\tau)$ are much smaller than $p_{i,m,m}^t(\tau)$;

3. The wireless channels among different local nodes are independent;

4. The average transmission rate $(\overline{R}_i^e)$ can be accurately estimated by the outer-loop MAC, while the CG member with the highest instantaneous transmission rate can always be selected as the transmitter node by the inner-loop MAC.

The performance analysis consists of four parts. In Subsection 2.4.1, we derive an explicit expression for the average number of delivered packets over the visiting trajectory of a nomadic node, while the components in the expression are evaluated in the following subsections. In Subsection 2.4.2, the average packet transmission rate is calculated for a specific location of a nomadic node. In Subsection 2.4.3 and Subsection 2.4.4, the signalling overhead in terms of the durations of contention-by-invitation and CG attachment is evaluated, respectively.

2.4.1   Average Number of Delivered Packets over Visiting Trajectory

Suppose the AP is located at the pole, and the position of local node i $(i \in L)$ is (ρ_i, θ_i). In order to represent the movement of a nomadic node along the roadside (a straight
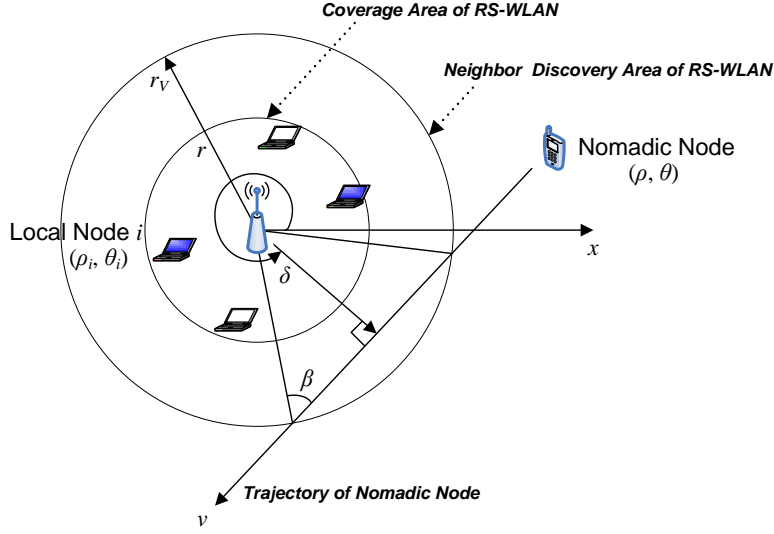
Figure 2.6: The visiting trajectory of a nomadic node to an RS-WLAN.

line), we define the visiting trajectory based on two parameters, i.e., δ and β, which are the angles related to the slope of the visiting trajectory and the shortest distance between the AP and the visiting trajectory, respectively. An illustration of the visiting trajectory is shown in Fig. 2.6 for the network topology in Fig. 2.1. If the nomadic node enters the neighbor discovery range of the RS-WLAN at time 0, then at time t, the positions of the nomadic node for the two opposite moving directions are given by[4]

$$\rho(t) = \sqrt{v^2t^2 + r_V^2 - 2vtr_V \cos\beta} \tag{2.8}$$

$$\theta(t) = \pm \arccos \frac{r_V - vt\cos\beta}{\rho(t)} + \delta \mp (\frac{\pi}{2} - \beta). \tag{2.9}$$

Based on the DRMAC scheme, the overhead of CG attachment should be calculated at the beginning of each dedicated phase, while the overhead of contention-by-invitation should be evaluated before each packet transmission. For analytical tractability, we consider both overhead at the beginning of each superframe since the average channel

---

[4]An extension of our analytical model to an arbitrary visiting trajectory is straightforward by using a different set of functions $\rho(t)$ and $\theta(t)$.

condition does not change significantly within a superframe for pedestrian nomadic nodes. With the kth superframe ($k \geq 1$) starting at time t_k ($t_k = (k-1)T_{SU}$), we denote the durations of contention-by-invitation and CG attachment as $\overline{T}_{CI}(t_k)$ and $\overline{T}_{AT}(t_k)$, respectively. Then the average number of packets delivered to the nomadic node during superframe k is given by

$$B_k^s = \frac{T_E - \overline{T}_{AT}(t_k)}{\left[1/\overline{R}_V(t_k)\right] + \overline{T}_{CI}(t_k)} \tag{2.10}$$

where $\overline{R}_V(t_k)$ is the average packet transmission rate without signalling overhead, given location $(\rho(t_k), \theta(t_k))$ of the nomadic node. For a sufficiently large B_0 value such that the data dissemination service cannot be completely delivered within a single RS-WLAN, the average number of delivered packets over the visiting trajectory is given by $B_V = \sum_{k=1}^{N_F} B_k^s$, where $N_F = \left\lfloor \frac{2r_V \cos\beta}{vT_{SU}} \right\rfloor$ is the number of superframes during the visiting period of the nomadic node. Note that the same average number of delivered packets is obtained for the two opposite moving directions as given in (2.9).

In order to obtain B_V, the values of $\overline{R}_V(t_k)$, $\overline{T}_{CI}(t_k)$, and $\overline{T}_{AT}(t_k)$ should be calculated for all $k \in \{1, 2, \cdots, N_F\}$, to be discussed in the following subsections. Without loss of generality, consider the beginning time of a tagged superframe with the position of the nomadic node given by (ρ, θ).

2.4.2 Average Packet Transmission Rate

We first derive the average packet transmission rate of each local node. The probability that the mth ($0 \leq m \leq M$) rate is chosen by the (one-hop) wireless transmission from

local node i to the nomadic node is given by

$$
P_{i,m} = \begin{cases} F_{\Gamma(d_i)}(\gamma_1^{th}), & \text{if } m = 0 \\ 1 - F_{\Gamma(d_i)}(\gamma_{M_R}^{th}), & \text{if } m = M_R \\ F_{\Gamma(d_i)}(\gamma_{m+1}^{th}) - F_{\Gamma(d_i)}(\gamma_m^{th}), & \text{otherwise} \end{cases} \tag{2.11}
$$

where $d_i = \sqrt{\rho^2 + \rho_i^2 - 2\rho\rho_i \cos(\theta - \theta_i)}$ is the distance between the nomadic node and local node i. Denoting the instantaneous transmission rate from local node i to the nomadic node as R_i, the average transmission rate can be calculated as

$$
\overline{R}_i = \sum_{m=0}^{M_R} \zeta_i(m) P\left(R_i = \zeta_i(m)\right) = \sum_{m=0}^{M_R} \zeta_i(m) P_{i,m}. \tag{2.12}
$$

Based on the estimated average transmission rate $(\overline{R}_i^e = \overline{R}_i)$, the CG memberships (L_C) can be determined for spatial diversity. According to assumption 4), we have $R_V = \max_{j \in L_C} \{R_j\}$ with its CDF given by

$$
F_{R_V}(a) = P\left(\max_{j \in L_C}\{R_j\} \le a\right) = \prod_{j \in L_C} P\left(R_j \le a\right) = \prod_{j \in L_C}\left[\sum_{m=1}^{M_R} P_{j,m} I\left(\zeta_j(m) \le a\right)\right] \tag{2.13}
$$

where the second equality holds as the channels are independent. From (2.11) and (2.13), the probability mass function (PMF) of R_V and the average packet transmission rate $\overline{R}_V$ can be obtained numerically.

2.4.3 Duration of Contention-by-Invitation

In addition to a constant T_{CR}, the duration of contention-by-invitation mainly consists of the duration of deterministic backoff, which depends on the the current transmitter node and the group of CG members in the channel contention. The probability that CG

member n is the transmitter node and the transmission rate index is m ($m \geq 1$) can be derived as

$$P_{n,m}^s = P_{n,m} \prod_{j \in L_C \backslash n} \sum_{l=0}^{M_R} [P_{j,l} I\left(\zeta_j(l) < \zeta_n(m)\right) + P_{j,l} I\left(\zeta_j(l) = \zeta_n(m)\right) I\left(f(j) > f(n)\right)]$$

(2.14)

where j denotes a CG member other than n and l the transmission rate index. The first and second terms in the summation of (2.14) are based on the temporal diversity and correspond to the two cases in the definition of $g(\cdot)$ in (2.4), respectively.

Given that the current transmitter node n is transmitting at the rate indexed m, the (conditional) probability for the rate index of a potential CG member i to be l is given by

$$P_{i,l|n,m} = \frac{P_{i,l}}{\sum_{l=0}^{\zeta_i^{-1}(R'_{i,\zeta_n(m)})-1} P_{i,l}}, \quad i \in L_{CP}, l \in \{0, 1, \cdots, \zeta_i^{-1}(R'_{i,\zeta_n(m)}) - 1\}$$

(2.15)

where L_{CP} can be calculated based on (2.2) by replacing i_{Tx} and R_{Tx} with n and $\zeta_n(m)$, respectively. In (2.15), we have $0 \leq l \leq \zeta_i^{-1}(R'_{i,\zeta_n(m)}) - 1$ since the rate of CG member i cannot exceed that of the current transmitter node. Given the current transmitter node n and its rate index m, the probability for a potential CG member $i \in L_{CP}$ to participate in the channel contention is given by

$$P_{i|n,m}^c = \sum_{l=0}^{\zeta_i^{-1}(R'_{i,\zeta_n(m)})-1} \sum_{h=\zeta_i^{-1}(R'_{i,\zeta_n(m)})}^{M_R} [P_{i,l|n,m} \cdot p_{i,l,h}^t\left(1/\zeta_n(m)\right)]$$

$$= P_{i,[\zeta_i^{-1}(R'_{i,\zeta_n(m)})-1]|n,m} \cdot p_{i,[\zeta_i^{-1}(R'_{i,\zeta_n(m)})-1],\zeta_i^{-1}(R'_{i,\zeta_n(m)})}^t \left(1/\zeta_n(m)\right)$$

(2.16)

where $1/\zeta_n(m)$ corresponds to the duration of one packet transmission from the current transmitter node. Based on assumption 2), the probability for two or more CG members to change their transmission rate (and join the channel contention) during the time of a packet transmission is negligible. Therefore, given the current transmitter node n and

its rate index m, the probability for CG member i to be the next transmitter is

$$P_{i|n,m}^x = P_{i|n,m}^c \prod_{\substack{j \in L_{CP} \\ j \neq i}} (1 - P_{j|n,m}^c). \tag{2.17}$$

Then, the duration (in s) of contention-by-invitation before each packet transmission can be calculated as

$$\overline{T}_{CI} = T_{CR} + \sum_{n \in L_C} \sum_{m=1}^{M_R} P_{n,m}^s \cdot \sum_{i \in L_{CP}} [(g(i) - 1) T_S] P_{i|n,m}^x \tag{2.18}$$

where $g(i)$ is given by (2.4), and the second term of the product represents the conditional expectation of the deterministic backoff duration, given the current transmitter node n and its rate index m.

2.4.4 Duration of CG Attachment

Since retransmission mechanism is considered in CG attachment, its duration can be calculated iteratively based on the success/failure of transmitting each dedicated phase assignment message. At the beginning of a dedicated phase, denote $\vec{\mathbf{m}} = \{\mathbf{m}_1, \cdots, \mathbf{m}_{N_c}\}$ as a vector of the rate indices of all CG members, where $\mathbf{m}_i$ is a random variable representing the rate index of the ith CG member according to the CG notification message. Conditioned on the success/failure of the first transmission of the dedicated phase assignment message, the average duration of CG attachment is given by

$$\begin{aligned}
\overline{T}_{AT} &= \overline{T}_{\vec{\mathbf{m}}|\mathbf{m}_1 \neq 0}^{at} P(\mathbf{m}_1 \neq 0) + \overline{T}_{\vec{\mathbf{m}}|\mathbf{m}_1 = 0}^{at} P(\mathbf{m}_1 = 0) \\
&= \overline{T}_{\vec{\mathbf{m}}|\mathbf{m}_1 \neq 0}^{at} \sum_{m=1}^{M} P_{f^{-1}(1),m} + \overline{T}_{\vec{\mathbf{m}}|\mathbf{m}_1 = 0}^{at} P_{f^{-1}(1),0}
\end{aligned} \tag{2.19}$$

where the inverse function $f^{-1}(\cdot)$ is used to map the rank in CG attachment to the ID of each CG member. In (2.19), $T_{\vec{\mathbf{m}}|\mathbf{m}_1 \neq 0}^{at}$ and $T_{\vec{\mathbf{m}}|\mathbf{m}_1 = 0}^{at}$ are the average durations of

CG attachment given the first transmission of the dedicated phase assignment message is successful and fails, respectively. The expressions of $T^{at}_{\vec{\mathbf{m}}|\mathbf{m}_1 \neq 0}$ and $T^{at}_{\vec{\mathbf{m}}|\mathbf{m}_1 = 0}$ are given in Appendix A. When no wireless transmission can be established from any of the CG members, the CG attachment procedure is also performed, which happens with a low probability (according to the neighbor discovery mechanism) and is neglected in (2.19).

2.5 Numerical Results

Our proposed MAC scheme can be applied to different WLAN standards. Here, the IEEE 802.11a standard with $M = 8$ is considered as an example [48]. By definition, the sizes of the dedicated phase assignment message, receiving request message, and helping request message are equal to the size of the CTS message, while the size of the rate notification message is equal to the size of the ACK message which piggybacks the instantaneous transmission rate index (4 bits) and the packet sequence number (12 bits) [48]. For the wireless channel condition, the pathloss exponent is 3 for a typical WLAN environment [21], and the Rayleigh fading is simulated based on the widely used Jake's model to reflect the time correlation [58]. The SNR threshold of each transmission rate (γ^{th}_m, $m = 1, \cdots, M$) is given in [52]. The RS-WLAN is fully connected with radius $r = 25$ m and neighbor discovery range $r_V = 50$ m. We consider a data dissemination service with a sufficiently large K value and let the size of each packet be 1000 bytes. The durations of the superframe and dedicated phase are $T = 150$ ms and $T_E = 50$ ms, respectively. Using a first-order autoregressive moving average (ARMA) model, the estimated average transmission rate from local node i to the nomadic node is updated by $\overline{R}^{e*}_i = (1 - \xi)\overline{R}^e_i + \xi R^e_i$, where $\overline{R}^e_i$ and $\overline{R}^{e*}_i$ are the estimated average transmission rate before and after the update, respectively, and ξ is an aging factor to keep a partial memory of the historic estimations and is set to $\xi = 0.1$. To simplify simulations with respect to the stationary local nodes, we investigate a ring topology [53] which achieves

36

approximately uniformly distributed node locations for different numbers of local nodes ($|L|$). The local nodes are evenly distributed on two circles with radius $\frac{r}{2}$ and $\frac{3r}{4}$, respectively. The two circles include the same number of nodes, and half of them can provide packet caching capabilities. Consider two visiting trajectories of the nomadic node with parameter sets $(\frac{\pi}{8}, 0)$ and $(\frac{\pi}{16}, \frac{3\pi}{4})$, and corresponding shortest distances between the AP and the nomadic node 19.13 m and 9.75 m, respectively. To incorporate the visiting trajectories of the nomadic node and the physical layer channel model (i.e., the Jake's model) into the MAC simulation, we develop our own event-driven simulator based on MATLAB. A similar simulator is used in previous research [23] without taking account of the trajectories and the time correlation of a wireless channel.

For performance comparison, we consider five MAC schemes, i.e., IEEE 802.11 MAC [48], direct transmission, transmitter-initiated cooperative MAC [23], receiver-initiated MAC [25], and the proposed DRMAC. For the IEEE 802.11 MAC scheme, all storage local nodes participate in the channel contention to deliver packets to the visiting nomadic node. The direct transmission scheme can be considered as a special case of the IEEE 802.11 MAC scheme, where a data packet is transmitted from the AP to the nomadic node after the RTS/CTS exchange. For fair comparison, we modify the transmitter-initiated cooperative MAC scheme by limiting the number of contending local nodes after the RTS/CTS exchange to N_C and ordering them based on the inner-loop MAC of the proposed scheme. In this manner, the channel contention can be reduced among multiple direct/relay links but still exists during the RTS message transmissions. Although the receiver-initiated MAC scheme (without multiple storage local nodes as traffic sources) is not applicable for RS-WLANs with pre-downloaded packets, we modify the scheme by always inviting the storage local node with the highest average transmission rate. Finally, for the newly proposed DRMAC scheme, the value of N_C is chosen from the set $\{1, 2, 3, 4\}$.

2.5.1 Performance Evaluation of the DRMAC Scheme

The effect of N_C on the performance of the proposed MAC scheme is shown in Fig. 2.7, without the signalling overhead. The nomadic node has a visiting trajectory with parameter set $(\frac{\pi}{8}, 0)$ at a speed of 1.5 m/s. We can see that the analytical results match well with the simulation results. As N_C increases, the average number of delivered packets increases, with a higher temporal diversity gain. However, the increment dwindles with a further increase of N_C because the temporal diversity gain becomes saturated. Moreover, for a given N_C, the average number of delivered packets increases with the number of local nodes, which offers more spatial diversity.

Taking account of the signalling overhead, the effect of N_C on the performance of the proposed MAC scheme is shown in Fig. 2.8, with accurate estimation of the average transmission rate. Although the signalling overhead slightly reduces the average number of delivered packets, the basic trends of the curves are the same as those in Fig. 2.7, thanks to both spatial and temporal diversity gains. With pedestrian nomadic nodes and the IEEE 802.11a based physical layer, the channel coherent time is in the order of tens of milliseconds, while the transmission duration of an ACK message is in the order of tens of microseconds. Therefore, the instantaneous transmission rate given in the ACK message is up-to-date with a high probability [56]. This observation confirms the utilization of the ACK message as a receiver-initiated contention invitation, which reduces the signalling overhead. Moreover, the analytical and simulation results agree with each other well, with a slight difference caused by the Markov chain based channel model and the one-step higher transmission rate based approximation.
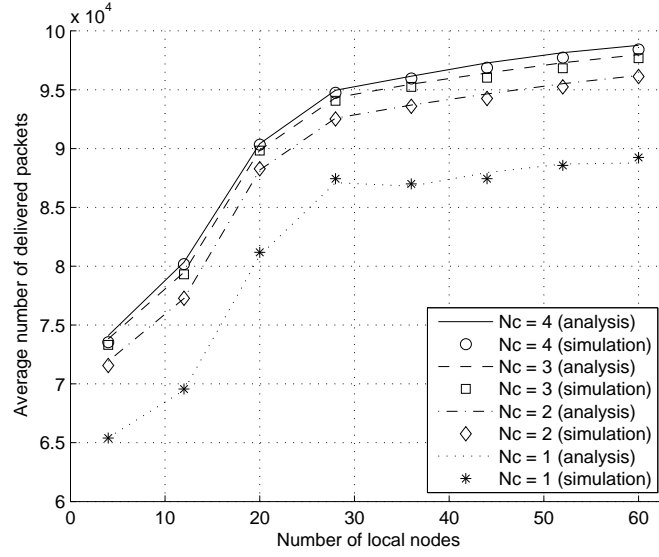
Figure 2.7: The average number of delivered packets using the proposed MAC scheme, without signalling overhead.
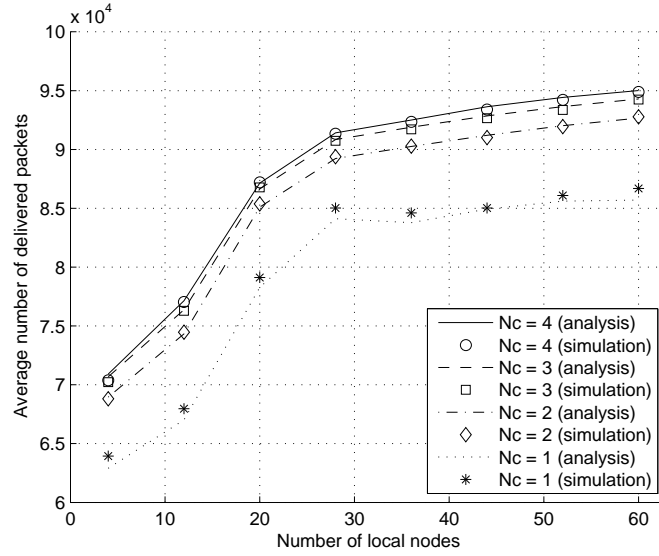
Figure 2.8: The average number of delivered packets using the proposed MAC scheme, taking account of the signalling overhead.

2.5.2   Performance Comparison among Different MAC Schemes

A performance comparison among all the five MAC schemes is shown in Fig. 2.9, using the first-order ARMA model based estimation of the average transmission rate. For the DRMAC scheme, we present the results for $N_C = 1$ and $N_C = 3$, respectively. The performance of the proposed MAC scheme slightly degrades as compared with that in Fig. 2.8, because of the estimation error of the average transmission rate, which results in an occasionally inaccurate selection of CG members. The performance of the direct transmission scheme is low in the absence of spatial and temporal diversity. The IEEE 802.11 MAC scheme performs poorly with packet pre-downloading, since the inherent random backoff before the RTS transmission is not based on the wireless channel condition of the storage local nodes. As the local nodes are scattered within the coverage area of the RS-WLAN, the storage local node with a poor channel condition may be selected as a transmitter, which degrades the packet delivery performance. Moreover, the number of packets delivered by the IEEE 802.11 MAC scheme decreases as the number of local nodes increases, because of a more intensive channel contention among the storage local nodes. By exploiting the diversity gain, the transmitter-initiated cooperative MAC scheme (with $N_C = 4$) can increase the average number of delivered packets. However, the performance improvement is not significant because of the RTS/CTS message exchange, and random backoff which does not adapt to the wireless channel condition. The average number of delivered packets first increases and then decreases with the number of local nodes, demonstrating a tradeoff between the spatial/temporal diversity gain and the intensity of the channel contention among multiple storage local nodes. The receiver-initiated MAC scheme can significantly increase the average number of delivered packets without RTS messages. When the number of local nodes increases, the average number of delivered packets increases with a higher spatial diversity gain. However, the performance of the receiver-initiated MAC scheme is inferior to the DRMAC scheme with $N_C = 1$
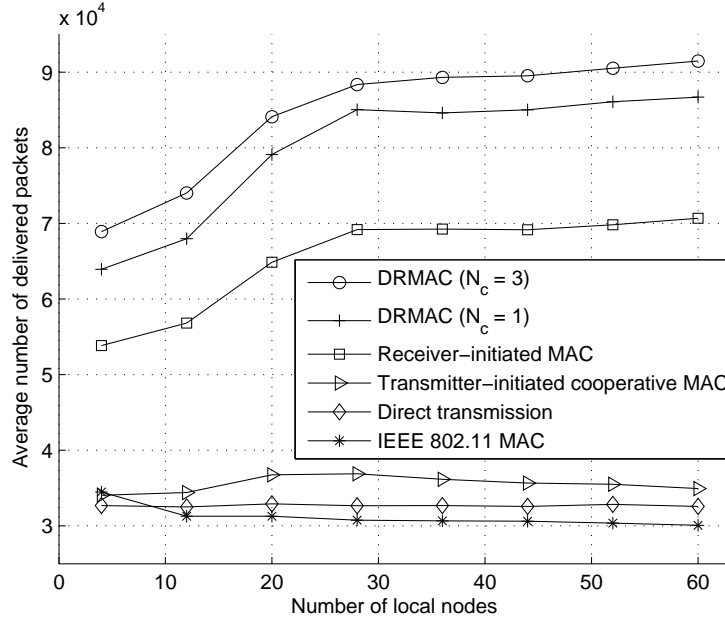
Figure 2.9: A comparison among different MAC schemes.

due to the overhead of CTS (or ready-to-receive (RTR) [25]) message transmission. By exploiting both spatial and temporal diversity gain and reducing the signalling overhead, the DRMAC scheme achieves the best performance among all the MAC schemes.

To study the effect of the movement speed and trajectory parameters of the visiting nomadic node, Figs. 2.10-2.11 show the average number of delivered packets versus movement speed for the different numbers of local nodes and visiting trajectory parameters. As the movement speed increases, the average number of delivered packets decreases with a shorter visiting period. However, the decrement is not linear since the movement speed also affects the channel fading statistics in terms of the maximum Doppler frequency. The relative performance among different schemes is the same as that in Fig. 2.9. More packets can be delivered by all the MAC schemes in Fig. 2.11, which has a longer visiting duration with the visiting trajectory closer to the AP. The transmitter-initiated cooper-
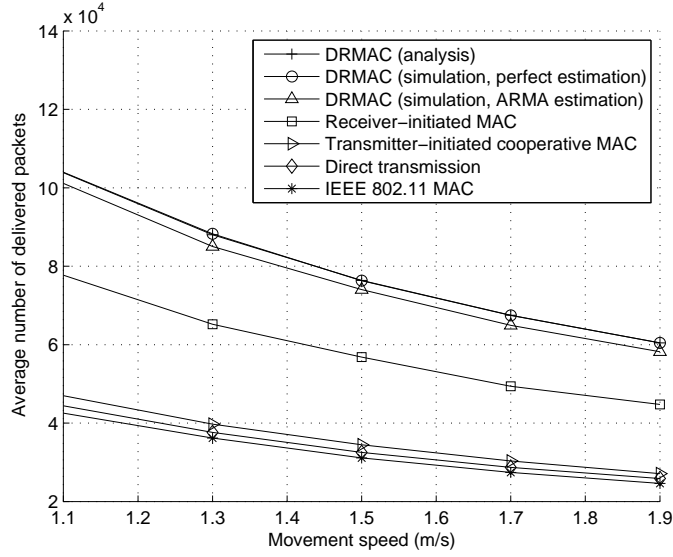
Figure 2.10: The effect of movement speed on different MAC schemes, 12 local nodes, $(\beta, \delta) = (\frac{\pi}{8}, 0)$.
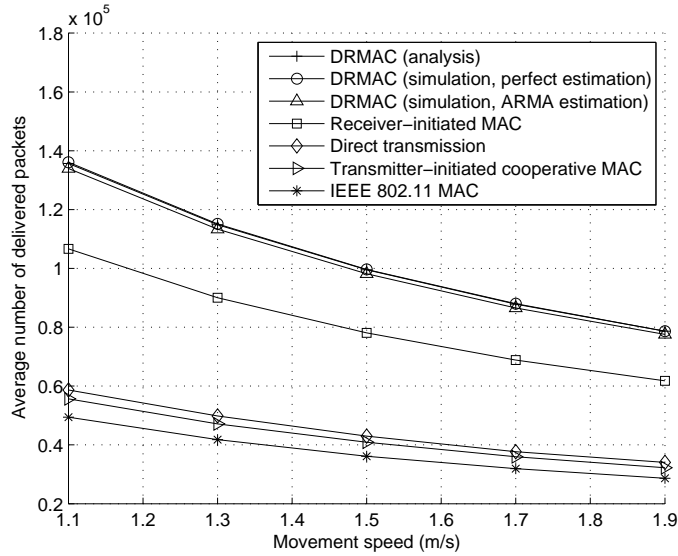
Figure 2.11: The effect of movement speed on different MAC schemes, 20 local nodes, $(\beta, \delta) = (\frac{\pi}{16}, \frac{3\pi}{4})$.

ative MAC scheme delivers slightly less packets to the nomadic node as compared with the direct transmission scheme since the channel contention is higher for an RS-WLAN with 20 local nodes and a visiting trajectory closer to the AP. In both Fig. 2.10 and Fig. 2.11, the analytical results of the DRMAC scheme match well with the simulation results with accurate average transmission rate information, and slightly better than the simulation results based on the first-order ARMA model for channel rate estimation.

2.6 Summary

In this chapter, a DRMAC scheme is proposed for cooperative data dissemination to improve the packet delivery rate from an RS-WLAN to a pedestrian nomadic node. The proposed MAC scheme exploits both spatial and temporal diversity gain while reducing the signalling overhead. An analytical model is derived for the proposed MAC scheme by using a finite-state Markov chain to characterize the time correlation of a wireless channel. Analytical and simulation results indicate that our proposed MAC scheme can achieve the best performance, in terms of the average number of delivered packets from an RS-WLAN to a nomadic node, as compared with the existing IEEE 802.11 MAC, transmitter-initiated cooperative MAC, and receiver-initiated MAC schemes.

Chapter 3

Efficient On-Demand Data Service Delivery to High-Speed Trains

In Chapter 2, the communication bandwidth management problem is addressed given the packet pre-downloading process is completed before the arrival of a nomadic node. In this chapter, we propose solutions for both communication bandwidth and buffer storage management problems for on-demand data service delivery to high-speed trains, taking into account intermittent network connectivity and multi-service demands. Specifically, the contribution is three-fold:

- The optimal resource allocation problem is formulated based on the trajectory of a train, data service demands, and network resources. In order to achieve efficient resource allocation with low computational complexity, the original frame-based formulation is transformed into a capacity-based formulation, which is a single-machine preemptive scheduling problem with integer request times, processing times, and deadlines. The transformation is based on a time-capacity mapping which exploits the predetermined high-speed train schedule.

- An online resource allocation algorithm is proposed to address the uncertainties in service demands, and the performance bound is characterized based on the theory of sequencing and scheduling. Given the link from the backbone network to an infostation is a bottleneck, we analyze the pre-downloading capacity and propose a service pre-downloading algorithm to facilitate the resource allocation.

- The performance of our proposed algorithms is evaluated based on a real high-speed train schedule.

3.1 Literature Review

The cellular network deployed near the rail lines can provide seamless coverage. However, the data transmission rate is limited for trains moving at extremely high speeds because of the Doppler effect [59]. With hundreds of passengers onboard and an ever-growing data-intensive service demand, high information traffic congestion in the cellular network is inevitable. An alternative or complementary solution is proposed in [28, 59, 60, 61], where trackside infostations (or repeaters) are deployed in close vicinity to the rail lines and connected to content servers in the Internet. Powerful antennas are installed on each train to communicate with the infostations. The antennas are further connected to a vehicle station which can be accessed by the passenger devices based on WLAN technologies. Various MAC protocols are studied for the communications between the infostations and vehicle stations. For instance, the IEEE 802.11p MAC can be used for video broadcasting in metro passenger information systems [61], while the MAC frame structure proposed in [59] can support data delivery to a high-speed train with a speed up to 360 km/h. Further, a cellular/infostation integrated network architecture is proposed in [18, 62] to better utilize the resources of both network infrastructures. A cellular network with seamless coverage is considered to support control channels for service

requests and acknowledgements to minimize their delay and avoid congestion, while data traffic is delivered via trackside infostations to achieve a high data transmission rate.

The optimal on-demand broadcast scheduling is investigated for satellite and cellular networks [26, 27]. The proposed algorithms can resolve the resource contention among multiple services. On the other hand, the data delivery in a vehicular network with intermittent links is studied based on the mobility patterns of vehicles [18, 29]. Service pre-downloading approaches are proposed to reduce the data fetching delay when the link from the backbone network to an infostation is a bottleneck [20, 28]. A service scheduling problem is discussed in [32] under the assumption that the bandwidth from the backbone network to an infostation is sufficiently large without addressing the service pre-downloading.

3.2 System Model

The network topology is shown in Fig. 3.1. Several trackside infostations are deployed along the rail line, whereas a cellular network provides a seamless coverage over the region. The base stations of the cellular network and the infostations are connected to the content servers in the Internet via wireline links[1]. When a passenger requests an on-demand data service, the service request is sent from the vehicle station to the corresponding content server via the cellular network. The data traffic of the requested service is delivered from the content server to the vehicle station via the infostations. After the service is delivered, an acknowledgement is made by the vehicle station via the cellular network. For simplicity, we assume that the probability of traffic congestion in the cellular and backbone networks is low, so that the service requests and acknowledgements can be delivered with a negligible delay. Moreover, the data transmission rate from a

---

[1]Note that a wireless link is possible for an infostation with two sets of wireless transceivers [60].
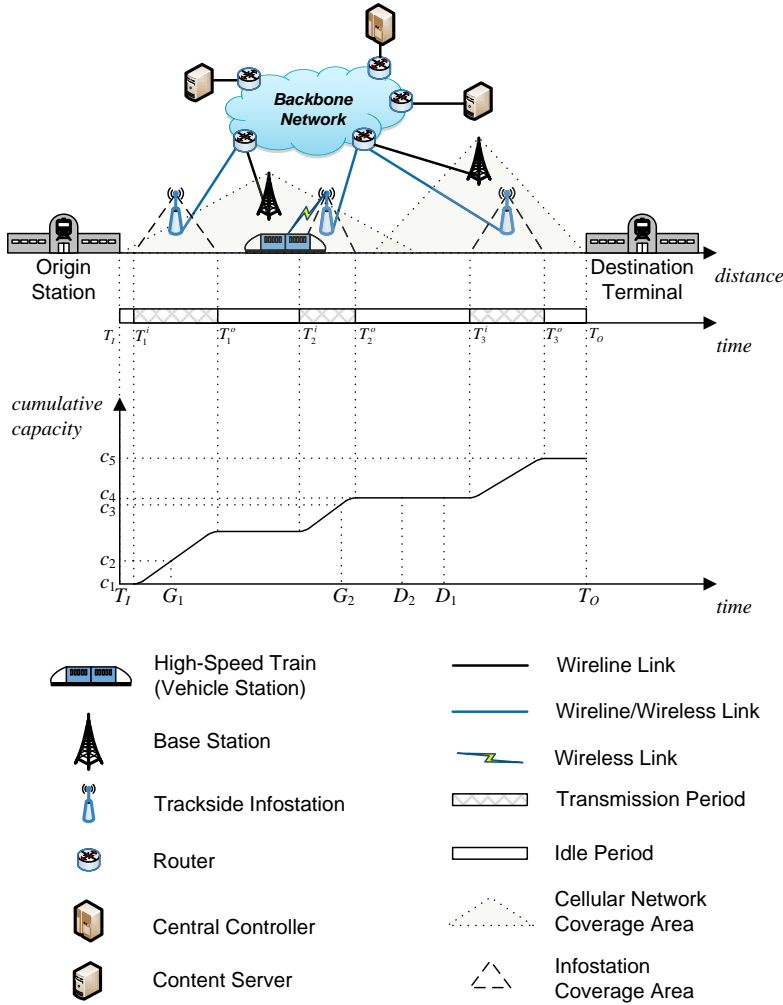
Figure 3.1: System model and time-capacity mapping.

vehicle station to a passenger device is sufficiently large. A data block can be successfully delivered to a passenger device if it is delivered to the vehicle station.

For the communications between the infostations and the vehicle station, we consider the MAC frame structure proposed in [59] which is specifically designed for high-speed trains with a speed up to 360 km/h. Time is partitioned into frames with equal duration T_F. At the beginning of each frame, one of the powerful antennas which are installed on

the train is selected as the master antenna to broadcast a beacon signal to the infostations in the vicinity. The infostations which can detect the beacon signal transmit their unique identification signals as acknowledgments. Each of the antennas on the train uses the acknowledgements for channel estimation and tunes to the infostation with the highest link gain. Then all the infostations which have detected the beacon signal start to broadcast data blocks. This scheme is referred to as the blind information raining. If a group of infostations are deployed in close vicinity with overlapped coverage area, an additional zone controller [59] should be deployed to control the group of infostations and schedule the broadcasting to reduce interference and improve data throughput. In this research, we mainly focus on a network with isolated infostations and intermittent link connectivity. However, the analytical model can be directly extended to a network with some densely deployed infostations, by replacing each infostation in the current model with a zone controller to take charge of scheduling the group of infostations in close vicinity.

A central controller is deployed and can communicate with the cellular network, infostations, and content servers. The central controller allocates the network radio resources based on the train trajectory and data service demands. The train trajectory defines the location of a train at a specific time, while the radio resources depend on the wireless channel condition from an infostation to a vehicle station. Since each train moves on a predetermined rail line and the schedule of a high-speed train is highly stable[2], the information of train trajectory and network resources can be obtained by the central controller in advance with high accuracy. However, the demand of a data service is not known a priori until the service request is received by the content server and delivered to the central controller.

---

[2]According to a recent report, the accuracy of train departure times of Huhang high-speed railway (also know as the Shanghai-Hangzhou high-speed railway) is about 99.5% [63, 64].

3.2.1 Train Trajectory

Consider a single trip of a train from an origin station to a destination terminal within the time duration $[T_I, T_O]$. A total number of H trackside infostations are deployed along the rail line. For instance, we have $H = 3$ in Fig. 3.1. Each infostation covers a segment of the rail line based on its wireless transmission range. Denote T_h^i and T_h^o as time instants for the train to come into and go out of the transmission range of the hth ($h \in [1, \cdots, H]$) infostation, respectively. For isolated infostations, we have $T_h^o \leq T_{h+1}^i$ for $1 \leq h \leq H - 1$. Taking into account the duration of a trip, we have $T_I \leq T_1^i$ and $T_H^o \leq T_O$. In Fig. 3.1, the transmission period and idle period are the time durations when the train is in and out of the coverage area of an infostation, respectively.

3.2.2 Data Service Demands

A set S of on-demand data services are supported over the trip. The request of service s ($s \in S$) is received by the content server at time G_s. If service s is delivered to the vehicle station before its deadline D_s, a reward ω_s can be obtained by the service provider. We consider $G_s \geq T_I$ and $D_s \leq T_O$, assuming that all other services can be delivered to the passengers when they are off-board. Erasure coding based service delivery is considered [59, 20]. The information data of service s is encoded and segmented into a large number $\tilde{Q}_s$ of blocks, each having an equal size of B bits. Service s can be decoded when at least Q_s ($Q_s < \tilde{Q}_s$) distinct blocks are received. The advantage of using erasure coding is that no recovery scheme is required for the transmission error or loss of a specific block. The infostations only need to keep transmitting (or "raining" according to [59]) the encoded blocks until the service can be decoded at the vehicle station, which significantly simplifies the protocol design for high-speed train applications subject to a highly dynamic wireless channel condition.

3.2.3 Network Resources

The duration that the train is within the coverage of the hth infostation corresponds to a number of frames, given by $K_h = \lfloor (T_h^o - T_h^i)/T_F \rfloor$. Note that the small difference between T_h^i and the beginning time of the first frame is omitted. The kth frame begins and ends at times $T_h^i + (k-1)T_F$ and $T_h^i + kT_F$, respectively. We define the capacity $(A_{h,k})$ of the kth frame as the maximum number of blocks that can be delivered from the hth infostation to the vehicle station within this frame. The value of $A_{h,k}$ is determined by the wireless channel condition according to (3) in [59]. If the wireless channel is in deep fading such that no block can be delivered to the vehicle station, we have $A_{h,k} = 0$. A round-robin scheduler[3] is applied when multiple trains are present in the coverage area of an infostation. If the kth frame within the hth infostation coverage is not allocated to the vehicle station under consideration, we have $A_{h,k} = 0$. Since the MAC is frame based, service request time (or deadline) is rounded to the beginning time of a frame.

Full-duplex infostations are considered such that data fetching from the content server and data delivery to the vehicle station can be achieved simultaneously. Two cases are considered for the link from the backbone network to an infostation: 1) The bandwidth of the link (e.g., a high data-rate wireline link [59]) is sufficiently large so that the capacity of each frame can be fully utilized; 2) The link (e.g., a T1 based wireline link at 1.5Mbps [65] or an IEEE 802.16j based wireless link [60]) is a bottleneck with limited bandwidth W_h to the hth infostation. For the second case, data services can be pre-downloaded at the infostations to achieve high radio resource utilization [18]. We consider an unlimited buffer space at the infostations.

---

[3]A scheduler with prioritization can potentially improve the performance of resource allocation when multiple trains are simultaneously within the coverage of an infostation. However, as the time for two high-speed trains to meet is extremely short according to the real train schedule (e.g., the one considered in Section 3.6), the performance improvement can be very limited.

3.3 Problem Formulation and Transformation

In this section, we first formulate the optimal resource allocation problem. Then we introduce a time-capacity mapping to transform the original problem formulation into a capacity-based problem formulation.

3.3.1 Problem Formulation

The objective in service provisioning is to maximize the total reward of delivered services over a trip of the train. Define $x_{h,k,s}$ as the number of blocks delivered to the vehicle station during the kth frame within the hth infostation coverage for service s. The resource allocation variable over the trip of the train is given by $X = \{x_{h,k,s} | h \in \{1, 2, \cdots, H\}, k \in \{1, 2, \cdots, K_h\}, s \in S\}$. For a specific X, define $\psi_{X,s}$ as a delivery indicator of service s, which equals 1 if service s is delivered before its deadline and 0 otherwise. Based on erasure coding, we have $\psi_{X,s} = 1$ if $\sum_{h=1}^{H} \sum_{k=1}^{K_h} x_{h,k,s} = Q_s$, and $\psi_{X,s} = 0$ if $\sum_{h=1}^{H} \sum_{k=1}^{K_h} x_{h,k,s} < Q_s$. Note that we do not consider the case $\sum_{h=1}^{H} \sum_{k=1}^{K_h} x_{h,k,s} > Q_s$ because, for erasure coding based service delivery, the resources are underutilized by delivering more than Q_s blocks for service s. The optimal resource allocation problem is formulated as

$$(\textbf{P1}) \max_{X} \quad \sum_{s \in S} \omega_s \psi_{X,s} \tag{3.1}$$

$$\text{subject to} \quad x_{h,k,s} \in \mathbb{Z}^+, \ h \in \{1, 2, \cdots, H\}, s \in S, k \in \{1, 2, \cdots, K_h\} \tag{3.2}$$

$$\sum_{h=1}^{H} \sum_{k=1}^{K_h} x_{h,k,s} \leq Q_s, \ s \in S \tag{3.3}$$

$$x_{h,k,s} = 0, \ \text{if } G_s \geq T_h^i + kT_F \text{ or } D_s \leq T_h^i + (k-1)T_F,$$

$$h \in \{1, 2, \cdots, H\}, s \in S, k \in \{1, 2, \cdots, K_h\} \tag{3.4}$$

$$\sum_{s \in S} x_{h,k,s} \leq A_{h,k}, \ h \in \{1, 2, \cdots, H\}, k \in \{1, 2, \cdots, K_h\}. \tag{3.5}$$

Constraint (3.2) implies that negative resource allocation is not allowed, where $\mathbb{Z}^+ = \mathbb{N} \cup \{0\}$ represents the set of nonnegative integers. Constraint (3.4) states that the blocks of a service can only be delivered after the request time and before the deadline. With (3.5), the number of blocks that can be delivered to the vehicle station during the kth frame within the hth infostation coverage is limited by the capacity $A_{h,k}$ of the frame.

Problem P1 is a mixed integer programming (MIP) problem which cannot be solved efficiently [66]. The main difficulty of analyzing problem P1 comes from the integer nature of constraint (3.2). However, based on further investigation, we observe that problem P1 can be potentially considered as a problem of sequencing and scheduling [67] because of the constant request time, deadline, size (in terms of the number of blocks), and reward of each service. However, the existing theory of sequencing and scheduling cannot be directly applied to analyze problem P1 since the services are not schedulable continuously over time because of the intermittent link connectivity. Moreover, the data transmission rate (in terms of $A_{h,k}$) from infostations to a vehicle station is not a constant. Therefore, the duration to complete each service is dependent on the time when the service is requested and scheduled.

In order to better characterize problem P1 and develop efficient algorithms to solve it, we consider a problem transformation in the rest of this section such that the time indices are virtually mapped to cumulative capacity values, as shown in Fig. 3.1. Here we define the cumulative capacity at time t ($t \in [T_I, T_O]$) as the summation of the capacities of all frames within $[T_I, t]$. The problem transformation consists of two steps, i.e., time-capacity mapping and capacity-based problem formulation as presented in the following. Here problem P1 is referred to as the frame-based problem formulation. The proofs of lemmas and Theorem 1 are given in Appendix B.

3.3.2 Time-Capacity Mapping

For a specific trip of the train, the maximum number of blocks that can be delivered to the vehicle station is limited by $\sum_{h=1}^{H} \sum_{k=1}^{K_h} A_{h,k}$. Define a time-capacity mapping function $f(t) : [T_I, T_O] \rightarrow \left[0, 1, \cdots, \sum_{h=1}^{H} \sum_{k=1}^{K_h} A_{h,k}\right]$ which maps time t to the corresponding cumulative capacity. Based on the information of train trajectory and network radio resources, we have the following lemma.

Lemma 1. *The value of $f(t)$ is given by*

$$f(t) = \begin{cases} \sum_{j=1}^{\left\lfloor (t-T_{h_t}^i)/T_F \right\rfloor} A_{h_t,j} + \sum_{l=1}^{h_t-1} \sum_{j=1}^{K_l} A_{l,j}, & \text{if } h_t \geq 1 \text{ and } t \leq T_{h_t}^o \\ \sum_{l=1}^{h_t} \sum_{j=1}^{K_l} A_{l,j}, & \text{otherwise} \end{cases} \tag{3.6}$$

where $h_t = \arg\max_h \{T_h^i \leq t\}$ if $t \geq T_1^i$, and $h_t = 0$ otherwise. Without loss of generality, we consider the summation $\sum_{l=a}^{b}(\cdot)$ equals zero if $b < a$.

Intuitively, more blocks can be potentially delivered to the vehicle station as time t increases. This property is inherent for $f(t)$ and stated by the following lemma.

Lemma 2. *The mapping $f(t)$ is a non-decreasing function with respect to t ($t \in [T_I, T_O]$).*

In problem P1, only constraint (3.4) is directly related to the time indices. Therefore, we can apply the time-capacity mapping function $f(t)$ on constraint (3.4) to transform it into a capacity-based constraint. Based on Lemma 1 and Lemma 2, the following theorem holds.

Theorem 1. *For problem P1, (3.4) is equivalent to a capacity-based constraint given by*

$$x_{h,k,s} = 0, \text{ if } G_s^c \geq \sum_{j=1}^{k} A_{h,j} + \sum_{l=1}^{h-1} \sum_{j=1}^{K_l} A_{l,j} \text{ or } D_s^c \leq \sum_{j=1}^{k-1} A_{h,j} + \sum_{l=1}^{h-1} \sum_{j=1}^{K_l} A_{l,j},$$

$$s \in S, h \in \{1, 2, \cdots, H\}, k \in \{1, 2, \cdots, K_h\} \tag{3.7}$$

where $G_s^c = f(G_s)$ and $D_s^c = f(D_s)$.

In (3.7), G_s^c and D_s^c can be considered as the virtual request time and deadline of service s, respectively, which are defined based on the cumulative capacity.

3.3.3 Capacity-Based Problem Formulation

By replacing (3.4) in problem P1 with (3.7), we can obtain problem P2. Since all constraints of problem P2 are defined based on the number of blocks, we can simplify problem P2 by introducing a capacity-based formulation.

By definition, we have $f(T_I) = 0$ and $f(T_O) = \sum_{h=1}^{H} \sum_{k=1}^{K_h} A_{h,k}$. Then the set $\{T_I, T_O, G_s, D_s | s \in S\}$ of time indices can be represented by a set C of unique cumulative capacity, given by

$$
\begin{aligned}
C &= \cup_{s \in S} \{f(G_s), f(D_s)\} \cup \{f(T_I), f(T_O)\} \\
&= \cup_{s \in S} \{G_s^c, D_s^c\} \cup \left\{0, \sum_{h=1}^{H} \sum_{k=1}^{K_h} A_{h,k}\right\}.
\end{aligned}
\tag{3.8}
$$

Let $|C| = N+1$ $(N \geq 1)$ and c_n $(1 \leq n \leq N+1)$ be the cardinality and elements of set C, respectively. Without loss of generality, we consider an ascending order of the elements in C, i.e., $c_1 < c_2 < \cdots < c_{N+1}$. An example is shown in Fig. 3.1, where two services are considered with request times G_1 and G_2, and deadlines D_1 and D_2, respectively. Then we have $N = 4$ and c_n $(1 \leq n \leq 5)$ given by

$$
c_1 = 0, \ c_2 = G_1^c, \ c_3 = G_2^c, c_4 = D_1^c = D_2^c, \ c_5 = \sum_{h=1}^{H} \sum_{k=1}^{K_h} A_{h,k}
\tag{3.9}
$$

where D_1 and D_2 are mapped to the same cumulative capacity c_4 since no block can be delivered during an idle period. Note that if $G_2^c < D_1^c \neq D_2^c < \sum_{h=1}^{H} \sum_{k=1}^{K_h} A_{h,k}$, we have $N = 5$, while each element in C (other than c_1 and c_6) corresponds to the request time or deadline of a service.

We partition the trip of the train into N non-overlapped virtual periods according to the cumulative capacity values in C. Within the nth virtual period (defined by $[c_n + 1, c_{n+1}]$), no new service is requested and no existing service expires since all service request times and deadlines are considered in the calculation of set C. Therefore, for a feasible resource allocation, changing the sequence of service scheduling within a virtual period does not affect the service delivery performance. This property is formally stated by the following lemma.

Lemma 3. *Consider a feasible resource allocation variable X with four elements x_{h_1,k_1,s_1}, x_{h_1,k_1,s_2}, x_{h_2,k_2,s_1}, x_{h_2,k_2,s_2}. Suppose $x_{h_1,k_1,s_1}, x_{h_2,k_2,s_2} \geq 1$, $x_{h_1,k_1,s_2}, x_{h_2,k_2,s_1} \geq 0$. All blocks of the two frames (i.e., the k_1th frame within the h_1th infostation coverage and the k_2th frame within the h_2th infostation coverage) belong to the same virtual period, while the two frames are not identical. Construct another resource allocation variable X' by replacing the elements x_{h_1,k_1,s_1}, x_{h_1,k_1,s_2}, x_{h_2,k_2,s_1}, x_{h_2,k_2,s_2} in X with $x_{h_1,k_1,s_1} - 1$, $x_{h_1,k_1,s_2} + 1$, $x_{h_2,k_2,s_1} + 1$, $x_{h_2,k_2,s_2} - 1$ and keeping all other elements unchanged. Then we have the same feasibilities and objective function values for X and X'.*

Based on Lemma 3, the optimal resource allocation can be achieved by considering the total number of blocks delivered for each service within each virtual period. Define $\tilde{y}_{n,s}$ as the number of blocks delivered to the vehicle station for service s within the nth virtual period. Then the resource allocation variable over the trip of the train is given by $\tilde{Y} = \{\tilde{y}_{n,s} | n \in \{1, 2, \cdots, N\}, s \in S\}$. Define the delivery indicator of service s as $\eta_{\tilde{Y},s}$. We have $\eta_{\tilde{Y},s} = 1$ if $\sum_{n=1}^{N} \tilde{y}_{n,s} = Q_s$, and $\eta_{\tilde{Y},s} = 0$ if $\sum_{n=1}^{N} \tilde{y}_{n,s} < Q_s$. Then problem P2 can be transformed into a capacity-based formulation as follows

$$(\textbf{P3}) \max_{\tilde{Y}} \quad \sum_{s \in S} \omega_s \eta_{\tilde{Y},s} \tag{3.10}$$

$$\text{subject to} \quad \tilde{y}_{n,s} \in \mathbb{Z}^+, \ n \in \{1, 2, \cdots, N\}, s \in S \tag{3.11}$$

$$\sum_{n=1}^{N} \tilde{y}_{n,s} \leq Q_s, \ s \in S \tag{3.12}$$

$$\tilde{y}_{n,s} = 0, \ \text{if } G_s^c \geq c_{n+1} + 1 \text{ or } D_s^c \leq c_n, n \in \{1, 2, \cdots, N\} \tag{3.13}$$

$$\sum_{s \in S} \tilde{y}_{n,s} \leq c_{n+1} - c_n, \ n \in \{1, 2, \cdots, N\} \tag{3.14}$$

where (3.14) states that the number of blocks which can be delivered to the vehicle station during the nth virtual period is limited to $c_{n+1} - c_n$.

3.4   Resource Allocation

Based on the problem transformation, time indices are virtually transformed to the cumulative capacity values, over which the services are continuously schedulable. According to the theory of sequencing and scheduling, problem P3 defines a single-machine preemptive scheduling problem with integer request (or release) times (G_s^c), processing times (Q_s), and deadlines (D_s^c) (formal notation: $1|G_s^c, preemption| \sum \omega_s \eta_{Y,s}$), which can be solved by a dynamic programming algorithm at complexity $O(|S| L_G^2 L_\omega^2)$, where L_G is the number of distinct request times, and L_ω represents the sum of the integer reward [67, 68, 69, 70]. The complexity is known as pseudo-polynomial [70] since the representation of all rewards ω_s ($s \in S$) by integers may result in a large L_ω and a high computational complexity accordingly. Moreover, for on-demand data services, the service demands are not known a priori. In order to achieve efficient resource allocation for on-demand data service delivery to high-speed trains, we devise an online algorithm in this section. As the online algorithm is devised based on problem P3, its performance bound can be characterized based on the theoretical results of the single-machine preemptive scheduling problem, to be discussed in the following.

As the train moves from the origin station to the destination terminal, the online algorithm allocates the network resources to multiple services frame-by-frame. Consider

the kth frame within the hth infostation coverage, with $x_{h,k,s}$ blocks delivered for service s ($s \in S^g_{h,k}$), where $S^g_{h,k} = \{s | s \in S, G_s \leq T^i_h + (k-1)T_F\}$ represents the set of requested services. The resource allocation algorithm is detailed in Algorithm 1, where $Q^r_{h,k,s}$ and $\tilde{Q}^r_{h,k,s}$ are the numbers of remaining blocks of service s before and after the kth frame, respectively. The algorithm needs to be performed only when $S^g_{h,k} \neq \emptyset$. For a newly requested service s, i.e.,

$$s \in \begin{cases} S^g_{h,k}, & \text{if } h = 1, k = 1 \\ S^g_{h,k} \setminus S^g_{h-1,K_{h-1}}, & \text{if } h \neq 1, k = 1 \\ S^g_{h,k} \setminus S^g_{h,k-1}, & \text{otherwise} \end{cases} \tag{3.15}$$

we have $Q^r_{h,k,s} = Q_s$; Otherwise, we have

$$Q^r_{h,k,s} = \begin{cases} \tilde{Q}^r_{h-1,K_{h-1},s}, & \text{if } k = 1 \\ \tilde{Q}^r_{h,k-1,s}, & \text{if } k > 1. \end{cases} \tag{3.16}$$

In (3.15) and (3.16), $k = 1$ corresponds to the first frame within an infostation coverage. In (3.16), if $k = 1$, we have $h \neq 1$ since the service is considered to be new in one of the previous frames.

Algorithm 1 iteratively allocates the capacity of a frame ($A_{h,k}$) to the on-demand data services in descending order of their utilities, until the capacity of the frame is fully utilized. In step 3, S_A represents the set of active services which can possibly be delivered before their deadlines, given by

$$S_A = \left\{ s | s \in S^g_{h,k}, \tilde{Q}^r_{h,k,s} > 0, D^c_s \geq \tilde{Q}^r_{h,k,s} + \sum_{j=1}^{k} A_{h,j} + \sum_{l=1}^{h-1} \sum_{j=1}^{K_l} A_{l,j} - m \right\}. \tag{3.17}$$

In step 7, U_s represents the utility of service s. We consider two kinds of utilities, i.e., Smith ratio and exponential capacity [69]. For Smith ratio based algorithm, $U_s = \omega_s / Q_s$. Intuitively, a service with a higher reward or smaller size can obtain a higher utility. For

---

Algorithm 1   Resource Allocation Algorithm

Input: k, h, G_s^c, D_s^c, ω_s, Q_s, $Q_{h,k,s}^r$ $(s \in S_{h,k}^g)$

Output: $x_{h,k,s}$, $\tilde{Q}_{h,k,s}^r$ $(s \in S_{h,k}^g)$

 1: Initialize $x_{h,k,s} = 0$, $\tilde{Q}_{h,k,s}^r = Q_{h,k,s}^r$ for $s \in S_{h,k}^g$, $m = A_{h,k}$;

 2: **while** $m \neq 0$ **do**

 3: S_A calculation;

 4: **if** $S_A = \emptyset$ **then**

 5: break;

 6: **end if**

 7: U_s calculation, for $s \in S_A$;

 8: $s^* = \arg\max_{s \in S_A} \{U_s\}$;

 9: Update $x_{h,k,s^*} \leftarrow x_{h,k,s^*} + 1$, $\tilde{Q}_{h,k,s^*}^r \leftarrow \tilde{Q}_{h,k,s^*}^r - 1$, $m \leftarrow m - 1$;

10: **end while**

---

the exponential capacity based algorithm, the utility function incorporates the number of remaining blocks $(\tilde{Q}_{h,k,s}^r)$ which corresponds to the current condition of each service, and is given by

$$U_s = \omega_s \left(1 - \frac{\ln\left(\max_{s \in S_{h,k}^g} Q_s\right)}{\max_{s \in S_{h,k}^g} Q_s} \right)^{\tilde{Q}_{h,k,s}^r - 1}. \tag{3.18}$$

The complexity of Algorithm 1 is $O\left(\max_{h,k}\{A_{h,k}\}|S|\right)$.

Define the competitive ratio of Algorithm 1 as the maximal ratio (corresponds to the worst-case performance of Algorithm 1 with respect to the randomness in service requests) of the total reward of delivered services based on the optimal solution of problem P3 to that of the delivered services based on Algorithm 1. The competitive ratio of the Smith ratio and exponential capacity based algorithm is given by $2\max_{s \in S}\{Q_s\}$ and $\max_{s \in S}\{Q_s\}/\ln(\max_{s \in S}\{Q_s\})$, respectively [69]. Since we have $1/\ln(\max_{s \in S}\{Q_s\}) < 2$ for typical on-demand data services which consist of a large number of blocks, the exponential capacity based algorithm can improve the performance of resource allocation in worst-case scenarios, at the cost of higher computational complexity in step 7. However, the computational complexity can be potentially reduced. For instance, a straightforward

approach is to maintain a queue of all active services and sort the services in descending order of their utilities. In this way, the head-of-line (HOL) service always represents the service with the highest utility to be scheduled. For the resource allocation in each frame, the order is updated only for the newly requested services or the services with some blocks being delivered. As a result, step 7 and step 8 do not need to be recalculated for each active service during each iteration with respect to m.

3.5   Service Pre-Downloading

When the link from the backbone network to an infostation is the bottleneck of service delivery, the capacity $A_{h,k}$ of a frame is underutilized if less than $A_{h,k}$ blocks are fetched from the content server within the frame. In order to address this problem, a service pre-downloading mechanism can be implemented [18, 20, 28]. In the cellular/infostation integrated network, after a service request is received by the content server, the data blocks of the service can be pre-downloaded to the infostations to be visited by the vehicle station, and then delivered to the vehicle station upon its arrival. A simple service pre-downloading approach is to buffer all data blocks of the available services at each infostation. However, this approach is not only infeasible (because of the limited bandwidth of the bottleneck link) but also inefficient (as some pre-downloaded blocks cannot be transmitted to the vehicle station during its short visit to each of the infostations).

In the following, we propose a service pre-downloading approach to facilitate the resource allocation of Algorithm 1. Let $S_{\hat{s}}^g = \{s | s \in S, G_s \leq G_{\hat{s}}\}$ denote the set of requested services at time $G_{\hat{s}}$. We want to determine the number of blocks ($M_{h,s}$) to be pre-downloaded at the hth ($h \in [1, \cdots, H]$) infostation for service $s \in S_{\hat{s}}^g$. Next, we first analyze the pre-downloading capacity to determine the maximum number of blocks to be pre-downloaded at each infostation, and then present a service pre-downloading algorithm to calculate $M_{h,s}$.

3.5.1 Pre-Downloading Capacity and Redundant Factor

Taking account of the limited capacity of each frame, the number of blocks to be pre-downloaded at the hth infostation ($\sum_{s \in S} M_{h,s}$) should be limited by the sum capacity of all frames within the infostation coverage ($\sum_{k \in K_h} A_{h,k}$). On the other hand, for a given time t ($t < T_h^o$), the duration of service pre-downloading to the hth infostation is given by $T_h^o - t$. Note that the transmission period with duration $T_h^o - T_h^i$ is taken into account since full-duplex infostations are considered. With the bandwidth W_h of the bottleneck link, the maximum number of blocks that can be fetched from the content server during $T_h^o - t$ is $\lfloor (T_h^o - t)W_h/B \rfloor$. Then the pre-downloading capacity of the hth infostation at time t is

$$Q_{h,t}^c = \min \left\{ \sum_{k \in K_h} A_{h,k}, \lfloor (T_h^o - t)W_h/B \rfloor \right\}. \tag{3.19}$$

As discussed in Section 5.2, service s can be successfully decoded if Q_s blocks are received by the vehicle station before D_s. However, because of the resource contention among multiple services, the number of pre-downloaded blocks of service s is dependent on other service demands. Therefore, we introduce a redundant factor β ($\beta \geq 0$) for service pre-downloading. Specifically, for each service, the number of pre-downloaded blocks at the infostations to be visited is β times the number of remaining blocks to be delivered. The larger the β, the more blocks can be pre-downloaded for each service and the less number of services can be pre-downloaded. Note that β can be larger than one since some pre-downloaded blocks of a service may not be delivered to the vehicle station when new services with high priorities arrive.

3.5.2 Service Pre-Downloading Algorithm

Based on the pre-downloading capacity and redundant factor, a service pre-downloading algorithm is devised. When the request of a service $\hat{s}$ is received at time $G_{\hat{s}}$, the service pre-downloading variables $(M_{h,s})$ are calculated according to Algorithm 2, where $Q^r_{\hat{s},s}$ represents the number of remaining blocks of service s at time $G_{\hat{s}}$. In step 5, only the set of active services which can possibly be delivered before their deadlines is considered. The minimum operation in step 9 is performed over two terms corresponding to the pre-downloading capacity and redundant factor, respectively. For the first term, a summation $\sum_{i=1}^{j-1} M_{h,s_i}$ is subtracted since the corresponding capacity is used to pre-download services with higher priorities, while for the second term, a summation $\sum_{l=h_{G_{\hat{s}}}+1}^{h-1} M_{l,s_j}$ is subtracted since this amount of blocks is to be pre-downloaded to the infostations before infostation h. The utility (U_s) of service s is given by the resource allocation Algorithm 1. The complexity of Algorithm 2 is $O(H|S|)$.

Let $M^d_{h,s}$ denote the number of blocks already pre-downloaded at infostation h for service s. Because of the arrival of services with higher priorities, we may have $M_{h,s} < M^d_{h,s}$. Therefore, the number of blocks to be pre-downloaded for service s at infostation h is given by $\max\{0, M_{h,s} - M^d_{h,s}\}$. For each infostation, the data blocks of the services are fetched from the content server in descending order of their utilities. When multiple trains are traveling on parallel high-speed rails between the origin station and destination terminal [63], Algorithm 2 is applied by letting $S^g_{\hat{s}}$ represent the set of services requested by all the trains.

When a train comes into the transmission range of an infostation, the pre-downloaded blocks are scheduled for transmission according to Algorithm 1. After all pre-downloaded blocks are delivered, the remaining blocks of available services are directly fetched from the content servers.

Algorithm 2   Service Pre-Downloading Algorithm

Input: G_s, D_s, G_s^c, D_s^c, ω_s, Q_s, $Q_{\hat{s},s}^r$ $(s \in S_{\hat{s}}^g)$

Output: $M_{h,s}$ $(h \in \{1, \cdots, H\}, s \in S_{\hat{s}}^g)$

 1: Initialize $M_{h,s} = 0$ for $h \in \{1, \cdots, H\}$, $s \in S_{\hat{s}}^g$;

 2: U_s calculation, for $s \in S_{\hat{s}}^g$;

 3: Sort services in $S_{\hat{s}}^g$ in descending order of their utilities and obtain the ordered set $\{s_1, s_2, \cdots, s_{|S_{\hat{s}}^g|}\}$;

 4: **for** $j = 1$ to $|S_{\hat{s}}^g|$ **do**

 5:   **if** $Q_{\hat{s},s_j}^r = 0$ or $D_{s_j}^c < G_{\hat{s}}^c + Q_{\hat{s},s_j}^r$ **then**

 6:     Continue;

 7:   **end if**

 8:   **for** $h = h_{G_{\hat{s}}} + 1$ to H **do**

 9:     $M_{h,s_j} = \min \left\{ Q_{h,G_{\hat{s}}}^c - \sum_{i=1}^{j-1} M_{h,s_i}, \beta Q_{\hat{s},s_j}^r - \sum_{l=h_{G_{\hat{s}}}+1}^{h-1} M_{l,s_j} \right\}$;

10:   **end for**

11: **end for**

3.6   Numerical Results

In order to evaluate performance of the proposed resource allocation algorithms, we consider a real train schedule based on the Huhang high-speed railway [71]. The railway is specially designed for high-speed trains with a maximum speed of 350 km/h. There are ten stations on the railway and the location of each station (in terms of the distance from the Shanghai station) is given in Table 3.1.

Since no mobility trace is available, we consider a synthetic train mobility model proposed in [72]. Each train moves at a constant speed when it travels from one station to another. When a train leaves (arrives at) a station, it accelerates (decelerates) according to a constant acceleration (deceleration). For simplicity, we consider the deceleration equals to the negative value of the acceleration (α). A typical value for the acceleration α of a high-speed train is given by 0.4 m/s^2 [73]. Five sample trajectories of the high-speed trains are shown in Fig. 3.2, for two trains from Hangzhou (G7403 and G7302) and three trains from Shanghai (G7401, G7301, and G7362). The starting time of train

Table 3.1: Locations of stations on the railway.

Station	Shanghai	Hongqiao	Songjiang	Jinshan	Jiashan
Distance (km)	0	33	64	81	100
Station	Jiaxing	Tongxiang	Haining	Yuhang	Hangzhou
Distance (km)	117	145	166	177	202
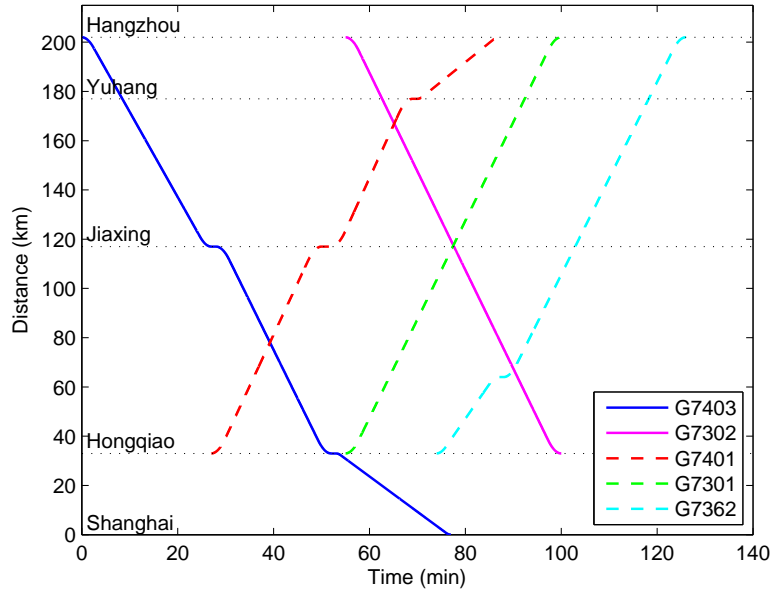
Figure 3.2: Trajectory of the high-speed trains.

G7403 (06:05 am) based on the February 2011 schedule is chosen to be time 0. Note that the trains G7301 and G7302 need less time to travel between Hongqiao and Hangzhou since they do not stop at two intermediate stations, Jiaxing and Yuhang.

For the wireless channel condition, we use a typical setting for a high-speed train [59], with $T_F = 53\mu$s, $B = 240$ bits, and $H = 40$. The wireless communication between an infostation and the vehicle station is established based on a carrier frequency of 2.4GHz and an approximate data rate of 50Mbps. On each train operating on Huhang high-

speed railway, 13 antennas can be deployed with a separation distance of 15 m between adjacent antennas. The distance between each infostation and the rail line is 3 m. The transmission range of each infostation is approximately 500 m. The service requests arrive at a train according to a Poisson process with average rate λ. The number of blocks of each service (Q_s) is uniformly distributed within $[Q_{\min} = 50000, Q_{\max} = 500000]$ (corresponding to a service size within $[1.5, 15]$ Mbytes). The lifetime $(D_s - G_s)$ of each service is exponentially distributed with average value 2 minutes. The reward of each service (ω_s) is uniformly distributed within $[1, 10]$[4].

In addition to the proposed resource allocation algorithms, we consider three existing algorithms for comparison, i.e., first-in-first-out (FIFO), earliest due date (EDD), and RAPID [29]. For the FIFO and EDD algorithms, the services are scheduled according to an ascending order of their request times and deadlines, respectively. RAPID is a typical single-service resource allocation algorithm for a network with intermittent links. Since the RAPID algorithm is originally proposed for randomized node mobility, we have modified the algorithm to incorporate the pre-determined train schedule for fair comparison. To calculate the utility function, we modify the algorithm by replacing the time indices with cumulative capacity values based on the time-capacity mapping. Moreover, the transfer opportunity [29] (which determines the maximum number of blocks that can be delivered from an infostation to the vehicle station) is changed from a constant defined by the original work to the sum of the capacity of all frames within each infostation, which is a variable with respect to different infostations according to the train schedule.

---

[4]In reality, the reward of each service may depend on many factors such as the service size, urgency (delivery deadline), and priority. How to map these factors to the reward for practical high-speed train applications is still an open issue and left for our future work.

3.6.1   Performance of Resource Allocation Algorithms

The performance of our proposed resource allocation algorithm is evaluated by extensive simulations under different system parameters, such as service arrival rate, train schedule, service size, and service lifetime. The total reward of delivered services versus average service arrival rate (λ) is shown in Fig. 3.3 for train G7302. The standard deviations are illustrated for reference. The total reward is low for the FIFO and EDF algorithms since they do not incorporate the train trajectory and data service demands. Although the EDF algorithm performs well when most services can be delivered before their deadlines, its performance degrades as λ increases [74]. For a large λ, the total rewards achieved by the RAPID algorithm and our proposed algorithm improve since more services can be potentially scheduled. However, the increment dwindles since the network throughput becomes saturated. The RAPID algorithm performs better than the FIFO and EDF algorithms since the mobility information of the train is taken into account. By further incorporating the demands of multiple services, our proposed resource allocation algorithm achieves the best performance. In comparison with the existing algorithms, the performance gain achieved by our proposed algorithm improves as the service arrival rate increases, which is a desirable property for high-speed trains with hundreds of passengers onboard and an ever-growing service demand. Although the competitive factor of the exponential capacity based algorithm is higher than that of the Smith ratio based algorithm, the performance of resource allocation is comparable since a worst case scenario for the algorithm (i.e., there is a large service with high reward which consumes most of the network resources [69]) happens with a low probability for the high-speed train applications.

Fig. 3.4 shows the total reward of delivered services versus λ for train G7401. For the same λ value, train G7401 has a higher total reward than train G7302, because the former has a longer trip duration, as shown in Fig. 3.2, resulting in more delivered services.
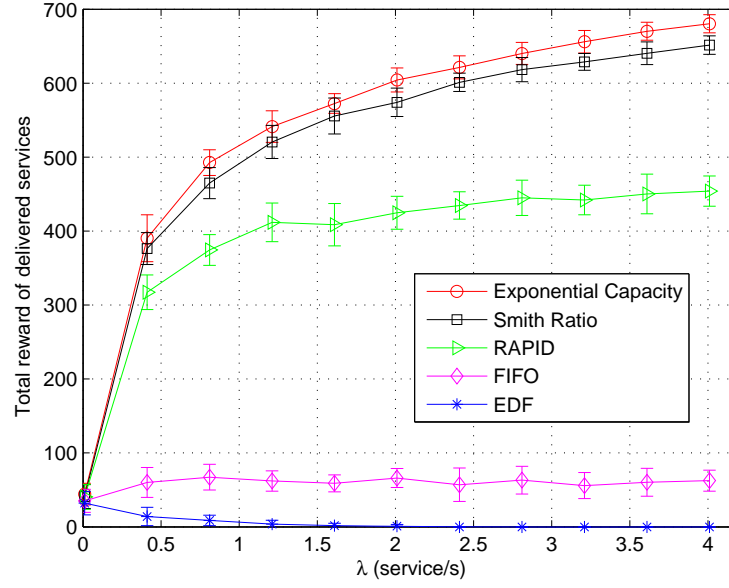
Figure 3.3: Impact of service arrival rate (G7302).
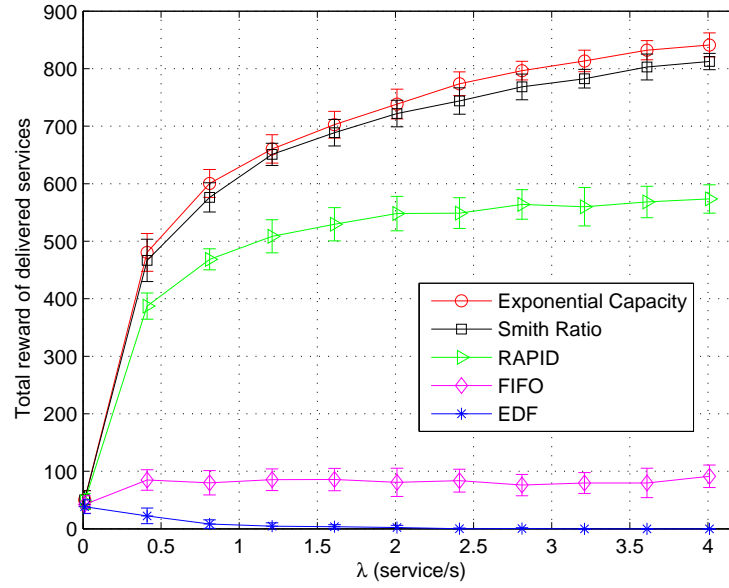
Figure 3.4: Impact of service arrival rate (G7401).
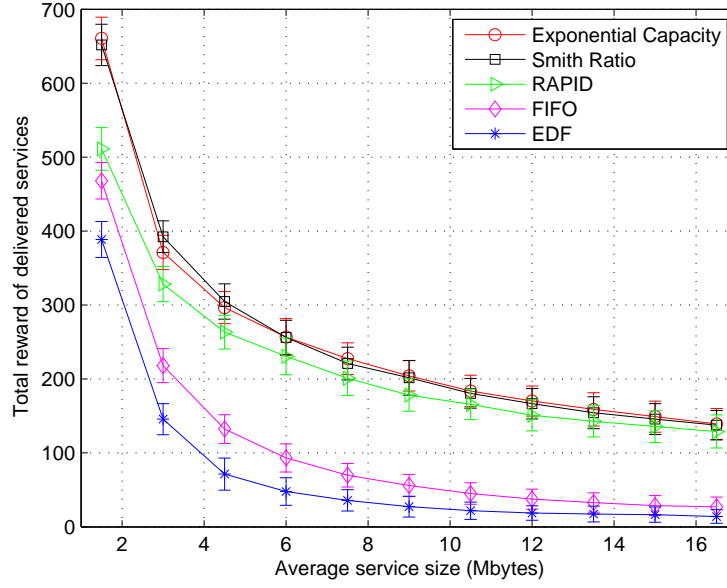
Figure 3.5: Impact of service size.
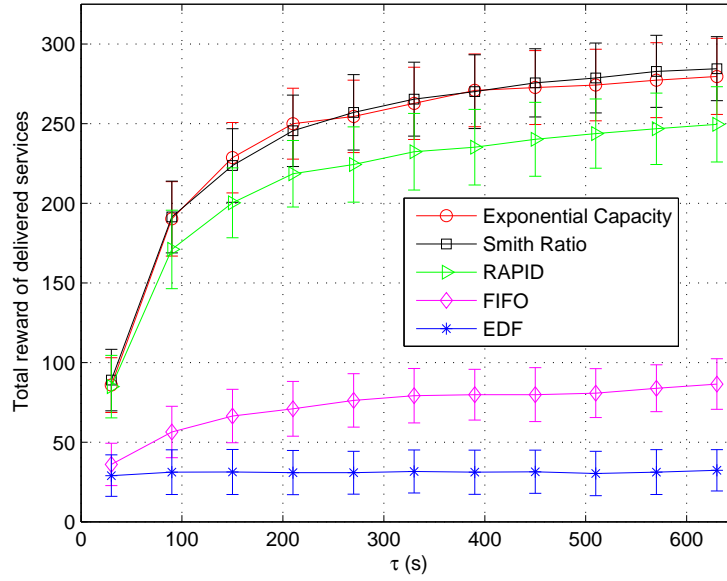
Figure 3.6: Impact of service lifetime.

Fig. 3.5 shows how the total reward of delivered services changes with the average service size, with $Q_{\min} = 50000$ and $Q_{\max}$ varying according to the average. We can see that the total reward decreases as the average downloading file size increases. For a larger average service size, more resources are needed to deliver each service. As a result, a less number of services can be delivered under the limited resources.

The total reward of delivered services increases with the average service lifetime (τ), as shown in Fig. 3.6. For a larger τ, more infostations can be visited by an vehicle station before a service expires, which increases the probability of delivering the service. However, the increment dwindles when τ is large since the network throughput becomes saturated. From Figs. 3.4-3.6, we can see that our proposed resource allocation algorithms outperform the existing algorithms under different system parameters. As similar performance is observed for Smith ratio and exponential capacity utilities, in the following performance evaluation, we consider the Smith ratio based algorithm as an example.

3.6.2   Performance of Service Pre-Downloading Algorithm

The effect of the bottleneck link bandwidth (W_h) in service pre-downloading is shown in Fig. 3.7 for train G7403, where all infostations have the same bandwidth $W_h = W$ ($h \in [1, \cdots, H]$). The total reward is significantly improved by the service pre-downloading. As the bandwidth increases, the total reward improves slowly without service pre-downloading since all data blocks need to be fetched directly from the content servers upon the arrival of a vehicle station, which underutilizes the capacity of the wireless channel (in frames). On the other hand, with service pre-downloading, a higher reward can be achieved even for a small W_h since the disconnected period of a vehicle station is effectively exploited by the infostations to pre-download data blocks.

Fig. 3.8 and Fig. 3.9 show that the redundant factor (β) has a critical impact on
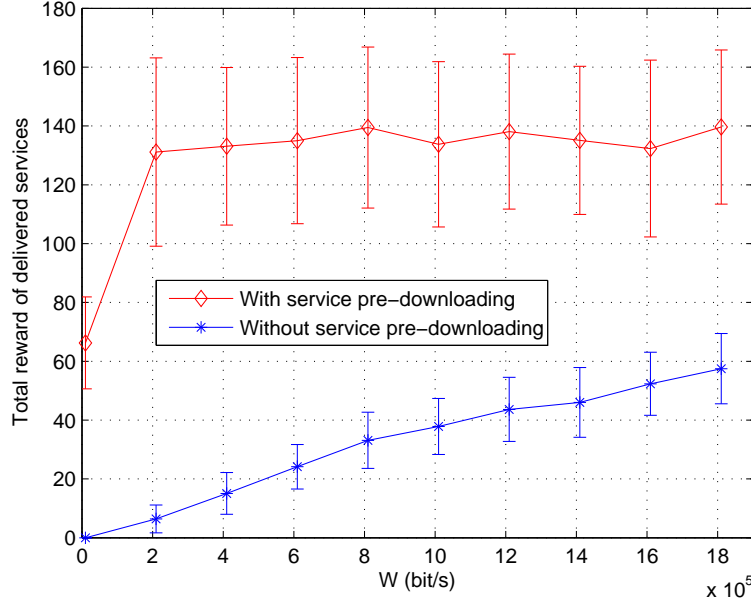
Figure 3.7: The total reward with and without service pre-downloading ($\lambda = 0.02$ service/s).

the resource allocation performance. As demonstrated in Fig. 3.8, the number of pre-downloaded blocks increases as β increases. However, the increment decreases for a large β because of a saturated throughput of the bottleneck link. Also, the number of pre-downloaded blocks increases with λ. From Fig. 3.9, we can see that, as β increases, the total reward first increases and then decreases. When β is small, more services can be pre-downloaded at each infostation while the number of blocks pre-downloaded for each service is small. The highest total reward is achieved at $\beta = 0.6$ and $\beta = 1.4$ for $\alpha = 0.05$ service/s and $\alpha = 0.01$ service/s, respectively. This observation indicates that, for a lower service arrival rate, more blocks should be pre-downloaded for each service, and vice versa. However, further investigation is needed to determine the optimal value of β and to strike a balance between the overhead of service pre-downloading and the total reward of delivered services.
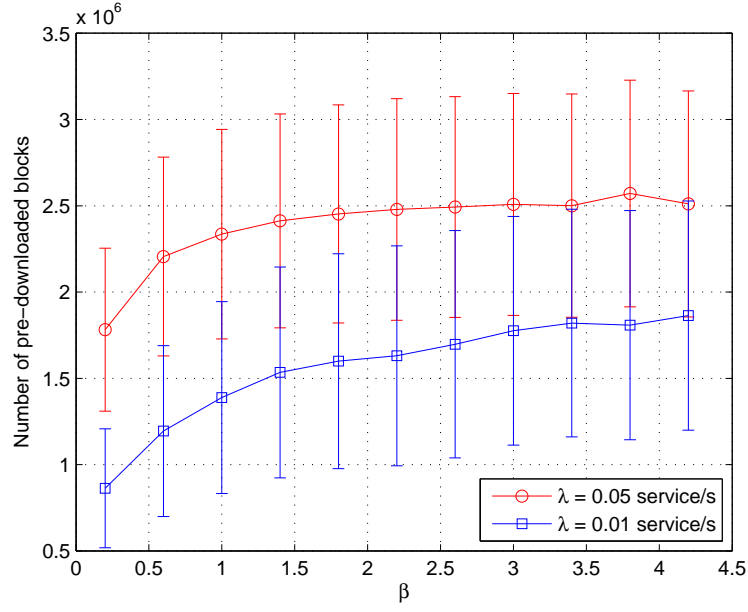
Figure 3.8: Number of pre-downloaded blocks versus redundant factor ($W = 10^4$ bit/s).
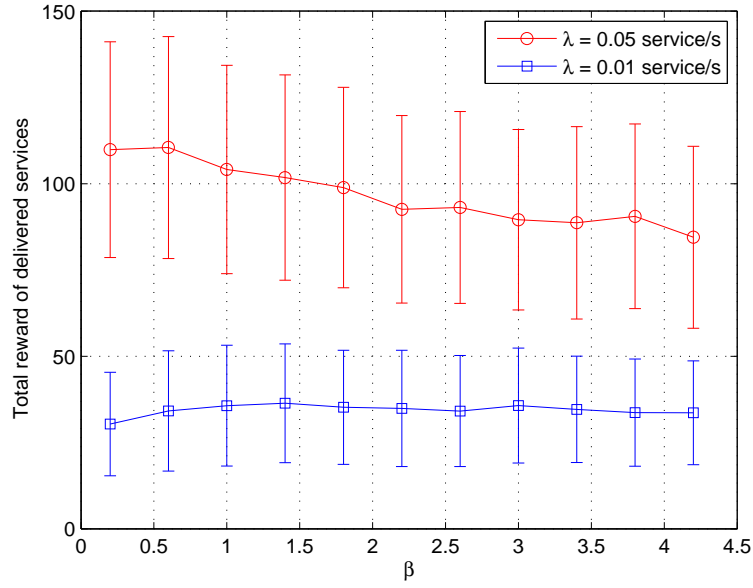
Figure 3.9: Total reward of delivered services versus redundant factor ($W = 10^4$ bit/s).

3.7   Summary

In this chapter, we present an optimal resource allocation problem for on-demand data delivery to high-speed trains in a cellular/infostation integrated network. The problem is transformed into a single-machine preemptive scheduling problem with integer request times, processing times, and deadlines. An online resource allocation algorithm with the Smith ratio and exponential capacity based utility functions is proposed. The performance bound of the online algorithm is characterized based on the theory of sequencing and scheduling with respect to the single-machine preemptive scheduling problem. Further, a service pre-downloading algorithm is presented to achieve efficient resource allocation when the link from the backbone network to an infostation is a bottleneck. It is demonstrated that the proposed resource allocation algorithm can improve the total reward of delivered services over the existing approaches such as FIFO, EDF, and RAPID, and that the service pre-downloading algorithm can significantly improve the efficiency of resource allocation when the bandwidth of the link to the infostation is a limiting factor. By tuning the redundant factor, different tradeoff can be achieved between the overhead of service pre-downloading (in terms of the number of pre-downloaded blocks) and total reward of delivered services.

Part II: Resource Management in Smart Grid

Chapter 4

Optimal Energy Delivery via V2G Systems

As discussed in Chapter 1, although the energy store-carry-and-deliver mechanism in a V2G system is analogous to the packet store-carry-and-forward routing concept in a DTN which can exploit node mobility statistics, the unidirectional energy delivery and simplified battery model in a DTN energy management [75, 76, 77] are not suitable for the battery storage management in a V2G system. In this chapter, we develop an optimal energy delivery scheme for PHEV in V2G system by jointly considering bi-directional energy flow, vehicle mobility pattern, realistic battery model, and TOU electricity price.

4.1 Literature Review

Daily energy cost minimization of vehicle owners under TOU electricity pricing is one of the main thrusts of the load shaving applications in V2G systems [13]. TOU is one category of time-based electricity pricing where the price is predetermined (typically on

73

a half-yearly basis) and can be utilized by the customers. An example is shown Fig. 1.2 for the Ontario electricity TOU price established since May 2011 [78]. Smart meters are installed to automatically record energy demand on an hourly basis to implement the TOU pricing. Currently, the TOU based recharging controller is already adopted by plug-in hybrid electric vehicles (PHEVs) such as Chevrolet Volt [79]. For developing V2G systems, the electricity pricing and energy demand information is automatically transmitted to a vehicle controller via wireline/wireless communications to facilitate the decision on bi-directional energy delivery [80].

The energy cost minimization problems of V2G systems are addressed in [35, 36]. The proposed schemes are tailored for frequency regulation applications with stationary vehicles. Taking account of stochastic energy demand information, the energy cost minimization problem is investigated for data centers with uninterrupted power supply (UPS) units [37]. In order to reduce the computational complexity for large-scale data center applications, a Lyapunov optimization technique is used by assuming i.i.d. demand to provide an average performance guarantee. Similarly, an online algorithm can be designed based on the i.i.d. demand assumption with worst-case performance guarantee [38]. However, for a V2G system where the vehicle mobility in daily commute is highly non-stationary, the i.i.d. assumption on demand statistics is no longer valid. The economic issues of using PHEV battery packs for grid storage are discussed in [13] which targets at household energy saving when the vehicle is parked at home, without taking account of daily commute.

4.2   System Model

An illustration of the system model is given in Fig. 4.1. The PHEV controller manages battery recharging/discharging when the PHEV is connected to the power grid, and
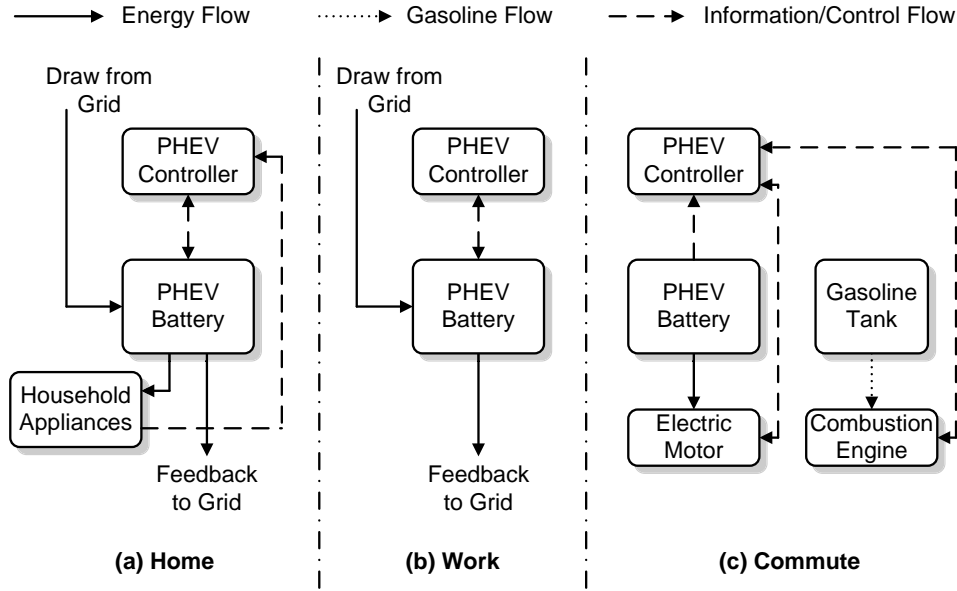
Figure 4.1: An illustration of the system model.

operates the electric motor and combustion engine when the PHEV is commuting. The battery status and commute energy demand can be directly monitored by the PHEV controller. Based on the communication functionality of the V2G system, the information of electricity price, PHEV mobility status, and household energy demand is acquired by the PHEV controller via wireline/wireless links. We consider a time slotted system. Time is partitioned into periods with equal duration T_P. Within each period, the mobility status of the PHEV stays unchange and the price of electricity remains constant.

4.2.1   PHEV Mobility and Energy Demand

The PHEV mobility is modeled as a Markov chain [81]. Without loss of generality, we consider three states of the PHEV mobility, i.e., home ($\mathcal{H}$), work ($\mathcal{W}$), and commute ($\mathcal{C}$). An extension is straightforward to include more locations by increasing the state space. Taking account of the non-stationary PHEV mobility, the state transition probabilities

are time-dependent. Given period n ($n = 0, 1, 2, \cdots$) and the current state s_n, the probability for the state to be s_{n+1} in period $n+1$ is $P_n(s_{n+1}|s_n)$ ($s_n, s_{n+1} \in \{\mathcal{H}, \mathcal{W}, \mathcal{C}\}$), where period 0 corresponds to the first period of a day.

Fig. 4.1 shows the grid connections of the PHEV for the three states. The PHEV battery can be used by household appliances and the V2G system [13]. When $s_n = \mathcal{H}$ or $\mathcal{W}$, energy can be either drawn from or fed back to the grid. However, the household appliances can use the energy in the battery only when $s_n = \mathcal{H}$. Let random variable ξ_n denote the household energy demand in period n based on the smart meter readings. When $s_n = \mathcal{C}$, the energy in the battery is used to drive the electric motor. Let random variable ζ_n denote the transport demand in period n given $s_n = \mathcal{C}$.

4.2.2 Electricity Pricing

TOU electricity pricing is considered for the V2G system [13]. In period n, the cost of drawing z units of energy from the grid is given by $c_n^g(z) = r_n z$, where r_n is the TOU price. The net metering arrangement is considered for the pricing of energy feedback to the grid. Rather than paying cash, the net meter spins backward as the excess energy is fed into the grid [82]. As a result, the same TOU price can be achieved for buying and selling energy[1], while selling energy can be considered the same as reducing the energy drawn from the grid by the neighborhood (when $s_n = \mathcal{H}$) or workplace appliances (when $s_n = \mathcal{W}$) [13]. We do not consider the spatial difference in electricity price since most daily commute is over a relatively short distance. For instance, 75% of Americans commute 65 km or less round-trip [79]. However, an extension is straightforward by considering the specific locations of home and work.

---

[1]Specifically, in September 2009, the Delaware governor has signed a bill for V2G system which requires electric utilities to compensate for the energy feedback to the grid at the same price as it is drawn from the grid [80].

If battery is depleted when $s_n = \mathcal{C}$, gasoline is used to drive the combustion engine and thus the PHEV[2]. The average cost of using gasoline to satisfy z units of energy demand in period n is $c_n^m(z) = r_n' z$. Since the gasoline price fluctuates at a much slower rate than the electricity price, constant approximation is typically used, i.e., $r_n' = r'$ [79].

4.2.3   Battery Model

Consider a realistic battery model which includes energy and value loss in recharging/discharging, limited battery capacity, limited recharging/discharging rate, and self-discharge effect [13, 37, 38, 83]. For each recharge and discharge of the battery, a certain amount of energy is lost because of the battery conversion loss. Therefore, we use a virtual capacity of the battery such that all stored energy can be used. Specifically, when z units of energy is used to recharge the battery, the energy that can be fed back to the grid or used by the household appliances is ηz $(0 < \eta < 1)$, where η is the round-trip efficiency which merges the energy loss in both recharging and discharging [38]. Moreover, the lifetime of a battery is shortened for each recharging/discharging cycle since the capacity of the battery slowly deteriorates following the depth-of-discharge (DoD). As the deterioration is almost imperceptible on a daily basis [83], the capacity of the battery (denoted by $x_{\max}$) is approximately unchanged for the time frame that we consider. However, the loss of the battery value is modeled as a cost which is proportional to the recharged (or discharged) energy with a factor $\tilde{r}$ [13]. As a result, the cost to increase the energy level of the battery by z $(z > 0)$ in period n $(n = 0, 1, 2, \cdots)$ is given by

$$c_n^{rc}(z) = c_n^g\left(\frac{z}{\eta}\right) + \tilde{r}z = \left(\frac{r_n}{\eta} + \tilde{r}\right)z. \tag{4.1}$$

---

[2]For instance, either a series hybrid or a series-parallel hybrid operation mode can be used by Chevrolet Volt based on the vehicle speed [79].

In order to prolong the battery lifetime, the energy level of the battery should not drop below $x_{\min}$ according to certain state-of-charge (SOC) [35]. Since virtual capacity is used in this work, we consider $x_{\min} = 0$ for simplicity. We assume $r' \geq \left(\frac{r_n}{\eta} + \tilde{r} \right)$ for the PHEVs. That is, the cost of using combustion engine is higher than using the electric motor, taking account of all cost in the recharging/discharging process, which is one of the key features of PHEVs [79].

Within each period, the battery can be either recharged or discharged, but not both [37]. Because of a limited recharging/discharging rate, the maximum energy that can be recharged into and discharged from the battery in a period is given by $u^{rc}_{\max}$ and $u^{dc}_{\max}$, respectively. Because of the self-discharge effect, the energy stored in the battery decreases by a percentage, β $(0 < \beta < 1)$, for each period. Specifically, suppose the remaining energy in the battery at the end of a period is x, the maximum amount of energy that can be used in the next period is βx.

4.3 Problem Formulation

Consider a daily energy cost minimization problem. Each day consists of $N + 1$ periods, i.e., $n \in \{0, 1, \cdots, N\}$. The duration of period $n \in \{0, 1, \cdots, N - 1\}$ is T. Since the PHEV mobility is negligible during the midnight off-peak period, we define period N as an aggregate period to reduce the computational complexity. For instance, if $\{0, 1, \cdots, N-1\}$ corresponds to the periods between 6:00am and 10:00pm, then period N aggregates all night periods between 10:00pm and next 6:00am. The analytical method of stochastic inventory theory [84, 85, 86] is used. For a V2G system considered in this work, we extend the theory by incorporating the bi-directional energy flow, PHEV mobility pattern, and realistic battery model.

Denote the energy level of the battery at the beginning of period n $(n \in \{0, 1, \cdots, N\})$

as x_n, where x_0 is the initial energy level. The decision variable is given by $U = (u_0, u_1, \cdots, u_{N-1})$, where u_n denotes the energy level of the battery at the end of period n. The decision of u_n is made at the beginning of period n given that the PHEV is connected to the grid, i.e., $s_n = \mathcal{H}$ or $\mathcal{W}$. Since recharge and discharge cannot be performed simultaneously, we have $u_n > x_n$ and $u_n < x_n$ if the battery is recharged and discharged, respectively, while $u_n = x_n$ if the battery is not used (or idle) in period n. Taking account of the limited battery capacity and recharging/discharging rate, we have

$$u_n \in \left[\max\{0, x_n - u_{\max}^{dc}\}, \min\{x_{\max}, x_n + u_{\max}^{rc}\}\right]. \tag{4.2}$$

Denote the energy cost in period k ($k \in \{0, 1, \cdots, N-1\}$) as $C_k^{s_k}(x_k, u_k)$ which depends on the system states (s_k and x_k) and the decision variable u_k. When $s_k = \mathcal{H}$, we have

$$C_k^{\mathcal{H}}(x_k, u_k) = \left(c_k^g(\xi_k) + c_k^{rc}(u_k - x_k)\right) I_{u_k > x_k} + c_k^g(\xi_k) I_{u_k = x_k} - c_k^g(x_k - u_k - \xi_k) I_{u_k < x_k}$$

$$= r_k \xi_k + H_k(x_k, u_k) \tag{4.3}$$

where I_A is an indication function which equals 1 if A is true and 0 otherwise, while $H_k(x, u)$ is defined as

$$H_k(x, u) = \left(\frac{r_k}{\eta} + \tilde{r}\right)(u - x)I_{u > x} + r_k(u - x)I_{u \leq x}. \tag{4.4}$$

Note that for a recharging or idle period with $u_k \geq x_k$, all household demand resorts to drawing energy from the grid at a cost $c_k^g(\xi_k)$ since the battery cannot be discharged at the same time. For a discharging period with $u_k < x_k$, if $x_k - u_k < \xi_k$, the unsatisfied demand resorts to drawing energy from the grid, while if $x_k - u_k > \xi_k$, the energy unused by the demand is fed back to the grid with a negative cost representing the revenue. Since the same price is used for buying and selling energy, the benefit of selling energy back to the grid is the same as compensating for the household demand. Therefore, the

cost of household demand $(r_k \xi_k)$ can be considered as irrelevant to the decision u_k, as shown in (4.3). When $s_k = \mathcal{W}$, we have

$$C_k^{\mathcal{W}}(x_k, u_k) = c_k^{rc}(u_k - x_k)I_{u_k > x_k} - c_k^g(x_k - u_k)I_{u_k \leq x_k} = H_k(x_k, u_k) \qquad (4.5)$$

where the only difference from (4.3) is that the household demand is not considered since the PHEV is away from the home. When $s_k = \mathcal{C}$, we have

$$C_k^{\mathcal{C}}(x_k, u_k) = c_k^m \left((\zeta_k - x_k)^+ \right) = r'(\zeta_k - x_k)^+ \qquad (4.6)$$

where $(x)^+$ equals x if $x > 0$ and 0 otherwise, while $(\zeta_k - x_k)^+$ represents the energy deficit in commute which needs to be compensated by using gasoline. In (4.6), there is no decision on buying or selling of energy since the PHEV is not connected to the grid.

For period N, we consider that the PHEV battery should be fully recharged during the off-peak hours overnight [13], based on the assumption that all the energy can be used or sold during the daytime. Otherwise, a battery with a smaller capacity and lower cost should be equipped by the PHEV. Therefore, the end-of-day cost function $(C_N(x))$ is proportional to the energy to be recharged according to the off-peak price r_N, and is given by $C_N(x) = \left(\frac{r_N}{\eta} + \tilde{r} \right) (x_{\max} - x)$. For simplicity, we neglect the cost to compensate for the self-discharge effect during period N for the off-peak hours.

The daily energy cost minimization problem is defined as

$$(\mathbf{P1}) \quad \min_{U \in \mathscr{U}} C_{0, s_0, x_0}(U) \qquad (4.7)$$

where $\mathscr{U}$ represents the class of all admissible decisions satisfying (4.2), while $C_{n, s_n, x_n}(U)$ is the expected energy cost during periods $\{n, n+1, \cdots, N\}$, and is given by

$$C_{n, s_n, x_n}(U) = E\left[\sum_{k=n}^{N-1} C_k^{s_k}(x_k, u_k) \right] + C_N(x_N). \qquad (4.8)$$

In (4.8), the expectation is taken with respect to the random variables ξ_k and ζ_k in (4.3) and (4.6), respectively. Taking account of the self-discharge effect, the energy level of period k ($k \in \{0, 1, \cdots, N-1\}$) evolves as

$$
x_{k+1} = \begin{cases} \beta u_k, & \text{if } s_k = \mathcal{H} \text{ or } \mathcal{W} \\ \beta(x_k - \zeta_k)^+, & \text{otherwise} \end{cases} \tag{4.9}
$$

where $(x_k - \zeta_k)^+$ denotes the remaining energy in the battery after the commute in period k. It is worth mentioning that problem P1 can be directly extended for weekly, monthly, and seasonal energy cost minimization based on the time frame that the PHEV mobility and energy demand statistics are investigated.

4.4 The Optimal Energy Delivery Policy

In this section, we first transform the original problem formulation P1 into a dynamic programming formulation and show the existence of an optimal Markov policy. In order to reduce the computational complexity, we further investigate the problem and prove the optimality of a state-dependent (S, S') policy, where S and S' are independent of the current energy amount x in the battery.

4.4.1 Existence of Optimal Markov Policy

Suppose $s_n = s$ and $x_n = x$, we define the value function within periods $\{n, n+1, \cdots, N\}$ as $V_n(s, x) = \min_{U \in \mathscr{U}} C_{n,s,x}(U)$. For $n \in \{0, 1, \cdots, N-1\}$, the dynamic programming equation of the value function is given by

$$V_n(s,x) = \begin{cases} r_n\bar{\xi}_n + \min_u\{H_n(x,u) + E[V_{n+1}(s_{n+1},\beta u)|s_n = \mathcal{H}]\}, & \text{if } s = \mathcal{H} \\ \min_u\{H_n(x,u) + E[V_{n+1}(s_{n+1},\beta u)|s_n = \mathcal{W}]\}, & \text{if } s = \mathcal{W} \\ E[V_{n+1}(s_{n+1},\beta(x-\zeta_n)^+)|s_n = \mathcal{C}] + r'E[(\zeta_n - x)^+], & \text{otherwise} \end{cases} \quad (4.10)$$

where the values of u are taken from a set as defined in (4.2), while $\bar{\xi}_k$ represents the expectation of ξ_k. For $n = N$, we have

$$V_N(s,x) = C_N(x). \tag{4.11}$$

A policy is a Markov policy if it depends only on the current state (n, s_n, x_n) and not on the past states (k, s_k, x_k) $(k \in \{0, 1, \cdots, n-1\})$. The following theorem shows the existence of an optimal Markov policy for problem P1. The proof is omitted here since it is similar to the inventory control problem [84].

Theorem 2. *There exists a function $u_n^*(s,x) : \mathbb{I}\times\mathbb{I}\times\mathbb{R} \to \mathbb{R}$, which provides the minimum of (4.10) for any x and $s = \mathcal{H}$ or $\mathcal{W}$. Moreover, the decision $U^* = (u_0^*, u_1^*, \cdots, u_{N-1}^*)$ is optimal for the problem P1, where $u_n^* = u_n^*(s_n, x_n^*)$ and x_{n+1}^* evolves according to (4.9) with respect to u_n^* and x_n^*.*

4.4.2 Optimality of State-Dependent (S, S') Policy

Based on Theorem 2, the optimal Markov policy exists. However, the computational complexity for the optimal policy is prohibitive even for a small N since the function $u_n^*(s,x)$ should be optimized for each combination of s and x [87]. Therefore, we further investigate the properties of the value functions in this subsection, and show that a state-dependent (S, S') policy is optimal. The proofs of lemmas, theorems, and propositions are given in Appendix B.

Definition 1. *Given $S \leq S'$ and the current energy level x, an (S, S') policy is defined as*

$$u^*(x) = \begin{cases} x + u^{rc}_{\max}, & \text{if } x < S - u^{rc}_{\max} \\ S, & \text{if } S - u^{rc}_{\max} \leq x < S \\ x, & \text{if } S \leq x \leq S' \\ S', & \text{if } S' < x < S' + u^{dc}_{\max} \\ x - u^{dc}_{\max}, & \text{otherwise.} \end{cases} \tag{4.12}$$

Note that the (S, S') policy is essentially a double-threshold policy by incorporating the limited recharging/discharging rate. That is, when the energy level is below S (above S'), the battery is recharged (discharged) as much as possible up to S (down to S'). When the energy level is between S and S', the battery is kept in an idle state.

The optimality of the state-dependent (S, S') policy can be established based on the convexity of the value function. We first investigate $H_n(x, u)$ and have the following lemma.

Lemma 4. *Function $H_n(x, u)$ is convex with respect to $u \in [0, x_{\max}]$ for any x.*

Consider a convex function $q(u)$ ($u \in [0, x_{\max}]$) with minimum value $q^* = \min_{u \in [0, x_{\max}]}\{q(u)\}$. Since $\arg\min_{u \in [0, x_{\max}]}\{q(u)\}$ is a convex set, we define its boundary points as

$$S = \min\{u \in [0, x_{\max}] | q(u) = q^*\} \tag{4.13}$$

$$S' = \max\{u \in [0, x_{\max}] | q(u) = q^*\}. \tag{4.14}$$

Then we have the following lemma:

Lemma 5. *If $q(u)$ is convex with respect to $u \in [0, x_{\max}]$, then the minimum of $q(u)$ for any $x \in [0, x_{\max}]$ and $u \in \left[\max\{0, x - u^{dc}_{\max}\}, \min\{x_{\max}, x + u^{rc}_{\max}\}\right]$ is achieved by choosing u according to the (S, S') policy, where S and S' are given by (4.13) and (4.14), respectively.*

Lemma 5 indicates that, with limited recharging/discharging rate, the optimal value of a convex function is achieved by the (S, S') policy. After applying (S, S') policy to a convex function, we have the following lemma:

Lemma 6. *For a convex function $q(u)$ $(u \in [0, x_{\max}])$, define $Q(x)$ $(x \in [0, x_{\max}])$ as*

$$Q(x) = q(u^*(x)) = \begin{cases} q(x + u^{rc}_{\max}), & \text{if } x < S - u^{rc}_{\max} \\ q^*, & \text{if } S - u^{rc}_{\max} \leq x < S' + u^{dc}_{\max} \\ q(x - u^{dc}_{\max}), & \text{otherwise} \end{cases} \quad (4.15)$$

where $u^*(x)$ is given by (4.12), while S and S' are given by (4.13) and (4.14), respectively. Then $Q(x)$ is convex.

Lemma 6 indicates that, by applying the (S, S') policy to a convex function $q(u)$ for any $x \in [0, x_{\max}]$ and $u \in \left[\max\{0, x - u^{dc}_{\max}\}, \min\{x_{\max}, x + u^{rc}_{\max}\}\right]$, the resulting function is still convex with respect to x.

Then we investigate the properties of the value functions and have the following lemma:

Lemma 7. *For any $\epsilon > 0$, and $x, x + \epsilon \in [0, x_{\max}]$, we have $V_n(s, x + \epsilon) \geq V_n(s, x) - r'\epsilon$ for $n \in \{0, 1, \cdots, N\}$ and $s \in \{\mathcal{H}, \mathcal{W}, \mathcal{C}\}$.*

Based on Lemmas 4-7, we have the following Theorem, which is the main result for the optimality of a state-dependant (S, S') policy. For presentation clarity, we first denote the state-dependent S and S' as functions of x by $S_n(s, x)$ and $S'_n(s, x)$, respectively. In the following subsection, we will show that $S_n(s, x)$ and $S'_n(s, x)$ are independent of x.

Theorem 3. *Given state s $(s = \mathcal{H}$ or $\mathcal{W})$ in period n, a state-dependant (S, S') policy is optimal. In other words, the optimal policy $u^*_n(s, x)$ is given by (4.12) with $S_n(s, x)$ and*

$S'_n(s, x)$ given by (4.13) and (4.14), respectively, based on the following convex function with respect to u:

$$q_n(s, x, u) = H_n(x, u) + E\left[V_{n+1}(s_{n+1}, \beta u)|s_n = s\right]. \tag{4.16}$$

4.4.3 Characterizing S and S'

Note that for the (S, S') policy defined by Theorem 3, the S and S' values depend on the energy level x, which makes the calculation complicated. In this subsection, we analyze $q_n(s, x, u)$ and show that S and S' are constant with respect to x. Based on (4.16), $q_n(s, x, u)$ can be rewritten as

$$q_n(s, x, u) = \left[H_n^r(s, u) - \left(\frac{r_n}{\eta} + \tilde{r}\right)x\right]I_{u>x} + \left[H_n^d(s, u) - r_n x\right]I_{u \le x} \tag{4.17}$$

where

$$H_n^r(s, u) = \left(\frac{r_n}{\eta} + \tilde{r}\right)u + E\left[V_{n+1}(s_{n+1}, \beta u)|s_n = s\right] \tag{4.18}$$

$$H_n^d(s, u) = r_n u + E\left[V_{n+1}(s_{n+1}, \beta u)|s_n = s\right]. \tag{4.19}$$

Obviously, $H_n^r(s, u)$ and $H_n^d(s, u)$ are convex with respect to u. Denote the minimum of $H_n^r(s, u)$ with respect to u as

$$H_n^{r*}(s) = \min_{u \in [0, x_{\max}]}\{H_n^r(s, u)\}. \tag{4.20}$$

Since $\arg\min_{u \in [0, x_{\max}]}\{H_n^r(s, u)\}$ is a convex set, we define the minimum and maximum values of u to achieve $H_n^{r*}(s)$ as

$$u_n^{r1}(s) = \min\{u \in [0, x_{\max}]|H_n^r(s, u) = H_n^{r*}(s)\} \tag{4.21}$$

$$u_n^{r2}(s) = \max\{u \in [0, x_{\max}]|H_n^r(s, u) = H_n^{r*}(s)\}. \tag{4.22}$$

Similarly, we can define $u_n^{d1}(s)$ and $u_n^{d2}(s)$ for $H_n^d(s, u)$. Then we have the following proposition:

Proposition 1. *For sets* $[u_n^{r1}(s), u_n^{r2}(s)]$ *and* $[u_n^{d1}(s), u_n^{d2}(s)]$, *we have* $u_n^{r2}(s) \leq u_n^{d1}(s)$.

Proposition 1 implies that the overlapping between the two sets $[u_n^{r1}(s), u_n^{r2}(s)]$ and $[u_n^{d1}(s), u_n^{d2}(s)]$ is at most one point. Since $q_n(s, x, u)$ is convex with respect to u, any local minimum of $q_n(s, x, u)$ is also global minimum [89]. By definition (4.17), $H_n^r(s, u)$ takes value on $u > x$ while $H_n^d(s, u)$ takes value on $u \leq x$. Therefore, the minimum of $q_n(s, x, u)$ can only be achieved at the minimum points of $H_n^r(s, u)$ (within $[u_n^{r1}(s), u_n^{r2}(s)]$), the minimum points of $H_n^d(s, u)$ (within $[u_n^{d1}(s), u_n^{d2}(s)]$), or the boundary point x. Based on the value of x, $(S_n(s, x), S_n'(s, x))$ is given by

$$(S_n(s, x), S_n'(s, x)) = \begin{cases} (u_n^{r1}(s), u_n^{r2}(s)), & \text{if } x < u_n^{r1}(s) \\ (x, u_n^{r2}(s)), & \text{if } u_n^{r1}(s) \leq x < u_n^{r2}(s) \\ (x, x), & \text{if } u_n^{r2}(s) \leq x \leq u_n^{d1}(s) \\ (u_n^{d1}(s), x), & \text{if } u_n^{d1}(s) < x \leq u_n^{d2}(s) \\ (u_n^{d1}(s), u_n^{d2}(s)), & \text{otherwise.} \end{cases} \quad (4.23)$$

By jointly considering (4.12) and (4.23), we have

$$u_n^*(s, x) = \begin{cases} x + u_{\max}^{rc}, & \text{if } x < u_n^{r1}(s) - u_{\max}^{rc} \\ u_n^{r1}(s), & \text{if } u_n^{r1}(s) - u_{\max}^{rc} \leq x < u_n^{r1}(s) \\ x, & \text{if } u_n^{r1}(s) \leq x \leq u_n^{d2}(s) \\ u_n^{d2}(s), & \text{if } u_n^{d2}(s) < x < u_n^{d2}(s) + u_{\max}^{dc} \\ x - u_{\max}^{dc}, & \text{otherwise.} \end{cases} \quad (4.24)$$

Therefore, the optimal policy can be simply denoted as an $(S_n(s), S_n'(s))$ policy, where $S_n(s) = u_n^{r1}(s)$ and $S_n'(s) = u_n^{d2}(s)$. As a result, we need to calculate only two parameters for the optimal policy with respect to each state and each period (instate of a function $u_n^*(s, x)$ with respect to x), which significantly reduces the computational complexity for practical applications.

4.5   Approximation Algorithm

The calculation of the optimal policy requires the daily statistics of the PHEV mobility $(P_n(j|s))$, average household energy demand $(\bar{\xi}_n)$, and probability density function (PDF) of transport energy demand $(f_{\zeta_n}(y), y \geq 0)$, for $n \in \{0, 1, \cdots, N-1\}$ and $s, j \in \{\mathcal{H}, \mathcal{W}, \mathcal{C}\}$. However, since the statistics are not known a priori, we have to use the historic information to estimate the statistics. The rationale behind the approximation is that both commute pattern and electricity demand are periodic in nature on a daily basis. We consider an exponentially weighted moving average (EWMA) algorithm which is typically used for load estimation in smart grid [88]. The EWMA algorithm utilizes the historic observations over previous days and captures the long-term statistic change (e.g., from summer to winter) by a weighted average. To apply the EWMA algorithm, we quantize ζ_n into discrete values and estimate the probability mass function (PMF). Denote $\hat{P}_n(j|s)$, $\hat{\bar{\xi}}_n$, and $\hat{f}_{\zeta_n}(y)$ as the estimates of $P_n(j|s)$, $\bar{\xi}_n$, and $f_{\zeta_n}(y)$, respectively. Then we devise a modified backward iteration algorithm to calculate the parameters of the optimal policy [84]. Based on the analysis in Section 4.4, we summarize the steps of the backward iteration in Algorithm 3. Note that step 5 involves two convex optimization problems which are readily solved by sophisticated algorithms [89].

4.6   Numerical Results

The performance of our proposed scheme is evaluated by simulations. The simulation is based on the ONE simulator [90] version 1.4.1 with an additional implementation of the V2G components. The simulator uses sample parameters and data from a real scenario. Hourly household energy demand data during the month of June, 2011, obtained from volunteers of two different households (John and Terry) subscribed to the Waterloo North

---

Algorithm 3 Modified Backward Iteration Algorithm

Input: r_n $(n \in \{0, 1, \cdots, N\})$, $\tilde{r}$, r', η, β, $u_{\max}^{rc}$, $u_{\max}^{dc}$, $x_{\max}$, $\hat{P}_n(j|s)$, $\hat{\bar{\xi}}_n$, and $\hat{f}_{\zeta_n}(y)$
        $(n \in \{0, 1, \cdots, N-1\}$, $s, j \in \{\mathcal{H}, \mathcal{W}, \mathcal{C}\}$, and $y \geq 0)$;
Output: $S_n(s)$ and $S_n'(s)$ $(n \in \{0, 1, \cdots, N-1\}, s \in \{\mathcal{H}, \mathcal{W}\})$;
 1: Initialize: $V_N(s, x)$ based on (4.11);
 2: **for** $n = N - 1$ to 0 **do**
 3:    **for** $s = \mathcal{H}$ or $\mathcal{W}$ or $\mathcal{C}$ **do**
 4:      **if** $s = \mathcal{H}$ or $\mathcal{W}$ **then**
 5:         Calculate: $H_n^{r*}(s)$ and $H_n^{d*}(s)$ according to (4.20);
 6:         Calculate: $u_n^{r1}(s)$, $u_n^{r2}(s)$, $u_n^{d1}(s)$, and $u_n^{d2}(s)$ according to (4.21) and (4.22);
 7:      **end if**
 8:      Update: $V_n(s, x)$ according to (4.10);
 9:    **end for**
10: **end for**
11: **return** $S_n(s) = u_n^{r1}(s)$ and $S_n'(s) = u_n^{d2}(s)$ $(n \in \{0, 1, \cdots, N-1\}, s \in \{\mathcal{H}, \mathcal{W}\})$

Hydro, is used [34]. Fig. 1.1 shows the hourly electricity usage of John's household during June 20 (Monday) and June 24 (Friday). The TOU pricing of Waterloo North Hydro is in accordance with the Ontario electricity TOU price under the summer schedule, as shown in Fig. 1.2. Traces of vehicle mobility patterns of these individuals are generated using the ONE simulator based on the survey information which includes the locations of their homes, work places, points of interests, and commute patterns. For example, John usually leaves from home to work between 9:55am and 10:05am, works until 5:00pm. About 3 times a week, he goes to a grocery or a mall after work, and spends 30 to 60 minutes. Finally, he returns home and stays at home until the next morning. The trace is generated considering a map based mobility model where the vehicle follows main roads of the Waterloo Region as shown in Fig. 4.2. The energy cost during weekdays is considered since the TOU price is constant during weekends.

    The default battery parameters are given in Table 4.1, which is based on a lithium-ion battery [91]. The round-trip efficiency of lithium-ion battery is typically between 80% and 90% [92]. A medium value 85% is used as the default parameter of our simulations.
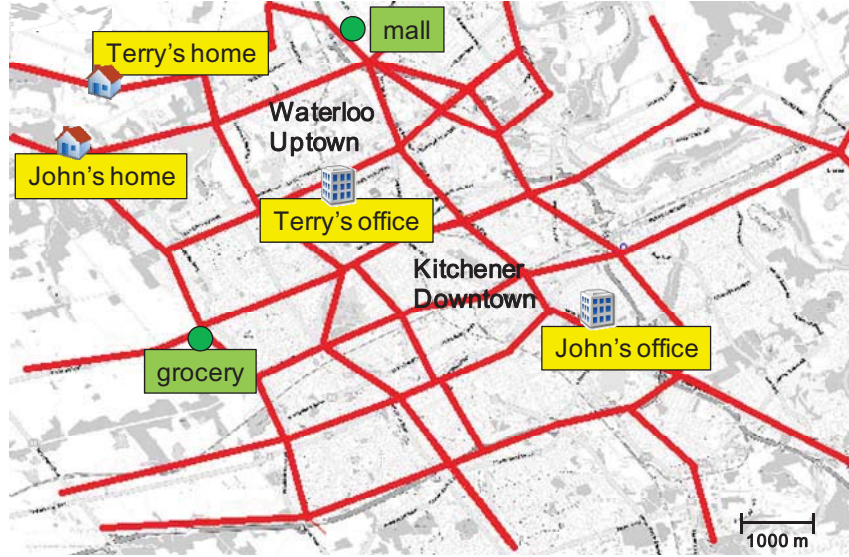
Figure 4.2: The topology of the main roads in Waterlo Region and the locations of homes, work places, and points of interests of John and Terry.

Table 4.1: Default battery parameters.

Parameter	Value
Round-trip efficiency (η)	85%
Self-discharging percentage (β)	99.993%
Battery value loss in recharging ($\tilde{r}$)	1.1 c / kWh
Equivalent gasoline cost (r')	67 c / kWh
Battery capacity ($x_{\max}$)	8 kWh

High efficiency (97%) of lithium-ion battery is also reported in literature [93]. We only use the value for comparison purpose since experimental data for PHEV applications is not available. The equivalent gasoline cost is based on the average gasoline price in Waterloo Region in June 2011 (130.0 c/L) and the eletricity/gasoline efficiency reported by Chevrolet Volt (0.125 kWh/km in all-electric mode and 6.4 L/100 km in gasoline-only mode) [79]. The battery value loss in recharging is calculated based on the statistics of

Chevrolet Volt with a 8000-dollar battery pack (rated at 16 kWh and about 10 kWh available for use) and a 10% capacity loss after 10 years of use with two full recharging/discharging cycles for daily commute. The recharging/discharging rate of individual PHEV is in accordance with level 2 (3.3 kW) infrastructures [94]. For performance optimization, we consider 16 hours of a day from 6:00am to 10:00pm with a period duration $T_P = 10$ minutes. The transport energy demand $\zeta_{i,n}$ is quantized by a 0.5 kWh interval.

4.6.1   Recharging/Discharging Pattern

In order to demonstrate how a PHEV battery is managed according to the optimal policy, we consider a specific day of Terry and John, and assume that the PHEV mobility and energy demand information is known a priori. Suppose John leaves home and work at 10:00am and 5:00pm, respectively, with a single-trip commute time 20 minutes and energy consumption 2 kWh. Terry leaves home and work at 8:00am and 5:00pm, respectively, with a single-trip commute time 10 minutes and energy consumption 1 kWh. For comparison purpose, we assume that the PHEV of Terry has a lower recharging/discharging rate (1.2 kW in accordance with level 1 infrastructures [94]) and a higher round-trip energy efficiency (97%).

The results are presented in Fig. 4.3 and Fig. 4.4 for John and Terry, respectively, where the lower bound of discharging region and the upper bound of idle region correspond to S', while the lower bound of idle region and the upper bound of recharging region correspond to S. The midnight off-peak periods (which only include a recharging region) are not shown. We can see that, the round-trip energy efficiency has a critical impact on the optimal policy. For Terry, since the round-trip energy efficiency is high (97% as compared with 85% of John's PHEV), energy is bought as much as possible during the mid-peak periods, and sold during the on-peak periods. On the contrary, John buys energy during the mid-peak periods only for commute use since no benefit can be
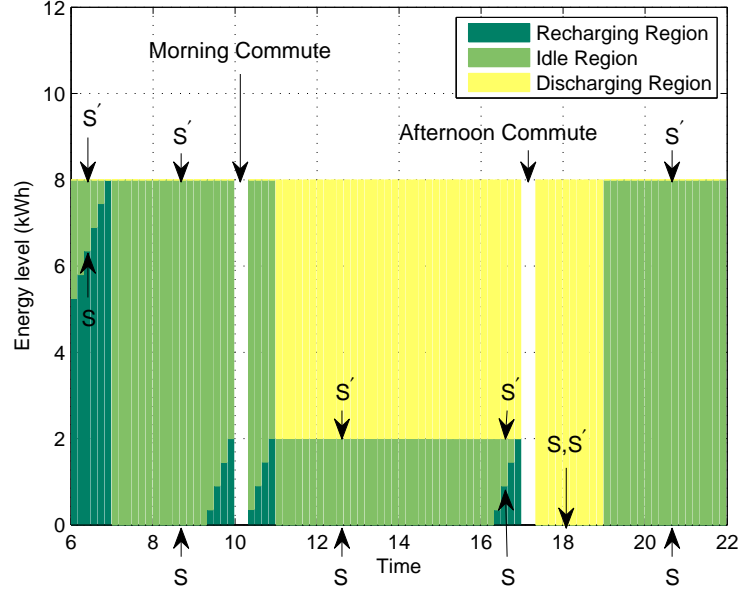
Figure 4.3: The values of S and S' at different times of a day (John).
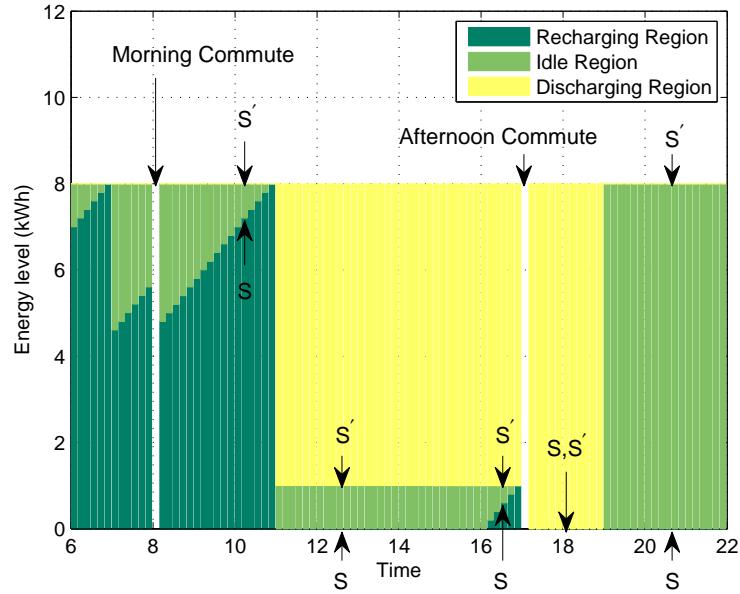
Figure 4.4: The values of S and S' at different times of a day (Terry).

gained by selling the "mid-peak energy" during the on-peak periods, taking account of the energy loss in recharging and discharging. For instance, Terry buys energy at 9:30am (which is a mid-peak hour) as much as possible by setting a large S, while John buys energy at the same time only for commute use with a small S. Moreover, due to the self-discharge effect, energy for selling or commute is bought as late as possible with the maximum recharging rate.

4.6.2 Performance Comparison

We evaluate the performance of the proposed scheme in comparison with three other schemes: i) W/O V2G – Without a V2G system, the energy drawn from the grid can only be used for daily commute, and the battery is fully recharged during the off-peak periods [80]; ii) SD – The energy store-and-deliver scheme utilizes commute statistics [13]. The PHEV battery is fully recharged during off-peak periods and a certain amount of energy is reserved for average daily commute demand. The remaining energy is used to compensate for the household demand during the on-peak and mid-peak periods when the PHEV is at home. The benefit of the SD scheme is the same as feeding energy back to the grid, but the amount of energy is bounded by the household demand; iii) OPT – As our proposed scheme uses estimated statistics, we also show the performance of a scheme with a priori knowledge of the PHEV mobility and energy demand information, which provides the best performance but cannot be realized in practical applications.

A comparison among different schemes is shown in Fig. 4.5 for daily energy cost over 20 days. Note that the first day is removed since no historic information is available. The trace of John is used as an example. With a constant cost of household demand every day, we only consider the cost of recharging PHEV battery and using combustion engine, and the benefit of feeding energy back to the grid (or equivalently, compensating for household demand). We can see that, the cost without V2G is the highest since the

92
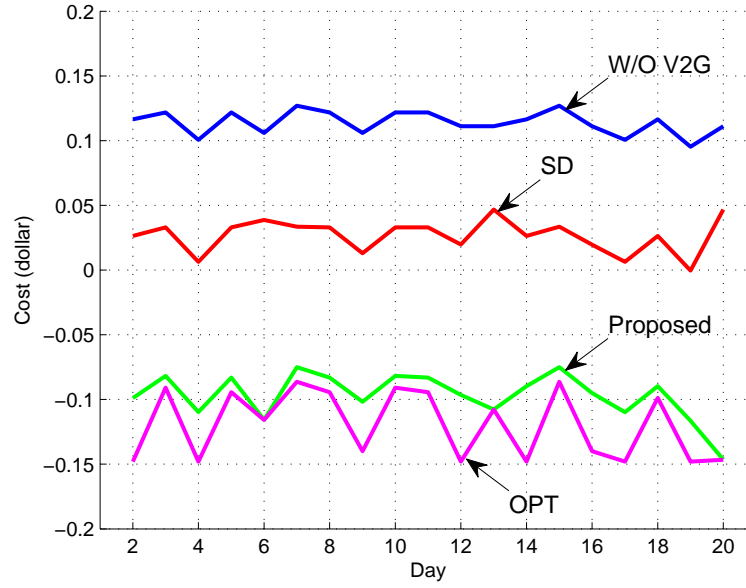
Figure 4.5: Daily energy cost.
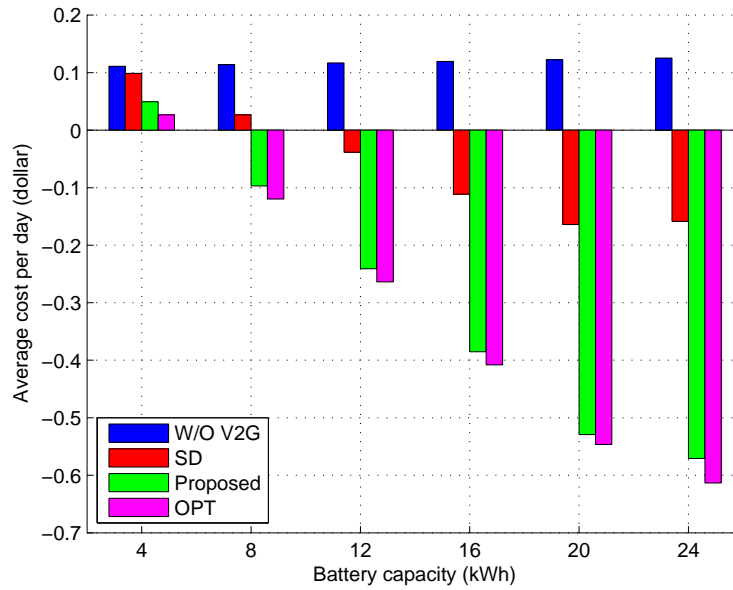
Figure 4.6: Average energy cost per day versus battery capacity.

energy in the PHEV battery cannot be used by the household demand or fed back to the grid. By compensating for the household demand during on-peak and mid-peak periods, the SD scheme can reduce the energy cost. But the reduction is inferior to that with our proposed scheme, since most on-peak periods are not considered for energy feedback when the PHEV is at work place. Our proposed scheme using estimated statistics achieves slightly higher cost than the scheme with a priori knowledge.

The average energy cost per day versus battery capacity is shown in Fig. 4.6. We can see that, the cost without a V2G scheme increases as the battery capacity increases since the self-discharge effect gradually decreases the level of the unused energy in battery. The cost achieved by the SD scheme decreases as the battery capacity increases since more battery energy can be used by household appliances. However, the decrement is saturated from 20 kWh because of the limited household demand. By further enlarging the battery capacity, the cost again increases because of the self-discharge effect, similar to that without a V2G system. For all battery capacities, the cost achieved by our proposed scheme is close to that of the scheme with a priori knowledge. As compared with the SD scheme, the cost reduction of our proposed scheme is more evident for a larger battery capacity.

4.7 Summary

In this chapter, the energy cost minimization problem under TOU electricity pricing is investigated for a PHEV with a realistic battery model. A state-dependent (S, S') policy is proved to be optimal. For practical applications, we proposed a modified backward iteration algorithm with an EWMA estimation of the statistics of PHEV mobility and energy demand. The performance of our proposed scheme is evaluated based on realistic commute and energy demand data and is compared with the existing schemes.

Chapter 5

Decentralized Economic Dispatch in Microgrids

In this chapter, we address the electric power and communication bandwidth management issues for decentralized economic dispatch in microgrids. We propose a heterogeneous wireless network architecture for microgrids. Each node is equipped with a short-range (e.g., WiFi or ZigBee) wireless communication device for information exchange in an ad hoc mode. Several nodes are further equipped with cellular communication devices and are referred to as dual-mode nodes for connectivity improvement. By activating the cellular communication devices, information exchange beyond the one-hop neighbors in the ad hoc network can be enabled such that the performance of decentralized economic dispatch can be improved. However, the monetary cost of using cellular communication devices is comparable to the incremental generation cost incurred by the error in multiagent coordination. For economic dispatch in microgrids which addresses the cost minimization issues, a tradeoff between the communication and power generation costs is obtained.

5.1 Literature Review

Both centralized and decentralized approaches can be used to achieve economic dispatch. Most existing centralized approaches assume that the estimates or statistics of power generation and loads acquired by a central controller are accurate [39, 40, 41]. Although the centralized economic dispatch has the advantage of high efficiency, it suffers from the problem of a single point of failure and high deployment cost in terms of a powerful central controller and a communication infrastructure (such as a fiber-optic network [15] to connect each DG unit or load to the central controller). On the other hand, the decentralized economic dispatch can avoid a single point of failure and fits the plug-and-play nature of DG units and loads in microgrids [95]. Since information exchange only needs to be established among neighboring nodes (corresponding to the DG units or loads), low-cost short-range wireless communication devices such as WiFi and ZigBee devices can be implemented to establish the network infrastructure [12]. In order to achieve the same efficiency in cost minimization as the centralized counterpart, the DG units should acquire the accurate power generation and load information in a decentralized manner [42].

Multiagent coordination is a promising solution for decentralized information acquisition and load restoration [96] in microgrids since the accuracy of information discovery is guaranteed based on the average consensus theory. Several MAC schemes are proposed to facilitate multiagent coordination in microgrids via wireless networks [97]. However, as the convergence speed decreases significantly as the network size increases, how to implement multiagent coordination to achieve economic dispatch in a small time scale is still an open issue. Although better network connectivity can improve the convergence speed of multiagent coordination according to the small-world phenomenon [98], simply increasing the transmission power of wireless devices is not helpful since the connectivity benefit is reduced by increased wireless transmission interference [99].

5.2   System Model

As shown in Fig. 5.1, we consider a microgrid built for a small residential community. Electric power is delivered from the DG units (e.g., the wind turbines and PV panels) to the loads (e.g., the residential houses) via the power grid infrastructure. The power generation and loads are balanced via economic dispatch every T_D (hour), where $T_D < 1$ for typical renewable energy source integration [16]. The information exchange for the economic dispatch is based on a heterogeneous wireless network infrastructure[1] and is completed at the beginning of each economic dispatch period with a short duration T ($T < T_D$) [17], as shown in Fig. 5.2(a). In the following, we consider one economic dispatch period as an example. Each DG unit or load is represented by a node in the microgrid. The set of all nodes in the microgrid is denoted as $\mathcal{V}$ and is indexed by $1, 2, \cdots, |\mathcal{V}|$.

5.2.1   Microgrid and Electricity Pricing

The microgrid is connected to the main grid (i.e., the utility grid) via a point of common coupling (PCC) [15]. The microgrid can operate either in a grid-connected mode or an islanded mode, by closing or opening the circuit breaker (CB) between the PCC and microgrid bus, respectively. Without loss of generality, we consider an islanded mode in this research with an opened CB. An example of the microgrid is shown in Fig. 5.1. There are three feeders in the microgrid. On feeder 1, there are two DG units (DG1 and DG2). On feeder 2, there are two loads (L1 and L2) and two DG units (DG3 and DG4). On feeder 3, there are two loads (L3 and L4) and three DG units (DG5, DG6, and DG7).

Suppose there are G types of DG units in the microgrid. For each node v ($v \in \mathcal{V}$),

---

[1]The power supply of the network infrastructure is considered to be independent of the microgrid since the supervisory control should be uninterruptible even when fault occurs in the power grid [96].

Figure 5.1: An illustration of the microgrid configuration with a heterogeneous wireless network infrastructure.

its type g ($g \in \{1, 2, \cdots, G\}$) power generation (in kW) is given by x_{gv}. Specifically, we have $x_{gv} > 0$ if node v is a DG unit and belongs to type g, and $x_{gv} = 0$ otherwise. Take wind turbine as an example, the value of x_{gv} is equal to the maximum output of the wind turbine given the wind speed during the economic dispatch period[2]. Similarly, let y_v denote the power demand (in kW) of each node with $y_v > 0$ if node v represents

---

[2]For simplicity, we consider all the DG units to be dispatchable based on an accurate generation forecast and/or certain energy storage devices. An extension is straightforward by considering the non-dispatchable DG units as negative loads.

Figure 5.2: Economic dispatch and multiagent coordination: (a) Period definition. (b) Single-stage multiagent coordination. (c) Hierarchical multiagent coordination.

a load and $y_v = 0$ otherwise. Note that we use the generalized definitions of x_{gv} and y_v for all nodes in $\mathcal{V}$ for notation clarity. Denote $\mathbf{x} = \{x_{gv} | g \in \{1, 2, \cdots, G\}, v \in \mathcal{V}\}$ and $\mathbf{y} = \{y_v | v \in \mathcal{V}\}$ as the sets of power generation and loads, respectively. The values of $\mathbf{x}$ and $\mathbf{y}$ are assumed to be constant within each economic dispatch period[3] and vary randomly among different periods.

In this work, we consider a linear generation cost/pricing model, similar to the one used by the feed-in tariff (FIT) program of Ontario Power Authority [100]. The cost of unit power generation of type g DG unit is denoted as c_g (in dollar/kWh). Without loss of generality, we consider ordered costs, i.e., $0 < c_1 \leq c_2 \leq \cdots \leq c_G$. For instance, the solar energy is more expensive than wind or hydro energy according to the FIT program. The economic dispatch in a microgrid aims at balancing the power generation and loads at a minimum cost. In this research, we neglect the line flow limit and power losses. Potential

---

[3]According to experimental results, there is typically a 3%-5% relative error for wind farm power estimation in a 10-minute interval [101].

extensions will be discussed in Chapter 6. However, because of the uncertainty in DG output and/or the error in information discovery, the power generation and loads may not be balanced perfectly. Specifically, if the power generation of DG units is not enough to supply the loads, the undelivered power should be purchased from alternative sources such as traditional thermal energy power generators at a cost of c_A (in dollar/kWh). On the other hand, the extra power in the microgrid is compensated by negative spinning reserves[4] at a cost of c_E (in dollar/kWh). The energy waste can be reduced based on distributed energy storage systems [15] and V2G systems [43], which is left for our future research. Generally, we have $c_A > c_G$ and $c_E \geq 0$. The set of all possible costs in economic dispatch is denoted as $\mathbf{c} = \{c_g | g \in \{1, 2, \cdots, G\}\} \cup \{c_A, c_E\}$ and is assumed to be constant for the time frame under consideration.

5.2.2   Heterogeneous Wireless Networks

Each node in $\mathcal{V}$ is equipped with a short-range wireless communication device, such as the access point (AP) of a WiFi or ZigBee based device. An extension to power line communications (PLC) is straightforward since the PLC channel is interference limited and the transmission range of PLC devices is limited in general [96][102]. Multi-channel wireless communication is supported. For instance, we have 23 wireless channels for IEEE 802.11a based WiFi devises and 16 wireless channels for IEEE 802.15.4 based ZigBee devices. Because of a limited wireless transmission range, each node can only communicate with (or cause interference to) its one-hop neighbors operating on the same channel. For instance, in Fig. 5.1, the node corresponding to DG5 can communicate with the nodes corresponding to L1, L4, DG4, and DG7, given that they operate on the same channel. Concurrent transmissions over the non-overlapping channels are considered interference

---

[4]If the service is purchased before real-time operation, an estimation of the maximum extra power is required.

free. We denote the network based on the short-range wireless communication devices as an ad hoc network and the set of neighbors of node v ($v \in \mathcal{V}$) as $\mathcal{N}_v$ ($\mathcal{N}_v \subseteq \mathcal{V} \setminus \{v\}$). The wireless devices have a constant transmission rate and a transmission range equal to the interference range. Specifically, a transmission of node v can interfere with another transmission to node n only if $n \in \mathcal{N}_v$, which results in an unsuccessful reception at node n. For the ad hoc network, there exists a (multi-hop) communication path between any pair of two nodes. In other words, the ad hoc network is strongly connected.

A subset $\mathcal{B}$ ($\mathcal{B} \subseteq \mathcal{V}$) of nodes are further equipped with cellular communication devices, such as the user equipments (UEs) in a universal mobile telecommunications system (UMTS) [103]. Since the base stations (BSs) of the cellular network are connected by the base station controllers (BSCs) and are further connected to a backbone network, the $\mathcal{B}$ nodes can communicate with each other even if they are not one-hop neighbors in the ad hoc network. For instance, in Fig. 5.1, DG1, DG7, L1, and L3 can communicate with each other. For simplicity, we neglect the delay of information exchange via a cellular network which can support services with stringent delay requirements [104]. The cost of sending a message from one node to another via the cellular network is c_M, which depends on the size of the data message.

5.3   Decentralized Economic Dispatch based on Multiagent Coordination

In this section, we first analyze the economic dispatch problem and show that solving the economic dispatch problem is equivalent to achieving average consensus in the microgrid. Then, we propose a decentralized economic dispatch approach where each node makes a local decision on power generation based on the average values of the cumulative gener-

ation of each type of DG units and the aggregated loads. The information required for decision making is discovered by each node via multiagent coordination with guaranteed convergence.

5.3.1 Economic Dispatch

The economic dispatch in a microgrid schedules the power generation (or output) of DG units optimally such that the electric loads are served at a minimum cost. Denote the actual power generation of a type g DG unit v as u_{gv}, where $0 \leq u_{gv} \leq x_{gv}$ since the generation of a DG unit can be curtailed based on economic dispatch. The total generation cost (in dollar/h) equals the cost of purchasing power from the DG units and alternative energy sources plus the cost of purchasing negative spinning reserves, given by

$$C_P(\mathbf{x}, \mathbf{y}, \mathbf{c}, \mathbf{u}) = \sum_{g \in \{1,2,\cdots,G\}} \sum_{v \in \mathcal{V}} c_g u_{gv} + c_A z_A + c_E z_E \tag{5.1}$$

where z_A and z_E denote the undelivered power which should be purchased from the alternative sources and the extra power, respectively. Denote $\mathbf{u} = \{u_{gv} | g \in \{1, 2, \cdots, G\}, v \in \mathcal{V}\}$ as a specific policy of economic dispatch. Based on the power balance (or demand-supply balance) equation [39], we have $z_A = \left(\sum_{v \in \mathcal{V}} y_v - \sum_{g \in \{1,2,\cdots,G\}} \sum_{v \in \mathcal{V}} u_{gv}\right)^+$ and $z_E = \left(\sum_{g \in \{1,2,\cdots,G\}} \sum_{v \in \mathcal{V}} u_{gv} - \sum_{v \in \mathcal{V}} y_v\right)^+$. Then, the optimal economic dispatch policy $\mathbf{u}^*$ is determined by problem P1 as

$$(\mathbf{P1}) \quad \min_{\mathbf{u}} \quad C_P(\mathbf{x}, \mathbf{y}, \mathbf{c}, \mathbf{u}) \tag{5.2}$$

$$\text{subject to} \quad 0 \leq u_{gv} \leq x_{gv}, \ g \in \{1, 2, \cdots, G\}, v \in \mathcal{V}. \tag{5.3}$$

Accordingly, we denote the minimum generation cost based on $\mathbf{u}^*$ as $C_P^*(\mathbf{x}, \mathbf{y}, \mathbf{c}) = C_P(\mathbf{x}, \mathbf{y}, \mathbf{c}, \mathbf{u}^*)$. It is worth mentioning that z_A and z_E are included in the generation cost definition (5.1) to facilitate the analysis of the impact of information discovery error in the following sections.

5.3.2 Optimal Economic Dispatch and Average Consensus

In general, problem P1 is a linear programming (LP) problem which can be solved by existing methods. However, in order to solve problem P1 in a decentralized manner, the values of all elements in $\mathbf{x}$ and $\mathbf{y}$ should be obtained by each node, which results in a high communication overhead. In this subsection, we derive a closed-form expression of the optimal economic dispatch policy based on the ordered generation costs. The information required by each node for decentralized decision making is reduced to the average values of the cumulative generation of each type of DG units and the aggregated loads.

We first have the following two lemmas with respect to the extra and undelivered power in a microgrid. The proofs of both lemmas are straightforward based on contradiction and are omitted here.

Lemma 8. *For an optimal economic dispatch policy* $\mathbf{u}^* = \{u_{gv}^*|g \in \{1, 2, \cdots, G\}, v \in \mathcal{V}\}$ *based on problem P1, there is no extra power in the microgrid, i.e.,* $z_E^* = 0$.

Lemma 9. *If* $\sum_{g \in \{1,2,\cdots,G\}} \sum_{v \in \mathcal{V}} x_{gv} > \sum_{v \in \mathcal{V}} y_v$, *there is no undelivered power, i.e.,* $z_A^* = 0$. *Taking account of Lemma 8, we have* $\sum_{g \in \{1,2,\cdots,G\}} \sum_{v \in \mathcal{V}} u_{gv}^* = \sum_{v \in \mathcal{V}} y_v$, *i.e., the optimal aggregated power generation of the G types of DG units and the aggregated loads are balanced in a microgrid.*

Denote the cumulative generation of the DG units and the aggregated loads as $\mathbf{X} = \{X_g | g \in \{1, 2, \cdots, G\}\}$ and $Y = \sum_{v \in \mathcal{V}} y_v$, respectively, where $X_g = \sum_{v \in \mathcal{V}} x_{gv}$ represents the cumulative generation of type g DG units. Define an economic dispatch policy as follows:

$$u_{gv}(\bar{\mathbf{X}}, \bar{Y}, \mathbf{c}) = \begin{cases} x_{gv}, & \text{if } \bar{Y} \geq \sum_{k \in \{1,2,\cdots,g\}} \bar{X}_k \\ 0, & \text{if } \bar{Y} \leq \sum_{k \in \{1,2,\cdots,g-1\}} \bar{X}_k \\ \frac{x_{gv}}{X_g} \left[\bar{Y} - \sum_{k \in \{1,2,\cdots,g-1\}} \bar{X}_k \right], & \text{elsewhere} \end{cases} \quad (5.4)$$

where $\bar{\mathbf{X}} = \{\bar{X}_g | g \in \{1, 2, \cdots, G\}\}$, $\bar{X}_g = X_g/|\mathcal{V}|$ and $\bar{Y} = Y/|\mathcal{V}|$ are the average values of cumulative generation and aggregated loads, respectively. For the third case in (5.4), the power generation of the DG units is proportional to their generation, also known as the proportional fairness. Then, we have the following theorem which is proved in Appendix B.

Theorem 4. *Given the average values of the cumulative generation $\bar{\mathbf{X}}$ and aggregated loads $\bar{Y}$, the decentralized economic dispatch policy in (5.4) is optimal for problem P1.*

Based on Theorem 4, the problem of decentralized economic dispatch is transformed into the discovery (by each node) of the the average values of the cumulative generation $(\bar{X}_g)$ of each type of DG units and aggregated loads $(\bar{Y})$. Intuitively, the results follow the power balance equation which is based on the summation of power generation and/or loads. In this work, we consider a multiagent coordination scheme since the convergence of information discovery can be guaranteed based on the average consensus theory.

5.3.3 Multiagent Coordination via Ad Hoc Network

In this subsection, we investigate the multiagent coordination via the ad hoc network and show the convergence of the information discovery process. Take the discovery of the average cumulative generation of type g DG units $(\bar{X}_g)$ as an example. The information update takes place in a discrete-time manner, where each round of update is referred to as an iteration. Suppose the iterations are completed at time steps t_k $(k \in \{0, 1, 2, \cdots\})$ with $t_0 = 0 < t_1 < t_2 < \cdots \leq T$. Denote the state value kept by node v $(v \in \mathcal{V})$ at time t_k as $\bar{X}_g(v, t_k)$. For the initial value, we have $\bar{X}_g(v, t_0) = x_{gv}$. For the kth iteration, node v $(v \in \mathcal{V})$ acquires the state values $\bar{X}_g(n, t_{k-1})$ $(n \in \mathcal{N}_v)$ kept by its neighboring nodes via ad hoc communication links. Then, the state value kept by node v is updated based

on a weighted average of the acquired values, given by

$$\bar{X}_g(v, t_k) = \sum_{n \in \mathcal{V}} \omega_{\mathcal{V}}^a(v, n) \bar{X}_g(n, t_{k-1}) \tag{5.5}$$

where $\omega_{\mathcal{V}}^a(v, n) \geq 0$ is the weight used by node v with respect to node n. Here, we study a symmetric version of the natural random walk [99] which is analytically tractable. The weight values are given by

$$\omega_{\mathcal{V}}^a(v, n) = \begin{cases} \frac{1}{2 \max\{|\mathcal{N}_v|, |\mathcal{N}_n|\}}, & \text{if } n \in \mathcal{N}_v \\ 1 - \sum_{j \in \mathcal{N}_v} \frac{1}{2 \max\{|\mathcal{N}_v|, |\mathcal{N}_j|\}}, & \text{if } n = v \\ 0, & \text{elsewhere.} \end{cases} \tag{5.6}$$

Based on (5.6), we have $\omega_{\mathcal{V}}^a(v, n) > 0$ if $n \in \mathcal{N}_v \cup \{v\}$ and $\omega_{\mathcal{V}}^a(v, n) = 0$ otherwise. The update in (5.5) is fully decentralized such that each node only needs the information from its direct neighbors. Denote the weight matrix of each iteration as $W_{\mathcal{V}}^a = [\omega_{\mathcal{V}}^a(v, n)]_{|\mathcal{V}| \times |\mathcal{V}|}$, we have

$$\bar{X}_{g,\mathcal{V}}(t_k) = W_{\mathcal{V}}^a \bar{X}_{g,\mathcal{V}}(t_{k-1}) \tag{5.7}$$

where $\bar{X}_{g,\mathcal{V}}(t_k) = (\bar{X}_g(1, t_k), \cdots, \bar{X}_g(|\mathcal{V}|, t_k))^\top$. The wireless links for each iteration may be scheduled sequentially to avoid interference since we may have $\mathcal{N}_v \cap \mathcal{N}_j \neq \emptyset$ for some $v, j \in \mathcal{V}$.

Define a directed graph associated with $W_{\mathcal{V}}^a$ such that the vertex set is $\mathcal{V}$ and there is an edge from vertex i to vertex j $(i, j \in \mathcal{V})$ if and only if $\omega_{\mathcal{V}}^a(i, j) > 0$. Since $W_{\mathcal{V}}^a$ is doubly stochastic and the directed graph associated with $W_{\mathcal{V}}^a$ is strongly connected (based on the assumption that the ad hoc network is strongly connected), the state value of each node converges to a constant [105][106], given by

$$\lim_{t \to \infty} \bar{X}_g(v, t) = \bar{X}_g, \ v \in \mathcal{V}. \tag{5.8}$$

In other words, all nodes in the network can eventually obtain the same state value on the average cumulative generation of type g DG units. Similarly, we can show the convergence of the state values with respect to the average aggregated loads $\bar{Y}$ which is updated as

$$\bar{Y}_{\mathcal{V}}(t_k) = W_{\mathcal{V}}^a \bar{Y}_{\mathcal{V}}(t_{k-1}) \tag{5.9}$$

where $\bar{Y}_{\mathcal{V}}(t_k) = (\bar{Y}(1, t_k), \cdots, \bar{Y}(|\mathcal{V}|, t_k))^\top$.

The convergence of the multiagent coordination ensures that an accurate decentralized decision can be made by each node if T is sufficiently large. However, for the economic dispatch in a small time scale, the convergence should be reached in a short time. The error of multiagent coordination at time T is bounded by

$$||\Phi_{g,\mathcal{V}}(T)||_2 \leq |\lambda_2(W_{\mathcal{V}}^a)|^{\lfloor \frac{T}{T_I(\mathcal{V})} \rfloor} ||\Phi_{g,\mathcal{V}}(0)||_2 \tag{5.10}$$

where $\lambda_k(\cdot)$ represents the kth largest eigenvalue (in module), and $\Phi_{g,\mathcal{V}}(t)$ is the disagreement vector [106], given by

$$\Phi_{g,\mathcal{V}}(t) = \left(\bar{X}_g(1, t) - \bar{X}_g, \bar{X}_g(2, t) - \bar{X}_g, \cdots, \bar{X}_g(|\mathcal{V}|, t) - \bar{X}_g\right)^\top. \tag{5.11}$$

In (5.10), $T_I(\mathcal{V})$ is the duration of each iteration via the ad hoc network with respect to nodes in $\mathcal{V}$, which depends on the wireless link scheduling.

As the network size increases, the convergence speed of multiagent coordination in the ad hoc network decreases significantly [96] [99]. We propose to utilize the cellular communication links to improve network connectivity and thus the convergence speed according to the small-world phenomenon [98]. Denote $\mathcal{M}$ ($\mathcal{M} \subseteq \mathcal{B}$) as the set of dual-mode nodes for which the cellular communication devices are activated, where $M = |\mathcal{M}|$ ($M \geq 2$) represents the number of activated cellular communication devices. In the next two sections, we present two multiagent coordination schemes to utilize both the ad hoc and cellular communication links.

5.4   Single-Stage Multiagent Coordination

The single-stage multiagent coordination utilizes the cellular network to deliver information among the nodes in $\mathcal{M}$ after each iteration in the ad hoc network, as shown in Fig. 5.2(b). The single-stage multiagent coordination is fully decentralized such that the network topology information is not required. Given the value of M, the nodes in $\mathcal{M}$ are randomly selected. All nodes in $\mathcal{V}$ operate on the same frequency channel to ensure successful information exchanges via the ad hoc network.

5.4.1   Update-and-Continue based Random Access

For the information exchange via the ad hoc network, the wireless link access is random without requiring network topology information. Since multiagent coordination operates in a synchronous manner according to (5.5), after each update, node v should wait until the next iteration begins (i.e., all other nodes finish their current update) to guarantee the convergence. However, the time of each iteration (i.e., $T_I(\mathcal{V})$ in (5.10)) becomes a random variable because of the random access scheme. In order to avoid that each node waits for the worst-case iteration time (refereed to as the update-and-wait based random access scheme [96]), we consider an update-and-continue based random access scheme [97] such that each node starts to transmit the updated state values to its neighbors following the completion of its own update. The neighboring nodes store the received state values and use them for the next iteration following the completion of the current update. In order to implement the update-and-continue based random access, an index number is assigned to each iteration.

5.4.2 Iteration via Cellular Network

Since all cellular BSs are connected to a backbone network, we consider all nodes in $\mathcal{M}$ as direct neighbors of each other during the iteration via cellular network. An iteration via the cellular network includes the information exchange among each pair of nodes in $\mathcal{M}$. A uniform weight matrix [107] without the need of network topology information is used for the update of the state values, given by $W_{\mathcal{M}}^c = [\omega_{\mathcal{M}}^c(v,n)]_{|\mathcal{V}|\times|\mathcal{V}|}$, where $\omega_{\mathcal{M}}^c(v,n)$ is given by

$$\omega_{\mathcal{M}}^c(v,n) = \begin{cases} 1/M, & \text{if } v,n \in \mathcal{M} \\ 1, & \text{if } v,n \in \mathcal{V}\setminus\mathcal{M} \text{ and } v=n \\ 0, & \text{elsewhere} \end{cases} \tag{5.12}$$

where the second case corresponds to the ad hoc nodes or the dual-mode nodes with inactivated cellular communication devices. For an iteration via both the ad hoc and cellular networks, the weight matrix is given by $W_{\mathcal{M}}^c W_{\mathcal{V}}^a$, i.e.,

$$\bar{X}_{g,\mathcal{V}}(t_k) = W_{\mathcal{M}}^c W_{\mathcal{V}}^a \bar{X}_{g,\mathcal{V}}(t_{k-1}) \tag{5.13}$$

$$\bar{Y}_{\mathcal{V}}(t_k) = W_{\mathcal{M}}^c W_{\mathcal{V}}^a \bar{Y}_{\mathcal{V}}(t_{k-1}). \tag{5.14}$$

Since $W_{\mathcal{M}}^c$ is doubly stochastic, $W_{\mathcal{M}}^c W_{\mathcal{V}}^a$ is doubly stochastic. In the next section, we show that the graph associated with $W_{\mathcal{M}}^c W_{\mathcal{V}}^a$ is strongly connected. Therefore, the convergence of the single-stage multiagent coordination is guaranteed.

5.4.3 Performance Analysis

In this subsection, we analyze the benefit of using the cellular communication links to improve the convergence speed of multiagent coordination. According to (5.10), we focus on the second largest eigenvalue of the weight matrix. Consider a finite-state

Markov chain with state space $\mathcal{V}$ and state transition matrix (or stochastic matrix) $W = [w(i, j)]_{|\mathcal{V}| \times |\mathcal{V}|}$[5]. Define the closed subset and irreducible closed subset as follows.

Definition 2. *A set $\mathcal{M}$ of states is a closed subset of a Markov chain with state transition matrix W if and only if $w(i, j) = 0$ for any $i \in \mathcal{M}$ and $j \in \mathcal{V} \setminus \mathcal{M}$. A set $\mathcal{M}'$ of states is an irreducible closed subset if and only if $\mathcal{M}'$ is a closed subset, and no proper subset of $\mathcal{M}'$ is a closed subset.*

Then, the following lemma holds with respect to eigenvalues of the state transition matrix of a Markov chain [108].

Lemma 10. *The state transition matrix W has an eigenvalue 1, and the multiplicity of the eigenvalue 1 is equal to the number of irreducible closed subsets of the Markov chain.*

Based on Lemma 10, we have the following properties with respect to the weight matrices $W_{\mathcal{M}}^c$ and $W_{\mathcal{V}}^a$.

Lemma 11. *Both $W_{\mathcal{M}}^c$ and $W_{\mathcal{V}}^a$ are symmetric and positive semidefinite.*

The proof of Lemma 11 is given in Appendix B.

By comparing the second largest eigenvalue of $W_{\mathcal{M}}^c W_{\mathcal{V}}^a$ with that of $W_{\mathcal{V}}^a$, we have the following theorem with respect to the benefit of using cellular communication links, which is proved in in Appendix B.

Theorem 5. *Given $\mathcal{M} \subseteq \mathcal{V}$, $M \geq 2$, and the weight matrices $W_{\mathcal{V}}^a$ and $W_{\mathcal{M}}^c$, we have $\lambda_2(W_{\mathcal{M}}^c W_{\mathcal{V}}^a) \leq \lambda_2(W_{\mathcal{V}}^a)$.*

Theorem 5 indicates that the convergence speed of multiagent coordination can be improved by using the cellular communication links. On the other hand, since both $W_{\mathcal{M}}^c$

---

[5]Obviously, the doubly stochastic matrices $W_{\mathcal{V}}^a$, $W_{\mathcal{M}}^c$, and $W_{\mathcal{M}}^c W_{\mathcal{V}}^a$ can be considered as the transition matrices of Markov chains with a common state space $\mathcal{V}$.

and $W_{\mathcal{V}}^a$ are symmetric and positive semidefinite, the lower bound of $\sum_{i=1}^{k} \lambda_i(W_{\mathcal{M}}^c W_{\mathcal{V}}^a)$ for any $k \in \{1, 2, \cdots, |\mathcal{V}|\}$ is given by

$$\sum_{i=1}^{k} \lambda_i(W_{\mathcal{M}}^c W_{\mathcal{V}}^a) \geq \max_{m_1, \cdots, m_k} \sum_{i=1}^{k} \lambda_{|\mathcal{V}|-m_i+1}(W_{\mathcal{V}}^a) \lambda_{m_i}(W_{\mathcal{M}}^c) \tag{5.15}$$

where $1 \leq m_1 < m_2 < \cdots < m_k \leq |\mathcal{V}|$ are ordered integers [122]. Denote the lower and upper bounds of $\lambda_2(W_{\mathcal{M}}^c W_{\mathcal{V}}^a)$ with respect to $\mathcal{M}$ as $\theta(\mathcal{M})$ and $\varphi(\mathcal{M})$, respectively. Letting $k = 2$ in (5.15) and taking into account (6.38), we have

$$\theta(\mathcal{M}) = \max_{1 \leq m_1 < m_2 \leq |\mathcal{V}|} \{\lambda_{|\mathcal{V}|-m_1+1}(W_{\mathcal{V}}^a)\lambda_{m_1}(W_{\mathcal{M}}^c) + \lambda_{|\mathcal{V}|-m_2+1}(W_{\mathcal{V}}^a)\lambda_{m_2}(W_{\mathcal{M}}^c)\} - 1 \tag{5.16}$$

$$\varphi(\mathcal{M}) = \lambda_2(W_{\mathcal{V}}^a)\lambda_2(W_{\mathcal{M}}^c). \tag{5.17}$$

Based on $\mathcal{M}$, we consider another set $\mathcal{M}'$ with more activated cellular communication devices such that $\mathcal{M}' \subseteq \mathcal{B}$ and $\mathcal{M} \subseteq \mathcal{M}'$. Obviously, we have $M \leq |\mathcal{M}'|$. For the potential benefit of activating more cellular communication devices, we have the following proposition, which is proved in Appendix B.

Proposition 2. *Given $M \geq 2$ and $\mathcal{M} \subseteq \mathcal{M}'$, we have $\theta(\mathcal{M}') \leq \theta(\mathcal{M})$ and $\varphi(\mathcal{M}') \leq \varphi(\mathcal{M})$.*

5.5 Hierarchical Multiagent Coordination

Hierarchical multiagent coordination utilizes the network topology information for wireless link scheduling and clustering. Each of the dual-mode nodes in $\mathcal{M}$ is considered as a cluster head. As shown in Fig. 5.2(c), the hierarchical multiagent coordination consists of two levels. The first and second levels are performed via the ad hoc network and cellular network, respectively. Then, the dual-mode nodes in $\mathcal{M}$ broadcast (BC) the results based on the second level of multiagent coordination to the nodes within each cluster via

the ad hoc network. Since network topology information is available, the wireless links can be scheduled efficiently. Moreover, given the value of M, the selection of nodes in $\mathcal{M}$ and the node clustering can be optimized. Frequency reuse is considered such that the communication links within different clusters are interference free.

5.5.1 Deterministic Ad Hoc Communication Link Scheduling

Compared with the random access, deterministic scheduling improves the efficiency of information exchange by increasing the number of concurrent transmissions [97]. Denote the node set in the cluster corresponding to node m ($m \in \mathcal{M}$) as $\mathcal{Q}_m$. For each iteration, each node in $\mathcal{Q}_m$ broadcasts its own state values once. Suppose each broadcast corresponds to one time slot with duration T_B. Denote the deterministic scheduling scheme for the nodes in $\mathcal{Q}_m$ as $\mathfrak{D}_{\mathcal{Q}_m} = \{\mathcal{D}_{\mathcal{Q}_m}^s | s \in \{1, 2, \cdots, S_{\mathcal{Q}_m}\}\}$, where $\mathcal{D}_{\mathcal{Q}_m}^s$ represents the set of nodes scheduled to broadcast during time slot s, and $S_{\mathcal{Q}_m}$ is the number of time slots required to complete an iteration. The objective of the deterministic scheduling is to construct a broadcast sequence $\mathfrak{D}_{\mathcal{Q}_m}$ which uses the minimum number of time slots to complete the broadcasts of all nodes in $\mathcal{Q}_m$, given by

$$(\mathbf{P2}) \quad \min_{\mathfrak{D}_{\mathcal{Q}_m}} \quad S_{\mathcal{Q}_m} \tag{5.18}$$

$$\text{subject to} \quad (\mathcal{N}_{v_1} \cup \{v_1\}) \cap (\mathcal{N}_{v_2} \cup \{v_2\}) = \emptyset, v_1, v_2 \in \mathcal{D}_{\mathcal{Q}_m}^s, \ s \in \{1, 2, \cdots, S_{\mathcal{Q}_m}\} \tag{5.19}$$

$$\cup_{s \in \{1,2,\cdots,S_{\mathcal{Q}_m}\}} \mathcal{D}_{\mathcal{Q}_m}^s = \mathcal{Q}_m \tag{5.20}$$

$$\sum_{s \in \{1,2,\cdots,S_{\mathcal{Q}_m}\}} \sum_{n \in \mathcal{Q}_m} I_{n \in \mathcal{D}_{\mathcal{Q}_m}^s} = 1. \tag{5.21}$$

Constraint (5.19) indicates that there is no collision for the concurrent broadcasts during each time slot, while constraints (5.20) and (5.21) guarantee that each node broadcasts exactly once for each iteration. Problem P2 defines an integer programming problem which cannot be solved efficiently [66, 109]. In order to reduce the computational complexity, we consider a greedy algorithm, Algorithm 4. For each time slot, the algorithm

---

Algorithm 4   Deterministic Scheduling Algorithm

Input: $\mathcal{Q}_m$, $\mathcal{N}_i$ $(i \in \mathcal{Q}_m)$;
Output: $\mathfrak{D}_{\mathcal{Q}_m}$, $S_{\mathcal{Q}_m}$;

1: Initialize: $S = 1$, $\mathcal{Q}'_m = \mathcal{Q}_m$, and $\mathcal{D}^1_{\mathcal{Q}_m} = \emptyset$;
2: **while** $\cup_{s \in \{1,2,\cdots,S\}} \mathcal{D}^s_{\mathcal{Q}_m} \neq \mathcal{Q}_m$ **do**
3:     Calculate the maximum independent set of $\mathcal{G}_{\mathcal{Q}'_m}$ and denote the vertex set as $\mathcal{D}^S_h$;
4:     $\mathcal{Q}'_m = \mathcal{Q}_m - \cup_{s \in \{1,2,\cdots,S\}} \mathcal{D}^s_{\mathcal{Q}_m}$;
5:     Update $S \leftarrow S + 1$;
6: **end while**
7: **return** $\mathfrak{D}_{\mathcal{Q}_m} = \{\mathcal{D}^s_{\mathcal{Q}_m} | s \in \{1, 2, \cdots, S_{\mathcal{Q}_m}\}\}$, $S_{\mathcal{Q}_m} = S$

---

maximizes the number of concurrent (collision-free) broadcasts. Note that in step 1, $\mathcal{Q}'_m$ represents the set of nodes which have not completed the broadcast. In step 3, $\mathcal{G}_{\mathcal{Q}'_m}$ denotes a directed graph corresponding to the nodes in $\mathcal{Q}'_m$ based on the ad hoc network, i.e., there is an edge from node i to node j $(i, j \in \mathcal{Q}'_m)$ if and only if $j \in \mathcal{N}_i$, and vice versa. The maximum independent set can be calculated based on existing methods or heuristic algorithms [110].

5.5.2   Iteration via Cellular Network

Similar to the single-stage multiagent coordination scheme, all nodes in $\mathcal{M}$ are involved in the iteration via the cellular network. Denote the weight matrix with respect to the iteration via the cellular network as $W^h_{\mathcal{M}}(v, n) = [\omega^h_{\mathcal{M}}(v, n)]_{M \times M}$. Since each node $m \in \mathcal{M}$ is the cluster head of a set $\mathcal{Q}_m$ of nodes, the weight values should account for the cluster size, given by $\omega^h_{\mathcal{M}}(v, n) = |\mathcal{Q}_n| / |\mathcal{V}|$ for all $v, n \in \mathcal{M}$. Consider the information discovery of the average value of the aggregated generation of type g DG units. Given a sufficiently large duration for the iterations via the ad hoc network (T_A), we have

$$\lim_{T_A \to \infty} \bar{X}_g(i, T_A) = \frac{1}{|\mathcal{Q}_m|} \sum_{v \in \mathcal{Q}_m} x_{gv}, \; i \in \mathcal{Q}_m. \tag{5.22}$$

After the iteration via the cellular network, the state value broadcasted by each node in $\mathcal{M}$ to the cluster members is given by

$$\sum_{m \in \mathcal{M}} \frac{|\mathcal{Q}_m|}{|\mathcal{V}|} \cdot \frac{1}{|\mathcal{Q}_m|} \sum_{v \in \mathcal{Q}_m} x_{gv} = \frac{1}{|\mathcal{V}|} \sum_{m \in \mathcal{M}} \sum_{v \in \mathcal{Q}_m} x_{gv} = \frac{1}{|\mathcal{V}|} \sum_{v \in \mathcal{V}} x_{gv} = \bar{X}_g. \tag{5.23}$$

Therefore, the convergence of the hierarchical multiagent coordination is guaranteed.

5.5.3 Performance Analysis and Node Clustering

Since the cluster sizes ($|\mathcal{Q}_m|$) corresponding to the nodes $m \in \mathcal{M}$ are different, the performance of the hierarchical multiagent coordination is related to the clustering algorithm. The error of the hierarchical multiagent coordination at time T is given by

$$
\begin{aligned}
||\Phi_{g,\mathcal{V}}(T)||_2 &= \sqrt{|\mathcal{V}| \left[\left(\sum_{m \in \mathcal{M}} \frac{|\mathcal{Q}_m|}{|\mathcal{V}|} \bar{X}_g(m, T_A) \right) - \bar{X}_g \right]^2} \\
&= \sqrt{\frac{1}{|\mathcal{V}|} \left[\sum_{m \in \mathcal{M}} |\mathcal{Q}_m| \left(\bar{X}_g(m, T_A) - \bar{X}_g \right) \right]^2} \\
&\leq \sqrt{\sum_{m \in \mathcal{M}} |\mathcal{Q}_m| \left(\bar{X}_g(m, T_A) - \bar{X}_g \right)^2} \\
&\leq \sqrt{\sum_{m \in \mathcal{M}} |\mathcal{Q}_m| \cdot ||\Phi_{g,\mathcal{Q}_m}(T_A)||_2^2} \\
&\leq \sqrt{\sum_{m \in \mathcal{M}} |\mathcal{Q}_m| [\lambda_2(W_{\mathcal{Q}_m}^a)]^{\lfloor \frac{2T_A}{S_{\mathcal{Q}_m} T_B} \rfloor} ||\Phi_{g,\mathcal{Q}_m}(0)||_2^2} \\
&\leq ||\Phi_{g,\mathcal{V}}(0)||_\infty \sqrt{\sum_{m \in \mathcal{M}} |\mathcal{Q}_m|^2 [\lambda_2(W_{\mathcal{Q}_m}^a)]^{\lfloor \frac{2T_A}{S_{\mathcal{Q}_m} T_B} \rfloor}} \tag{5.24}
\end{aligned}
$$

where the second equality holds since $\sum_{m \in \mathcal{M}} |\mathcal{Q}_m| = |\mathcal{V}|$, and $||\Phi_{g,\mathcal{V}}(0)||_\infty$ equals the largest element of the initial disagreement vector. Compared with the multiagent coordination via the ad hoc network, the benefit of the hierarchical multiagent coordination

scheme is based on the potentially smaller $S_{\mathcal{Q}_m}$ and $\lambda_2(W^a_{\mathcal{Q}_m})$ for smaller graphs, i.e., $\mathcal{Q}_m \subset \mathcal{V}$. Similar observation can be obtained by decomposing an ad hoc network with long-range links [111].

According to (5.24), for a given number of activated cellular communication devices M, the convergence speed of the hierarchical multiagent coordination is determined by $\sum_{m \in \mathcal{M}} |\mathcal{Q}_m|^2 [\lambda_2(W^a_{\mathcal{Q}_m})]^{\lfloor \frac{2T_A}{S_{\mathcal{Q}_m} T_B} \rfloor}$, which needs to be minimized for all possible combinations of M nodes in $\mathcal{B}$ and all nodes in $\mathcal{V}$. However, the computational complexity is $O(|\mathcal{B}|^M |\mathcal{V}|^M)$, which is prohibitive as the network size increases. Note that the error of the hierarchical multiagent coordination scheme is dominated by the largest cluster (by a factor of $\max_{m \in \mathcal{M}} |\mathcal{Q}_m|^2$). Therefore, we consider a heuristic clustering algorithm which constructs the clusters by splitting [112] the largest cluster which includes at least two dual-mode nodes. The details are given in Algorithm 5, where the function $f(\cdot)$ is used to calculate an optimal split of a cluster with respect to a set $\mathcal{V}'$ of ad hoc nodes and a subset $\mathcal{B}'$ ($\mathcal{B}' \subseteq \mathcal{V}'$) of dual-mode nodes, given by

$$f(\mathcal{V}', \mathcal{B}') = \arg \min_{\substack{\{m_1, m_2\} \in \mathcal{B}' \times \mathcal{B}', m_1 \neq m_2 \\ \mathcal{Q}_{m_1} \cup \mathcal{Q}_{m_2} = \mathcal{V}'}} \{\sum_{k=1,2} |\mathcal{Q}_{m_k}|^2 [\lambda_2(W^a_{\mathcal{Q}_{m_k}})]^{\lfloor \frac{2T_A}{S_{\mathcal{Q}_{m_k}} T_B} \rfloor}\}. \qquad (5.25)$$

Note that if there is only one element in a cluster $\mathcal{Q}_m$ (i.e., $|\mathcal{Q}_m| = 1$), we denote $\lambda_2(W^a_{\mathcal{Q}_m}) = 0$ since each node has accurate power generation and load information of itself. For computational simplicity, the cluster members in terms of $\mathcal{Q}_{m_1}$ and $\mathcal{Q}_{m_2}$ are determined by the shortest-distance criteria, i.e., a Voronoi diagram with two points. In a case that $\mathcal{Q}_{m'}$ cannot be split into two clusters without isolated nodes, step 3 is recalculated with respect to the second largest cluster, and so on. Since each step of the cluster splitting only takes into account all possible pairs of dual-mode nodes in one cluster, the complexity of the algorithm is $O(M|\mathcal{B}|^2)$.

Algorithm 5 Clustering Algorithm

Input: $\mathcal{V}$, $\mathcal{B}$, $\mathcal{N}_v$ $(v \in \mathcal{V})$, M;
Output: $\mathcal{M}$, $\mathcal{Q}_m$, $m \in \mathcal{M}$;
 1: Initialize: $\mathcal{M} = \{m\}$ for any $m \in \mathcal{B}$, $Q_m = \mathcal{V}$;
 2: **for** $i = 2$ to M **do**
 3:     $m' = \arg\max_{m \in \mathcal{M}} \{|\mathcal{Q}_m| \mid |\mathcal{Q}_m \cap \mathcal{B}| \geq 2\}$;
 4:     $\mathcal{V}' = \mathcal{Q}_{m'}$, $\mathcal{B}' = \mathcal{Q}_{m'} \cap \mathcal{B}$;
 5:     Update $\mathcal{M} \leftarrow (\mathcal{M} \setminus m') \cup f(\mathcal{V}', \mathcal{B}')$;
 6:     Update $\mathcal{Q}_m$ for $m \in f(\mathcal{V}', \mathcal{B}')$;
 7: **end for**
 8: **return** $\mathcal{M}$, $\mathcal{Q}_m$, $m \in \mathcal{M}$

5.6 Communication Cost versus Energy Cost

Based on the discussions in Section 5.4 and Section 5.5, the error of multiagent coordination can be (potentially) reduced by activating more cellular communication devices. With more accurate information, each DG unit can make better decision on power generation for generation cost minimization. However, the communication cost increases as the number of activated cellular communication devices increases. In this section, we investigate a tradeoff between the communication and generation costs.

5.6.1 Cost Model

Consider one economic dispatch period as an example. The communication cost is defined based on the usage of network resources (such as communication bandwidth, buffer storage, and battery storage) to achieve economic dispatch. Specifically, we consider the usage of bandwidth resource which is the main concern of this chapter. Given the number of activated cellular communication devices (M), a total of $[M(M-1)]$ packets are transmitted via the cellular network for each iteration of multiagent coordination. The reason is that each activated cellular communication device needs to inform the other

$(M-1)$ devices about its own state values. As all data packets have the same size and transmitting each packet consumes a certain amount of bandwidth resource, the cost of using cellular network can be modeled as a function of M, given by $C_C^S(M)$ and $C_C^H(M)$ for the single-stage and hierarchical multiagent coordination schemes, respectively. In this research, we consider the monetary cost (in dollars) for simplicity since it is consistent with the definition of power generation cost in (5.1). In order to transmit a data packet via cellular network, a cost c_M (in dollars) is incurred. The value of c_M varies for different systems and depends on many factors such as the size of data packet, quality of service, power consumption in cellular communications, and billing system of the network operator. In the next section, we will present the numerical results based on a real data plan of a Canadian cellular network operator as an example. The ad hoc network (e.g., WiFi or ZigBee network) is used for both single-stage and hierarchical multiagent coordination. However, the ad hoc network is considered to be a less monetarily costly option, since it uses unlicensed radio frequency bands as opposed to licensed bands in cellular network. Therefore, the communication costs (in dollars) of the single-stage and hierarchical multiagent coordination schemes are, respectively, given by

$$C_C^S(M) = c_M M(M-1) E\left[T/T_I(\mathcal{V})\right] \tag{5.26}$$

$$C_C^H(M) = c_M M(M-1) \tag{5.27}$$

where $E\left[T/T_I(\mathcal{V})\right]$ is the average number of iterations of multiagent coordination via the ad hoc network. Note that the cost of single-stage multiagent coordination is enlarged by a factor of $E\left[T/T_I(\mathcal{V})\right]$ since an iteration via the cellular network is performed after each iteration via the ad hoc network.

The power generation cost is defined in (5.1). After the multiagent coordination, denote the state values of cumulative generation and aggregated loads obtained by node v as $\bar{\mathbf{X}}_v = \{\bar{X}_1(v,T), \bar{X}_2(v,T), \cdots, \bar{X}_G(v,T)\}$ and $\bar{Y}_v = \bar{Y}(v,T)$, respectively. Based on (5.4), the decentralized decision on the economic dispatch is given by $u_{gv}(\bar{\mathbf{X}}_v, \bar{Y}_v, \mathbf{c})$, where

$\bar{\mathbf{X}}$ and $\bar{Y}$ are replaced by $\bar{\mathbf{X}}_v$ and $\bar{Y}_v$, respectively. Given the minimum cost $C_P^*(\mathbf{x}, \mathbf{y}, \mathbf{c})$ based on problem P1 which is a constant within T_D, we consider the increment in the generation cost by using inaccurate information, which is a function of M and is given by

$$
\begin{aligned}
C_P^I(M) = \mathrm{E}\Bigg[& c_A(Y - \sum_{g \in \{1,2,\cdots,G\}} \sum_{v \in \mathcal{V}} u_{gv}(\bar{\mathbf{X}}_v, \bar{Y}_v, \mathbf{c}))^+ \\
& + c_E(\sum_{g \in \{1,2,\cdots,G\}} \sum_{v \in \mathcal{V}} u_{gv}(\bar{\mathbf{X}}_v, \bar{Y}_v, \mathbf{c}) - Y)^+ \\
& + \sum_{g \in \{1,2,\cdots,G\}} c_g \sum_{v \in \mathcal{V}} u_{gv}(\bar{\mathbf{X}}_v, \bar{Y}_v, \mathbf{c}) \Bigg] - \mathrm{E}\left[C_P^*(\mathbf{x}, \mathbf{y}, \mathbf{c}) \right]
\end{aligned}
\tag{5.28}
$$

where the first expectation is taken with respect to the random variables $\mathbf{x}$ and $\mathbf{y}$, and the set of randomly activated cellular communication devices $(\mathcal{M})$ for the single-stage multiagent coordination scheme. Denote the incremental generation cost of the single-stage and hierarchical multiagent coordination schemes as $C_P^{IS}(M)$ and $C_P^{IH}(M)$, respectively.

5.6.2 Cost Tradeoff

The objective is to minimize the combined communication and incremental generation costs by properly selecting the number of activated cellular communication devices M. The desired value of M for the single-stage multiagent coordination is given by problem P3 as follows:

$$
(\mathbf{P3}) \quad \min_{M \in \{1,2,\cdots,|\mathcal{B}|\}} \quad C_C^S(M) + C_P^{IS}(M) T_D
\tag{5.29}
$$

where the second term has a factor of T_D since we investigate the cost (in dollars) for one economic dispatch period. In other words, T_D is used to convert the unit of power generation cost from dollar/h to dollar/period. Similarly, we can calculate the desired value of M for the hierarchical multiagent coordination scheme. Problem P3 is an integer

programming problem which is NP-hard in general. Although an exhaustive search can be used to find the solution, the computational complexity can be prohibitive because of the expectation operation in (5.28). Moreover, the statistics of $\mathbf{x}$ and $\mathbf{y}$ (and the network topology information with respect to the single-stage multiagent coordination scheme) may not be available for a microgrid. Therefore, an approximation of the incremental generation cost $C_P^{IS}(M)$ is indispensable for practical applications.

For a self-sustained microgrid, the power generation by the G types of DG units and loads should be balanced for most of the time. Therefore, we can approximate the incremental generation cost based on the undelivered and extra power as

$$\tilde{C}_P^{IS}(M) = (c_A - c_1)\tilde{z}_A + (c_G + c_E)\tilde{z}_E \tag{5.30}$$

where $\tilde{z}_A$ and $\tilde{z}_E$ are the average values of z_A and z_E observed over a certain period of time (e.g., one day) by the alternative energy sources and negative spinning reserve service providers, respectively. Note that (5.30) provides an upper bound of $C_P^{IS}(M)$ since the price of purchasing power from the DG units is no less than c_1 and no greater than c_G. Based on the estimate $\tilde{C}_P^{IS}(M)$, an approximation of the desired tradeoff between the communication and generation costs can be achieved without resorting to the statistics of $\mathbf{x}$ and $\mathbf{y}$, which simplifies the network optimization of microgrids. Similarly, we can use the estimate $\tilde{C}_P^{IH}(M)$ for hierarchical multiagent coordination.

5.7 Numerical Results

The network topology used for simulations is shown in Fig. 5.3. We consider the Laurelwood neighborhood located in North-West Waterloo as a microgrid topology for the deployment of DG units and wireless devices. We plot the wind turbines, PV panels, and loads at adequate geographic locations on the map. For the generation data of
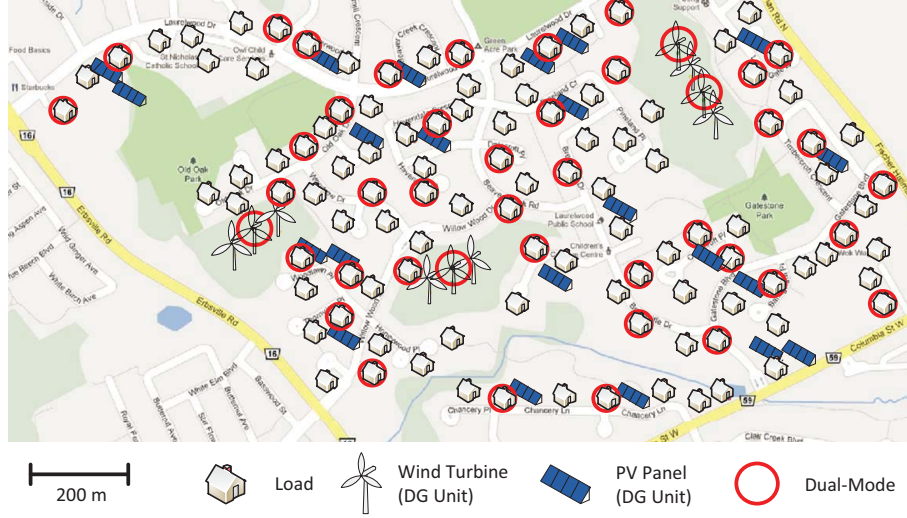
Figure 5.3: The network topology for simulations.

wind turbines, a probability distribution of the wind speed for Waterloo is obtained from Canadian Wind Energy Atlas [113] considering the 50 kW wind turbines located at 30 m height [114]. The power curve (which is the output power as a function of instantaneous wind speed) of the actual wind turbine is used to translate wind speeds to the amount of power generations. The probability distribution follows the Weibull distribution with a shape parameter 1.94 and scale parameter 4.48 m/s. The startup, cutout, and rated wind speeds are 2 m/s, 18 m/s, and 11 m/s, respectively. For the generation data of PV panels, hourly PV performance data of Toronto (100 km away from Waterloo) is obtained from NREL (National Renewable Energy Laboratory) PVWatts$^{\text{TM}}$ site specific calculator [115] which determines the power production of PV panels for a given geographic location. The AC rating of the PV panels is 3.08 kW. For the demand of loads, an hourly demand is obtained from the smart meters of two residences in the Laurelwood neighborhood subscribed to Waterloo North Hydro [34]. The demand data is approximated by a normal distribution [116]. For instance, the mean and standard deviation in kWh during the on-peak hours (i.e., 9 am and 6 pm) and off-peak hours (i.e., 1 am to 7 am and 1

pm to 4 pm) are, respectively, given by (1.5, 0.43) and (0.70, 0.04). For consistency, all power generation and load data are taken during the month of June in Waterloo. The costs are 0.135, 0.802, 2.080, and 0.000 (CAD) dollar/kWh for wind turbine, PV panel [100], diesel generator, and negative spinning reserves (i.e. the cost is neglected) [39], respectively. For the heterogeneous wireless network infrastructure, the transmission range of ad hoc communication devices is 150 m with a link layer data rate 2 Mbps and a PHY header according to the IEEE 802.11 standard [117]. For the update-and-wait and update-and-continue based random access schemes, we consider each ad hoc node accesses the wireless medium with probability 0.1 [54] and a retransmission mechanism is in place to guarantee the successful broadcast. We randomly select 44 dual-mode nodes with the cellular capability as shown in Fig. 5.3 and consider a basic data plan of Rogers Canada with 40 dollars for 100 MB data[6]. Since the power generation and demand state information can be represented by 16 bits [96], we have $c_M = 2.4 \times 10^{-6}$ dollars, which can be considered as a lower bound of communication cost since packetization overhead is not included. The durations of the economic dispatch and information exchange periods are $T_D = 300$ s (i.e., $\frac{1}{12}$ h) and $T(= T_A) = 2$ s, respectively [16, 17]. The generation of DG units and the loads are randomly generated for each economic dispatch period during the simulations. For a fair comparison, we focus on the average costs since random selection of dual-mode nodes is used by our proposed single-stage multiagent coordination scheme and random cluster splitting is studied in the following performance evaluation. Each simulation run lasts for one day from which the communication and generation costs are calculated, and the results are averaged over 30 days.

Fig. 5.4 shows the incremental generation cost ($C_P^I(M)$) on a daily basis versus the fraction of activated cellular communication devices ($M/|\mathcal{B}|$). As we can see, the gener-

---

[6]It is worth mentioning that this is a service plan for cell phone users. How to customize the plan for microgrid operation is still an open issue and left for our future work.

121
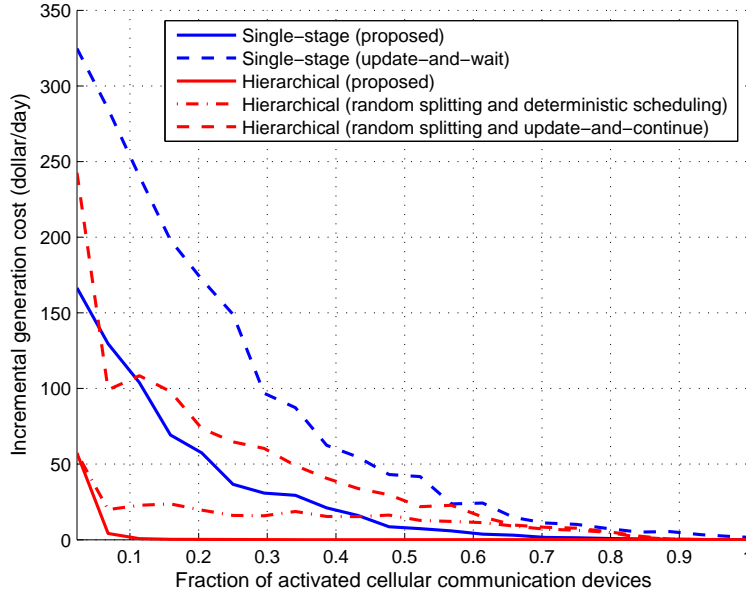
Figure 5.4: Incremental generation cost (per day) versus the fraction of activated cellular communication devices.

ation costs of both schemes decrease as the fraction of activated cellular communication devices increases since more cellular communication links can (potentially) improve the network connectivity and thus reduce the error in multiagent coordination. The update-and-continue based random access scheme which is used by our proposed single-stage multiagent coordination scheme can reduce the generation cost as compared with the update-and-wait scheme by reducing the duration of each iteration via the ad hoc network. The proposed hierarchical multiagent coordination scheme achieves the lowest generation cost based on deterministic scheduling and efficient clustering. For comparison, if random cluster splitting (without information of the cluster size and eigenvalues of weight matrices) is used, the generation cost decreases slowly with the fraction of activated cellular communication devices. Moreover, if update-and-continue based random access is also used (without network topology information for wireless link scheduling),

the generation cost further increases because of an increased iteration duration within each cluster. The generation cost is even higher than the single-stage counterpart since the error of the hierarchical multiagent coordination scheme is dominated by the potential large clusters as a result of random cluster splitting, according to our analysis in Subsection 5.5.3.

Taking account of the cost of using cellular communication links, a tradeoff between the communication and incremental generation costs is shown in Fig. 5.5. For presentation clarity, we normalize the combined communication and generation costs of both schemes by their maximum actual costs, given by 166.5 and 57.2 dollars, respectively. We can see that, the communication and generation costs are comparable with each other. As the fraction of activated cellular communication devices increases, the normalized cost first decreases since the generation cost decreases. Then, the normalized cost increases as the communication cost increases and exceeds the decrement in the generation cost. Therefore, there is a desired tradeoff point between the communication and generation costs for both single-stage and hierarchical multiagent coordination schemes, which provides the minimum normalized cost. Since the network topology information is used by the hierarchical multiagent coordination scheme, the desired tradeoff is achieved by activating less cellular communication devices. The normalized cost achieved at the tradeoff point based on the approximation of incremental generation cost is close to that of the desired tradeoff point, which implies a good estimate for the desired value of M. The normalized cost based on the existing schemes without using cellular communication devices [96] or with all cellular communication devices (or equivalently, all long-range links [111]) being activated is also shown. We can see that, the existing schemes can only achieve the boundary points of the cost tradeoff curves and may not be efficient in minimizing the combined communication and generation costs.
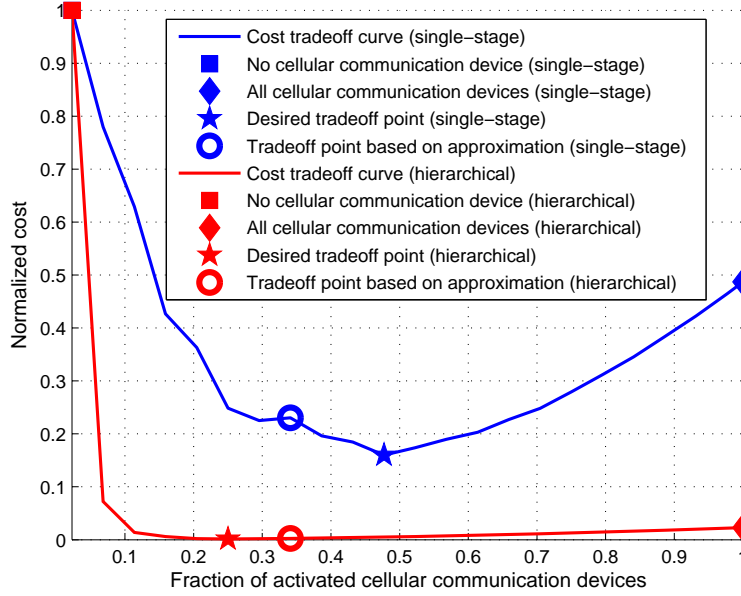
Figure 5.5: Tradeoff between the communication and generation costs.

5.8 Summary

In this chapter, we propose a decentralized economic dispatch approach for microgrids such that each DG unit makes local decisions on power generation based on a multiagent coordination with guaranteed convergence. A heterogeneous wireless network architecture is established. Each node uses an ad hoc communication device for basic information exchange, while some dual-mode nodes are equipped with optional cellular communication devices which can be activated to improve the convergence speed of multiagent coordination. Two multiagent coordination schemes are proposed to utilize the cellular communication links based on the single-stage and hierarchical operation modes, respectively. Numerical results indicate that our propose schemes can better utilized the cellular communication links and achieve more efficient tradeoff between the communication and generation costs in comparison with the existing schemes.

Chapter 6

Conclusions and Further Work

In this chapter, we summarize the major research contributions and discuss further research work.

6.1 Major Research Contributions

This research aims at developing efficient resource management schemes for DTNs and smart grid. Four research topics have been studied, namely medium access control for cooperative data dissemination via RS-WLANs, efficient on-demand data service delivery to high-speed trains, optimal energy delivery via V2G systems, and decentralized economic dispatch in microgrids. The proposed resource management schemes are able to address the intermittency of network connections in DTNs and the randomness of distributed generation and PHEV mobility in the smart grid. Specifically, the main contributions of this research are summarized as follows.

- We propose a DRMAC scheme for efficiency cooperative data dissemination via RS-WLANs. The proposed MAC scheme achieves the cooperative diversity gain based

on a receiver-initiated mechanism and utilizes the time correlation of a wireless channel to reduce the signalling overhead. A novel analytical model is established to evaluate the performance of the proposed MAC scheme by using a finitestate Markov chain based channel model to characterize the time correlation between two consecutive transmissions. From the users' point of view, the proposed MAC scheme improves quality of data dissemination services provided by RS-WLANs. From the service providers' point of view, the resources within each RS-WLAN can be better utilized, which in turn stimulates the sharing of the roadside communication infrastructures in terms of the WiFi based WLANs.

- We formulate an optimal resource allocation problem for on-demand data delivery to high-speed trains in a cellular/infostation integrated network. The problem is transformed into a single-machine preemptive scheduling problem and an online resource allocation algorithm is proposed for practical applications. The performance bound of the online algorithm is characterized based on the theory of sequencing and scheduling. Further, a service pre-downloading algorithm is used to achieve efficient resource allocation when the link from the backbone network to an infostation is a bottleneck. Compared with the existing approaches such as FIFO, EDF, and RAPID, our proposed algorithms can significantly improve the quality of on-demand data service provisioning over the trip of a train, which significantly improves the comfort of onboard passengers.

- We extend the traditional energy store-and-deliver mechanism for stationary battery management to an energy store-carry-and-deliver mechanism for PHEV battery management in V2G system. The energy cost minimization problem under TOU electricity pricing is mathematically formulated and a state-dependent (S, S') policy is proved to be optimal. Further, we proposed a modified backward iteration algorithm with an EWMA estimation of the statistics of PHEV mobility and

energy demand to facilitate practical applications. Compared with the existing approaches, the proposed scheme can achieve energy cost reduction, which increases with the battery capacity. The result obtained in this research can provide a good reference for PHEV operation cost reduction and utilities for better grid operation. Beyond PHEV applications, the optimal policy can also shed light on other energy management problems in DTNs and power systems which are (partially) featured by realistic battery model, non-stationary energy demand, and bi-directional energy flow.

- We propose a decentralized economic dispatch approach such that the optimal decision on power generation is made by each DG unit locally without a central controller. The prerequisite power generation and load information for decision making is discovered by each DG unit via a multiagent coordination with guaranteed convergence. To avoid a slow convergence speed which potentially increases the generation cost because of the time-varying nature of DG output, we present a heterogeneous wireless network architecture for microgrids along with two multiagent coordination schemes to utilize the cellular communication capabilities of dual-mode devices. The optimal number of activated cellular communication devices is obtained based on the tradeoff between communication and generation costs. From the utilities' point of view, the economic dispatch in microgrids can be achieved based on wireless communication devices at a low deployment cost and the minimum operation cost. From the environmental point of view, the use of traditional thermal energy power generators can be reduced via a better utilization of the renewable energy sources. At the same time, the customers can enjoy the monetary benefit in terms of reduced electricity bills which, in turn, promotes the use of the renewable energy sources.

6.2 Further Work

Resource management in DTNs and smart grid is a broad research area. Although several critical issues have been addressed in this thesis, there are still many open research issues to be investigated:

- This research focuses on pedestrian nomadic nodes. An extension to vehicular nomadic nodes is very interesting but challenging, in which the wireless channel is highly dynamic such that it is difficult to obtain the transmission rate information for temporal diversity and use the time correlation of a wireless channel for signalling overhead reduction. Moreover, joint design for packet pre-downloading to the storage local nodes and medium access control based on mobility statistics [18, 20] needs further investigation.

- This research investigates on-demand data service delivery to high-speed trains. For practical high-speed train applications (including safety-related applications), how to map the quality of service (QoS) parameters such as the service data size, relative deadline, and importance/priority to the reward of each service is an interesting topic and needs further studies.

- The optimal energy delivery problem is studied for a single PHEV in the V2G system. How to devise an efficient multi-vehicle aggregator management algorithm for grid stability enhancement should be investigated [35, 36]. In this case, the decision variable of multi-vehicle management becomes multidimensional and the solution may not be obtained in real-time. Moreover, vehicle owners always strive to minimize their own expense and may not want to be intervened by a third party. Therefore, decentralize algorithms based on certain incentives such as real-time electricity prices can be a potential solution. Further, the integration of sustainable

generation should be investigated [116], which may add a new dimension to the optimal energy store-carry-and-deliver problem.

- In this research, the proposed decentralized economic dispatch scheme requires reliable two-way communications. Further work includes an application of broadcast gossip which does not require two-way information exchange [118] and is less sensitive to packet losses. In addition, an optimization of the decentralized economic dispatch approach by taking account of the prediction error of power generation and load information [101] and the security/privacy issues in wireless networks [119, 120, 121] is interesting and needs further investigation. After all, knowing the dispatch point is only the first step of microgrid operation. How to utilize the information to facilitate microgrid control is an important and interesting topic, which needs further study.

Bibliography

[1] K. Fall, "A delay-tolerant network architecture for challenged Internets," in *Proceedings of ACM SIGCOMM'03*, pp. 27–34, Aug. 2003.

[2] S. Burleigh, A. Hooke, L. Torgerson, K. Fall, V. Cerf, B. Durst, K. Scott, and H. Weiss, "Delay-tolerant networking: an approach to interplanetary internet," *IEEE Communications Magazine*, vol. 41, no. 6, pp. 128–136, Jun. 2003.

[3] http://www.dtnrg.org/.

[4] P. Hui, A. Chaintreau, J. Scott, R. Gass, J. Crowcroft, and C. Diot, "Pocket switched networks and human mobility in conference environments," in *Proceedings of ACM WDTN'05*, pp. 244–251, Aug. 2005.

[5] N. Wisitpongphan, F. Bai, P. Mudalige, V. Sadekar, and O. Tonguz, "Routing in sparse vehicular ad hoc wireless networks," *IEEE Journal on Selected Areas in Communications*, vol. 25, no. 8, pp. 1538–1556, Oct. 2007.

[6] Y. Wang, H. Wu, F. Lin, and N. Tzeng, "Cross-layer protocol design and optimization for delay/fault-tolerant mobile sensor networks (dft-msn)," *IEEE Journal on Selected Areas of Communications*, vol. 26, no. 5, pp. 809–819, Jun. 2008.

[7] D. B. Johnson and D. A. Maltz, "Dynamic source routing in ad hoc wireless networks," *Mobile Computing*, edited by T. Imielinski and H. Korth, ch. 5, pp. 153–181, Kluwer Academic Publishers, 1996.

[8] C. Perkins, E. Belding-Royer, and S. Das, "Ad hoc on-demand distance vector (AODV) routing," RFC 3561, IETF Network Working Group, Jul. 2003.

[9] Z. Zhang, "Routing in intermittently connected mobile ad hoc networks and delay tolerant networks: overview and challenges," *IEEE Communications Surveys and Tutorials*, vol. 8, no. 1, pp. 24–37, 2006.

[10] International union of railways. http://www.uic.org/.

[11] Thales selects BelAir networks Wi-Fi for Bergen light rail project. http://www.belairnetworks.com/.

[12] H. Farhangi, "The path of the smart grid," *IEEE Power and Energy Magazine*, vol. 8, no. 1, pp. 18–28, Jan.-Feb. 2010.

[13] S. B. Peterson, J. F. Whitacre, and J. Apt, "The economics of using plug-in hybrid electric vehicle battery packs for grid storage," *Journal of Power Sources*, vol. 195, no. 8, pp. 2377–2384, Apr. 2010.

[14] C. Guille and G. Gross, "A conceptual framework for the vehicle-to-grid (V2G) implementation," *Energy Policy*, vol. 37, no. 11, pp. 4379–4390, 2009.

[15] S. Chowdhury, S. P. Chowdhury, and P. Crossley, *Microgrids and Active Distribution Networks*. Institution of Engineering and Technology, 2009.

[16] Y. V. Makarov, C. Loutan, J. Ma, and P. de Mello, "Operational impacts of wind generation on California power systems," *IEEE Transactions on Power Systems*, vol. 24, no. 2, pp. 1039–1050, May 2009.

[17] V. Vittal, "The impact of renewable resources on the performance and reliability of the electricity grid," *Bridge on Electricity Grid*, vol. 40, no. 1, Spring 2010.

[18] B. B. Chen and M. C. Chan, "MobTorrent: a framework for mobile Internet access from vehicles," in *Proc. IEEE INFOCOM'09*, pp. 1404-1412, Apr. 2009.

[19] H. Liang and W. Zhuang, "Cooperative data dissemination via roadside WLANs," *IEEE Communications Magazine*, vol. 50, no. 4, pp. 68–74, Apr. 2012.

[20] Y. Huang, Y. Gao, K. Nahrstedt, and W. He, "Optimizing file retrieval in delay-tolerant content distribution community," in *Proc. IEEE ICDCS'09*, pp. 308–316, Jul. 2009.

[21] P. Liu, Z. Tao, S. Narayanan, T. Korakis, and S. S. Panwar, "CoopMAC: a cooperative MAC for wireless LANs," *IEEE Journal on Selected Areas in Communications*, vol. 25, no. 2, pp. 340–354, Feb. 2007.

[22] T. Zhou, H. Sharif, M. Hempel, P. Mahasukhon, W. Wang, and T. Ma, "A novel adaptive distributed cooperative relaying MAC protocol for vehicular networks," *IEEE Journal on Selected Areas in Communications*, vol. 29, no. 1, pp. 72–82, Jan. 2011.

[23] H. Shan, W. Zhuang, and Z. Wang, "Distributed cooperative MAC for multi-hop wireless networks," *IEEE Communications Magazine*, vol. 47, no. 2, pp. 126–133, Feb. 2009.

[24] F. Talucci, M. Gerla, and L. Fratta, "MACA-BI (MACA by invitation) - a receiver oriented access protocol for wireless multihop networks," in *Proc. IEEE PIMRC'97*, pp. 435–439, Sept. 1997.

[25] J. J. Garcia-Luna-Aceves and A. Tzamaloukas, "Receiver-initiated collision avoidance in wireless networks," *ACM Wireless Networks*, vol. 8, no. 2–3, Mar. 2002.

[26] J. Xu, X. Tang, and W. Lee, "Time-critical on-demand data broadcast, algorithms, analysis, and performance evaluation," *IEEE Transactions on Parallel and Distributed Systems*, vol. 17, no. 1, pp. 3–14, Jan. 2006.

[27] R. Dewri, I. Ray, I. Ray, and D. Whitley, "Optimizing on-demand data broadcast scheduling in pervasive environments," in *Proc. ACM EDBT'08*, pp. 559–569, Mar. 2008.

[28] S. Motahari, E. Haghani, and S. Valaee, "Spatio-ternporal schedulers in IEEE 802.16," in *Proc. IEEE GLOBECOM'05*, pp. 566–570, Nov. 2005.

[29] A. Balasubramanian, B. N. Levine, and A. Venkataramani, "Replication routing in DTNs: a resource allocation approach," *IEEE/ACM Transactions on Networking*, vol. 18, no. 2, pp. 596–609, Apr. 2010.

[30] H. Liang and W. Zhuang, "Double-loop receiver-initiated MAC for cooperative data dissemination via roadside WLANs," *IEEE Transactions on Communications*, to appear.

[31] H. Liang and W. Zhuang, "A double-loop receiver-initiated medium access control scheme for data dissemination services with packet pre-downloading," in *Proc. IEEE GLOBECOM'10*, pp. 1-5, Dec. 2010.

[32] H. Liang and W. Zhuang, "Resource allocation for on-demand data delivery to high-speed trains via trackside infostations,"in *Proc. IEEE GLOBECOM'11*, Dec. 2011.

[33] H. Liang and W. Zhuang, "Efficient on-demand data service delivery to high-speed trains in cellular/infostation integrated networks," *IEEE Journal on Selected Areas in Communications*, vol. 30, no. 4, pp. 780-791, May 2012.

[34] Waterloo North Hydro. http://www.wnhydro.com/.

[35] S. Han and K. Sezaki, "Development of an optimal vehicle-to-grid aggregator for frequency regulation," *IEEE Transactions on Smart Grid*, vol. 1, no. 1, pp. 65–72, Jun. 2010.

[36] E. Sortomme and M. A. El-Sharkawi, "Optimal charging strategies for unidirectional vehicle-to-grid," *IEEE Transactions on Smart Grid*, vol. 2, no. 1, pp. 131–138, Mar. 2011.

[37] R. Urgaonkar, B. Urgaonkar, M. J. Neely, and A. Sivasubramaniam, "Optimal power cost management using stored energy in data centers," in *Proc. ACM SIGMETRICS'11*, Jun. 2011.

[38] A. Bar-Noy, Y. Feng, M. P. Johnson, and O. Liu, "When to reap and when to sow - lowering peak usage with realistic batteries," in *Proc. WEA'08*, pp. 194-207, 2008.

[39] H. Moraisa, P. Kadarb, P. Fariaa, Z. A. Valea, and H. M. Khodra, "Optimal scheduling of a renewable micro-grid in an isolated load area using mixed-integer linear programming," *Renewable Energy*, vol. 35, no. 1, pp. 151–156, Jan. 2010.

[40] J. Hetzer, D. C. Yu, and K. Bhattarai, "An economic dispatch model incorporating wind power," *IEEE Transactions on Energy Conversion*, vol. 23, no. 2, pp. 603–611, Jun. 2008.

[41] E. M. Constantinescu, V. M. Zavala, M. Rocklin, S. Lee, and M. Anitescu, "A computational framework for uncertainty quantification and stochastic optimization in

unit commitment with wind power generation," *IEEE Transactions on Power Systems*, vol. 26, no. 1, pp. 431–441, Feb. 2011.

[42] W. Gatterbauer. *Interdependencies of Electricity Market Characteristics and Bidding Strategies of Power Producers.* Master thesis, Massachusetts Institute of Technology, Cambridge, 2002.

[43] H. Liang, B. J. Choi, W. Zhuang, and X. Shen, "Towards optimal energy store-carry-and-deliver for PHEVs via V2G system," in *Proc. IEEE INFOCOM'12*, Mar. 2012.

[44] H. Liang, B. J. Choi, A. Abdrabou, W. Zhuang, and X. Shen, "Decentralized economic dispatch in microgrids via heterogeneous wireless networks," *IEEE Journal on Selected Areas in Communications*, vol. 30, no. 6, pp. 1061-1074, Jul. 2012.

[45] FON. http://www.fon.com.

[46] J. Ott and D. Kutscher, "A disconnection-tolerant transport for drive-thru Internet environments," in *Proc. IEEE INFOCOM'05*, pp. 1849–1862, Mar. 2005.

[47] H. Zhu, X. Lin, M. Shi, P. Ho, and X. Shen, "PPAB: a privacy preserving authentication and billing approach for metropolitan area sharing networks," *IEEE Transactions on Vehicular Technology*, vol. 58, no. 5, pp. 2529-2543, Jun. 2009.

[48] IEEE 802.11 WG, IEEE 802.11e/D11, "IEEE standard for information technology-telecommunications and information exchange between systems-Local and metropolitan area networks-Specific requirements-part 11: wireless medium access control (MAC) and physical layer (PHY) specifications: amendment 7: medium access control (MAC) quality of service (QoS) enhancements," Oct. 2004.

[49] K. Fall and S. Farrell, "DTN: an architectural retrospective," *IEEE Journal on Selected Areas in Communications*, vol. 26, no. 5, pp. 828–836, Jun. 2008.

[50] J. Zhang, Q. Zhang, and W. Jia, "VC-MAC: A cooperative MAC protocol in vehicular networks," *IEEE Transactions on Vehicular Technology*, vol. 58, no. 3, pp. 1561-1571, Mar. 2009.

[51] H. Liang and W. Zhuang, "DFMAC: DTN-friendly medium access control for wireless local area networks supporting voice/data services," *ACM Mobile Networks and Applications*, vol. 16, no. 5, Oct. 2011.

[52] X. Yang and N. Vaidya, "On physical carrier sensing in wireless ad hoc networks," in *Proc. IEEE INFOCOM'05*, pp. 2525-2535, Mar. 2005.

[53] Y. Xiao and J. Rosdahl, "Throughput and delay limits of IEEE 802.11," *IEEE Commununications Letters*, vol. 6, no. 8, pp. 355–357, Aug. 2002.

[54] G. Bianchi, "Performance analysis of the IEEE 802.11 distributed coordination function," *IEEE Journal on Selected Areas in Communications*, vol. 18, no. 3, pp. 535–547, Mar. 2000.

[55] Q. Liu, S. Zhou, and G. B. Giannakis, "Queuing with adaptive modulation and coding over wireless links: Cross-layer analysis and design," *IEEE Transactions on Wireless Commununications*, vol. 4, no. 3, pp. 1142–1153, May 2005.

[56] H. Wang and N. Moayeri, "Finite-state Markov channel - a useful model for radio communication channels," *IEEE Transactions on Vehicular Technology*, vol. 44, no. 1, pp. 163–171, Feb. 1995.

[57] F. Hou, L. X. Cai, P. H. Ho, X. Shen, and J. Zhang, "A cooperative multicast scheduling scheme for multimedia services in IEEE 802.16 networks," *IEEE Transactions on Wireless Commununications*, vol. 8, no. 3, pp. 1508–1519, Mar. 2009.

[58] T. S. Rappaport, *Wireless Communications Principles and Practice.* New Jersey: Prentice-Hall, 1996.

[59] D. H. Ho and S. Valaee, "Information raining and optimal link-layer design for mobile hotspots," *IEEE Transactions on Mobile Computing*, vol. 4, no. 3, pp. 271–284, May–Jun. 2005.

[60] C. Sue, S. Sorour, Y. Youngsoo, and S. Valaee, "Network coded information raining over high-speed rail through IEEE 802.16j," in *Proc. IEEE PIMRC'09*, pp. 1138–1142, Sept. 2009.

[61] L. Zhu, F. R. Yu, B. Ning, and T. Tang, "Cross-layer design for video transmissions in metro passenger information systems," *IEEE Transactions on Vehicular Technology*, vol. 60, no. 3, pp. 1171–1181, Mar. 2011.

[62] J. C.-P. Wang, H. El Gindy, and J. Lipman, "On cache prefetching strategies for integrated infostation-cellular network," in *Proc. IEEE LCN'06*, pp. 185–192, Nov. 2006.

[63] Shanghai-Hangzhou High-Speed Railway. http://en.wikipedia.org/.

[64] Zhejiang news. http://zjnews.zjol.com.cn/.

[65] M. Papadopouli and H. Schulzrinne, *Peer-to-Peer Computing for Mobile Networks - Information Discovery and Dissemination.* New York: Springer, 2008.

[66] G. L. Nemhauser and L. A. Wolsey, *Integer and Combinatorial Optimization.* New York: John Wiley & Sons, 1988.

[67] K. R. Baker and D. Trietsch, *Principles of Sequencing and Scheduling.* New Jersey: John Wiley & Sons, 2009.

[68] P. Baptistea, L. Peridy, and E. Pinson, "A branch and bound to minimize the number of late jobs on a single machine with release time constraints," *European Journal of Operational Research* , vol. 144, no. 1, pp. 1–11, Jan. 2003.

[69] C. Durr, L. Jez, and K. T. Nguyen, "Online scheduling of bounded length jobs to maximize throughput," *Lecture Notes in Computer Science (LNCS)*, vol. 5893, pp. 116–127, May 2010.

[70] E. L. Lawler, "A dynamic programming algorithm for the preemptive scheduling of a single machine to minimize the number of late jobs," *Annals of Operations Research*, vol. 26, no. 1, pp. 125–133, Dec. 1990.

[71] Train Schedule. http://lieche.58.com/.

[72] A. Ahmad, "Simulation-based local train mobility model," in *Proc. ACM SpringSim'10*, pp. 1–8, Apr. 2010.

[73] R. Liu and Y. Deng "Comparing operating characteristics of high-speed rail and maglev systems: case study of Beijing-Shanghai corridor," *Journal of the Transportation Research Board*, vol. 1863, pp. 19–27, Jan. 2004.

[74] S. K. Baruah, J. Haritsa, and N. Sharma, "On-line scheduling to maximize task completions," in *Proc. IEEE RTSS'94*, pp. 228–236, Dec. 1994.

[75] E. Altman, G. Neglia, F. De Pellegrini, and D. Miorandi, "Decentralized stochastic control of delay tolerant networks," in *Proc. IEEE INFOCOM'09*, pp. 1134–1142, Apr. 2009.

[76] B. J. Choi and X. Shen, "Adaptive asynchronous sleep scheduling protocols for delay tolerant networks," *IEEE Transactions on Mobile Computing*, vol. 10, no. 9, pp. 1283–1296, Sept. 2011.

[77] B. J. Choi, H. Liang, X. Shen, and W. Zhuang, "DCS: distributed asynchronous clock synchronization in delay tolerant networks," *IEEE Transactions on Parallel and Distributed Systems*, vol. 23, no. 3, pp. 491–504, Mar. 2012.

[78] Ontario electricity time-of-use price. http://www.ontarioenergyboard.ca.

[79] L. Ulrich, "Top 10 tech cars 2011," *IEEE Spectrum*, vol. 48, no. 4, pp.28–39, Apr. 2011.

[80] The grid-integrated vehicle with vehicle to grid technology. University of Delaware. http://www.udel.edu/V2G/.

[81] D. Niyato and P. Wang, "Optimization of the mobile router and traffic sources in vehicular delay tolerant network," *IEEE Transactions on Vehicular Technology*, vol. 58, no. 9, pp. 5095–5104, Nov. 2009.

[82] U.S. Department of Energy EERE Consumer's Guide: Metering and Rate Arrangements for Grid-Connected Systems. http://www.energysavers.gov.

[83] Battery performance characteristics. http://www.mpoweruk.com.

[84] D. Beyer, F. Cheng, S. Sethi, and M. Taksar, *Markovian Demand Inventory Models*. International Series in Operations Research and Management Science, vol. 108. New York: Springer, 2010.

[85] S. P. Sethi and F. Cheng, "Optimality of (s, S) policies in inventory models with Markovian demand," *Operations Research*, vol. 45, no. 6, pp. 931–939, Nov.-Dec. 1997.

[86] F. Cheng and S. P. Sethi, "Optimality of state-dependent (s, S) policies in inventory models with Markov-modulated demand and lost sales," *Production and Operations Management*, vol. 8, no. 2, pp. 183–192, Jun. 1999.

[87] D. P. Bertsekas, *Dynamic Programming and Optimal Control*, vols. 1 and 2. Athena Scientific, 2007.

[88] M. G. Kallitsis, G. Michailidis, and M. Devetsikiotis, "A framework for optimizing measurement-based power distribution under communication network constraints," in *Proc. IEEE SmartGridComm'10*, pp. 185–190, Oct. 2010.

[89] S. Boyd and L. Vandenberghe, *Convex Optimization*. Cambridge University Press, 2004.

[90] ONE Simulator. http://www.netlab.tkk.fi/.

[91] J. Voelcker, "Lithium Batteries for hybrid cars," *IEEE Spectrum*, Jan. 2007.

[92] L. Valoen and M. Shoesmith, "The effect of PHEV and HEV duty cycles on battery and battery pack performance," in *Proc. Plug-in Hybrid Vehicle Conference*, Nov. 2007.

[93] Ultralife Corporation, "Li-Ion vs. Lead Acid." [Online]. Available: ultralifecorporation.com/download/275/.

[94] K. Morrow, D. Karner, and J. Francfort, "Plug-in hybrid electric vehicle charging infrastructure review," Idaho National Laboratory, U.S. Department of Energy, Nov. 2008.

[95] F. Katiraei, R. Iravani, N. Hatziargyriou, and A. Dimeas, "Microgrids management," *IEEE Power and Energy Magazine*, vol. 6, no. 3, pp. 54–65, May-Jun. 2008.

[96] Y. Xu and W. Liu, "Novel multiagent based load restoration algorithm for microgrids," *IEEE Transactions on Smart Grid*, vol. 2, no. 1, pp. 152–161, Mar. 2011.

[97] H. Liang, A. Abdrabou, B. J. Choi, W. Zhuang, X. Shen, and A. S. A. Awad, "Multiagent coordination in microgrids via wireless networks," *IEEE Wireless Communications*, vol. 19, no. 3, pp. 14-22, Jun. 2012.

[98] A. Tahbaz-Salehi and A. Jadbabaie, "Small world phenomenon, rapidly mixing Markov chains, and average consensus algorithms," in *Proc. IEEE CDC'07*, pp. 276–281, Dec. 2007.

[99] S. Vanka, M. Haenggi, and V. Gupta, "Convergence speed of the consensus algorithm with interference and sparse long-range connectivity," *IEEE Journal of Selected Topics in Signal Processing*, vol. 5, no. 4, pp. 855–865, Aug. 2011.

[100] Ontario power authority. http://fit.powerauthority.on.ca/.

[101] A. Kusiak, H. Zheng, and Z. Song, "Short-term prediction of wind farm power: a data mining approach," *IEEE Transactions on Energy Conversion*, vol. 24, no. 1, pp. 125–136, Mar. 2009.

[102] S. Galli, A. Scaglione, and Z. Wang, "For the grid and through the grid: the role of power line communications in the smart grid," *Proceedings of the IEEE*, vol. 99, no. 6, pp. 998–1027, Jun. 2011.

[103] 3GPP. http://www.3gpp.org/.

[104] W. Song and W. Zhuang, "Multi-service load sharing for resource management in the cellular/WLAN integrated network," *IEEE Transactions on Wireless Communications*, vol. 8, no. 2, pp. 725–735, Feb. 2009.

[105] V. Blondel, J. Hendrickx, A. Olshevsky, and J. Tsitsiklis, "Convergence in multia-gent coordination, consensus, and flocking," *Proc. IEEE CDC-ECC*, pp. 2996–3000, Dec. 2005.

[106] R. Olfati-Saber, J. Fax, and R. Murray, "Consensus and cooperation in networked multi-node systems," *Proceedings of the IEEE*, vol. 95, pp. 215–233, Jan. 2007.

[107] L. Xiao and S. Boyd, "Fast linear iterations for distributed averaging," in *Proc. IEEE CDC'03*, vol. 5, pp. 4997–5002, Dec. 2003.

[108] D. L. Isaacson and R. W. Madsen. *Markov Chains: Theory and Applications*. Wiley, New York, 1976.

[109] E. Liu, Q. Zhang, and K. K. Leung, "Clique-based utility maximization in wireless mesh networks," *IEEE Transactions on Wireless Commununications*, vol. 10, no. 3, Mar. 2011, pp. 948–957.

[110] S. Balaji, V. Swaminathan, and K. Kannan, "A simple algorithm to optimize max-imum independent set," *Advanced Modeling and Optimization*, vol. 12, no. 1, pp. 107-118, 2010.

[111] M. Epstein. *Managing Information in Networked and Multi-Agent Control Systems*. PhD thesis, California Institute of Technology, 2007.

[112] D. Niyato, L. Xiao, and P. Wang, "Machine-to-machine communications for home energy management system in smart grid," *IEEE Commununications Magazine*, vol. 49, no. 4, pp. 53–59, Apr. 2011.

[113] Canadian Wind Energy Atlas, http://www.windatlas.ca/.

[114] ReDriven Power Inc. 50kw Wind Turbine, http://www.redriven.ca/products/50kw-wind-turbine.

[115] NREL (National Renewable Energy Laboratory): PVWatts^{TM} Site Specific Calculator, http://www.nrel.gov/rredc/pvwatts.

[116] M. He, S. Murugesan, and J. Zhang, "Multiple timescale dispatch and scheduling for stochastic reliability in smart grids with wind generation integration," in *Proc. IEEE INFOCOM'11*, Apr. 2011.

[117] Y. Xiao and J. Rosdahl, "Throughput and delay limits of IEEE 802.11," *IEEE Communication Letters*, vol. 6, no. 8, pp. 355–357, Aug. 2002.

[118] T. C. Aysal, M. E. Yildiz, A. D. Sarwate, and A. Scaglione, "Broadcast gossip algorithms for consensus," *IEEE Transactions on Singal Processing*, vol. 57, no. 7, pp. 2748–2761, Jul. 2009.

[119] M. E. Mahmoud and X. Shen, "PIS: a practical incentive system for multi-hop wireless networks," *IEEE Transactions on Vehicular Technology*, vol. 59, no. 8, pp. 4012–4025, Oct. 2010.

[120] M. E. Mahmoud and X. Shen, "An integrated stimulation and punishment mechanism for thwarting packet drop in multihop wireless networks," *IEEE Transactions on Vehicular Technology*, vol. 60, no. 8, pp. 3947–3962, Oct. 2011.

[121] X. Liang, X. Li, R. Lu, X. Lin, and X. Shen, "UDP: Usage-based dynamic pricing with privacy preservation for smart grid," *IEEE Transactions on Smart Grid*, 2013, to appear.

[122] F. Zhang and Q. Zhang, "Eigenvalue inequalities for matrix product," *IEEE Transactions on Automatic Control*, vol. 51, no. 9, pp. 1506–1509, Sept. 2006.

[123] C. D. Meyer. *Matrix Analysis and Applied Linear Algebra*. The Society for Industrial and Applied Mathematics (SIAM), 2000.

Appendices

Appendix A: Derivation of $\overline{T}^{at}_{\vec{\mathbf{m}}|\mathbf{m}_1\neq0}$ and $\overline{T}^{at}_{\vec{\mathbf{m}}|\mathbf{m}_1=0}$

We first derive the duration of CG attachment with respect to a deterministic set $\{m_1, \cdots, m_{N_c}\}$ of rate indices, given $m_1 \neq 0$. Define an indication function $A_{\{m_1, \cdots, m_{N_c}\}, k}$ which equals to 1 if the kth CG member has a higher transmission rate than all other CG members with lower ranks and 0 otherwise, given by

$$A_{\{m_1, \cdots, m_{N_c}\}, k} = I(\zeta_{f^{-1}(k)}(m_k) > \zeta_{f^{-1}(h)}(m_h), \forall\ 1 \leq h < k),\quad 2 \leq k \leq N_c. \tag{6.1}$$

In the DRMAC scheme, the kth CG member $(2 \leq k \leq N_c - 1)$ sends a rate notification message (with duration T_{RN}) only when $A_{\{m_1, \cdots, m_{N_c}\}, k} = 1$; Otherwise, it waits for an idle slot with duration T_S. Therefore, the duration of CG attachment with respect to the deterministic set of rate indices is given by

$$T^{at}_{\{m_1, \cdots, m_{N_c}\}|m_1\neq0} = T_{DA} + T_{RR} + T_{RN} + 3T_{SIFS} + \sum_{k=2}^{N_c-1} [(T_{RN} + T_{SIFS})\, A_{\{m_1, \cdots, m_{N_c}\}, k}$$

$$+ T_S \left(1 - A_{\{m_1, \cdots, m_{N_c}\}, k}\right)] + T_S \left(1 - A_{\{m_1, \cdots, m_{N_c}\}, N_c}\right). \tag{6.2}$$

Taking account of the randomness in transmission rates and independent channels,

144

the value of $\overline{T}^{at}_{\vec{\mathbf{m}}|\mathbf{m}_1\neq 0}$ is given by

$$\overline{T}^{at}_{\vec{\mathbf{m}}|\mathbf{m}_1\neq 0} = \sum_{\substack{1\leq m_1\leq M_R \\ 0\leq m_2,\cdots,m_{N_c}\leq M_R}} [T^{at}_{\{m_1,\cdots,m_{N_c}\}|m_1\neq 0} \cdot P(\vec{\mathbf{m}} = \{m_1,\cdots,m_{N_c}\}|\mathbf{m}_1\neq 0)]$$

$$= \sum_{m_1=1}^{M_R}\sum_{m_2=0}^{M_R}\cdots\sum_{m_{N_c}=0}^{M_R} [T^{at}_{\{m_1,\cdots,m_{N_c}\}|m_1\neq 0} \cdot \prod_{n=1}^{N_c} P(\mathbf{m}_n = m_n|\mathbf{m}_1\neq 0)]$$

$$= \sum_{m_1=1}^{M_R}\sum_{m_2=0}^{M_R}\cdots\sum_{m_{N_c}=0}^{M_R} [T^{at}_{\{m_1,\cdots,m_{N_c}\}|m_1\neq 0} \cdot P(\mathbf{m}_1 = m_1|\mathbf{m}_1\neq 0)\prod_{n=2}^{N_c} P(\mathbf{m}_n = m_n)]$$

$$= \sum_{m_1=1}^{M_R}\sum_{m_2=0}^{M_R}\cdots\sum_{m_{N_c}=0}^{M_R} [T^{at}_{\{m_1,\cdots,m_{N_c}\}|m_1\neq 0} \cdot \frac{P_{f^{-1}(1),m_1}}{\sum_{m=1}^{M} P_{f^{-1}(1),m}}\prod_{n=2}^{N_c} P_{f^{-1}(n),m_n}]. \qquad (6.3)$$

Define $\vec{\mathbf{m}}' = \{\mathbf{m}'_1,\cdots,\mathbf{m}'_{N_c}\}$ as the rate indices of CG members during the second transmission of the dedicated phase assignment message. Then, $\overline{T}^{at}_{\vec{\mathbf{m}}|\mathbf{m}_1=0}$ is given by

$$\overline{T}^{at}_{\vec{\mathbf{m}}|\mathbf{m}_1=0} = T_{DA} + T_{SIFS} + \overline{T}^{at}_{\vec{\mathbf{m}}'|\mathbf{m}_1=0,\mathbf{m}'_1\neq 0} \cdot p^t_{f^{-1}(1),0,1}(T_{DA} + T_{SIFS})$$

$$+ \overline{T}^{at}_{\vec{\mathbf{m}}'|\mathbf{m}_1=0,\mathbf{m}'_1=0} \cdot p^t_{f^{-1}(1),0,0}(T_{DA} + T_{SIFS}) \qquad (6.4)$$

where $\overline{T}^{at}_{\vec{\mathbf{m}}'|\mathbf{m}_1=0,\mathbf{m}'_1\neq 0}$ is the average duration of CG attachment after the first attempt (with duration $T_{DA}+T_{SIFS}$), given that the first and second transmissions of the dedicated phase assignment messages fail and are successful, respectively. Similar to (6.3), we have

$$\overline{T}^{at}_{\vec{\mathbf{m}}'|\mathbf{m}_1=0,\mathbf{m}'_1\neq 0} = \sum_{m'_1=1}^{M_R}\sum_{m'_2=0}^{M_R}\cdots\sum_{m'_{N_c}=0}^{M_R} [T^{at}_{\{m'_1,\cdots,m'_{N_c}\}|m'_1\neq 0} \cdot \frac{P_{f^{-1}(1),m'_1|m_1=0}}{\sum_{m=1}^{M_R} P_{f^{-1}(1),m|m_1=0}}\prod_{n=2}^{N_c} P_{f^{-1}(n),m'_n}]$$

$$(6.5)$$

where the value of $T^{at}_{\{m'_1,\cdots,m'_{N_c}\}|m'_1\neq 0}$ is given by (6.2) with $\{m_1,\cdots,m_{N_c}\}$ and $m_1 \neq 0$ being replaced by $\{m'_1,\cdots,m'_{N_c}\}$ and $m'_1 \neq 0$, respectively. In (6.5), $P_{f^{-1}(1),m|m_1=0}$ is the conditional PMF of the rate index of the second transmission of the dedicated phase assignment message, given that the first transmission fails. By considering the transition probabilities of the transmission rate indices in the finite-state Markov chain, we have

$$P_{f^{-1}(1),m|m_1=0} = \begin{cases} p^t_{f^{-1}(1),0,m}(T_{DA} + T_{SIFS}), & \text{if } m = 0 \text{ or } m = 1 \\ 0, & \text{otherwise} \end{cases} \qquad (6.6)$$

where the values of $p^t_{f^{-1}(1),0,0}(\cdot)$ and $p^t_{f^{-1}(1),0,1}(\cdot)$ are given by (2.5) and (2.7), respectively. Then, (6.5) can be simplified to

$$\overline{T}^{at}_{\vec{\mathbf{m}}'|\mathbf{m}_1=0,\mathbf{m}'_1\neq0} = \sum_{m'_2=0}^{M_R}\sum_{m'_3=0}^{M_R}\cdots\sum_{m'_{N_c}=0}^{M_R}[T^{at}_{\{1,m'_2,\cdots,m'_{N_c}\}|m'_1\neq0}\cdot\prod_{n=2}^{N_c}P_{f^{-1}(n),m'_n}]. \tag{6.7}$$

In (6.4), $\overline{T}^{at}_{\vec{\mathbf{m}}'|\mathbf{m}_1=0,\mathbf{m}'_1=0}$ is the average duration of CG attachment after the first attempt (with duration $T_{DA}+T_{SIFS}$), given that both first and second transmissions of the dedicated phase assignment messages fail. Define $\vec{\mathbf{m}}'' = \{\mathbf{m}''_1,\cdots,\mathbf{m}''_{N_c}\}$ as the rate indices of CG members during the third transmission of the dedicated phase assignment message. We have

$$\begin{aligned}\overline{T}^{at}_{\vec{\mathbf{m}}'|\mathbf{m}_1=0,\mathbf{m}'_1=0} &= T_{DA}+T_{SIFS}+[\overline{T}^{at}_{\vec{\mathbf{m}}''|\mathbf{m}_1=0,\mathbf{m}'_1=0,\mathbf{m}''_1\neq0}\cdot p^t_{f^{-1}(1),0,1}(T_{DA}+T_{SIFS})]\\ &\quad+[\overline{T}^{at}_{\vec{\mathbf{m}}''|\mathbf{m}_1=0,\mathbf{m}'_1=0,\mathbf{m}''_1=0}\cdot p^t_{f^{-1}(1),0,0}(T_{DA}+T_{SIFS})]\\ &= T_{DA}+T_{SIFS}+[\overline{T}^{at}_{\vec{\mathbf{m}}'|\mathbf{m}_1=0,\mathbf{m}'_1\neq0}\cdot p^t_{f^{-1}(1),0,1}(T_{DA}+T_{SIFS})]\\ &\quad+[\overline{T}^{at}_{\vec{\mathbf{m}}'|\mathbf{m}_1=0,\mathbf{m}'_1=0}\cdot p^t_{f^{-1}(1),0,0}(T_{DA}+T_{SIFS})]\end{aligned} \tag{6.8}$$

where the second equality of (6.8) is due to the one-step memory of finite-state Markov chain. By rearranging (6.8), we have

$$\overline{T}^{at}_{\vec{\mathbf{m}}'|\mathbf{m}_1=0,\mathbf{m}'_1=0} = \frac{T_{DA}+T_{SIFS}}{p^t_{f^{-1}(1),0,1}(T_{DA}+T_{SIFS})}+\overline{T}^{at}_{\vec{\mathbf{m}}'|\mathbf{m}_1=0,\mathbf{m}'_1\neq0}. \tag{6.9}$$

Substituting (6.9) into (6.4), we get

$$\begin{aligned}\overline{T}^{at}_{\vec{\mathbf{m}}|\mathbf{m}_1=0} &= T_{DA}+T_{SIFS}+\overline{T}^{at}_{\vec{\mathbf{m}}'|\mathbf{m}_1=0,\mathbf{m}'_1\neq0}\cdot p^t_{f^{-1}(1),0,1}(T_{DA}+T_{SIFS})\\ &\quad+[\frac{T_{DA}+T_{SIFS}}{p^t_{f^{-1}(1),0,1}(T_{DA}+T_{SIFS})}+\overline{T}^{at}_{\vec{\mathbf{m}}'|\mathbf{m}_1=0,\mathbf{m}'_1\neq0}]\cdot p^t_{f^{-1}(1),0,0}(T_{DA}+T_{SIFS})\\ &= \frac{T_{DA}+T_{SIFS}}{p^t_{f^{-1}(1),0,1}(T_{DA}+T_{SIFS})}+\overline{T}^{at}_{\vec{\mathbf{m}}'|\mathbf{m}_1=0,\mathbf{m}'_1\neq0}\end{aligned} \tag{6.10}$$

where $\overline{T}^{at}_{\vec{\mathbf{m}}'|\mathbf{m}_1=0,\mathbf{m}'_1\neq0}$ is given by (6.5).

146

Appendix B: Proofs of Lemmas, Theorems, and Propositions

Proof of Lemma 1: Two cases are considered for a given t. Case 1: t is in a transmission period (i.e., $\exists h, T_h^i \leq t \leq T_h^o$); Case 2: t is in an idle period (i.e., $\nexists h, T_h^i \leq t \leq T_h^o$).

Case 1: At time t, the infostation with which the vehicle station can communicate is $h_t = \arg\max_h \{T_h^i \leq t\}$. The number of frames within the h_tth infostation coverage before time t is $\lfloor (t - T_{h_t}^i)/T_F \rfloor$, and the sum capacity of these frames is given by $\sum_{j=1}^{\lfloor (t-T_{h_t}^i)/T_F \rfloor} A_{h_t,j}$. On the other hand, if $h_t > 1$, the sum capacity of the frames within the coverage of infostations $[1, \cdots, h_t - 1]$ is given by $\sum_{l=1}^{h_t-1} \sum_{j=1}^{K_l} A_{l,j}$.

Case 2: The infostation most recently visited by the train is $h_t = \arg\max_h \{T_h^i \leq t\}$. Since no block can be delivered during an idle period, the cumulative capacity is given by the sum capacity of all frames in infostations $[1, \cdots, h_t]$, i.e., $\sum_{l=1}^{h_t} \sum_{j=1}^{K_l} A_{l,j}$.

Proof of Lemma 2: Consider two time instants t_1 and t_2, such that $T_I \leq t_1 < t_2 \leq T_O$. There are four cases. Case 1: Both t_1 and t_2 are in a transmission period; Case 2: Both t_1 and t_2 are in an idle period; Case 3: t_1 is in a transmission period while t_2 is in an idle period; Case 4: t_1 is in an idle period while t_2 is in a transmission period. Since the proof is similar for the different cases, we show the proof of Case 1 in the following.

If both t_1 and t_2 are in the same transmission period, i.e., $h_{t_1} = h_{t_2}$, we have

$$
\begin{aligned}
f(t_1) &\leq \sum_{j=1}^{\left\lfloor (t_2 - T_{h_{t_1}}^i)/T_F \right\rfloor} A_{h_{t_1},j} + \sum_{l=1}^{h_{t_1}-1} \sum_{j=1}^{K_l} A_{l,j} \\
&= \sum_{j=1}^{\left\lfloor (t_2 - T_{h_{t_2}}^i)/T_F \right\rfloor} A_{h_{t_2},j} + \sum_{l=1}^{h_{t_2}-1} \sum_{j=1}^{K_l} A_{l,j} = f(t_2).
\end{aligned}
\tag{6.11}
$$

The inequality in (6.11) is due to $\left\lfloor (t - T_{h_{t_1}}^i)/T_F \right\rfloor$ being a non-decreasing function of t, and $A_{h,j}$ being non-negative.

If t_1 and t_2 are in different transmission periods, i.e., $h_{t_1} + 1 \leq h_{t_2}$, we have

$$f(t_1) \leq \sum_{j=1}^{\left\lfloor (T_{h_{t_1}}^o - T_{h_{t_1}}^i)/T_F \right\rfloor} A_{h_{t_1},j} + \sum_{l=1}^{h_{t_1}-1} \sum_{j=1}^{K_l} A_{l,j} = \sum_{l=1}^{h_{t_1}} \sum_{j=1}^{K_l} A_{l,j} \leq \sum_{l=1}^{h_{t_2}-1} \sum_{j=1}^{K_l} A_{l,j}$$

$$\leq \sum_{j=1}^{\left\lfloor (t_2 - T_{h_{t_2}}^i)/T_F \right\rfloor} A_{h_{t_2},j} + \sum_{l=1}^{h_{t_2}-1} \sum_{j=1}^{K_l} A_{l,j} = f(t_2). \tag{6.12}$$

The first inequality in (6.12) holds as $T_{h_{t_1}}^i \leq t_1 \leq T_{h_{t_1}}^o$.

Proof of Theorem 1: For sufficiency, we first consider the condition $G_s \geq T_h^i + kT_F$. Since $f(t)$ is a non-decreasing function with respect to t according to Lemma 2, we have

$$G_s^c = f(G_s) \geq f\left(T_h^i + kT_F\right) = \sum_{j=1}^{\left\lfloor (T_h^i + kT_F - T_h^i)/T_F \right\rfloor} A_{h,j} + \sum_{l=1}^{h-1} \sum_{j=1}^{K_l} A_{l,j}$$

$$= \sum_{j=1}^{k} A_{h,j} + \sum_{l=1}^{h-1} \sum_{j=1}^{K_l} A_{l,j}. \tag{6.13}$$

Similarly, we can obtain $D_s^c \leq \sum_{j=1}^{k-1} A_{h,j} + \sum_{l=1}^{h-1} \sum_{j=1}^{K_l} A_{l,j}$ for $D_s \leq T_h^i + (k-1)T_F$.

For necessity, we cannot derive (3.4) directly from (3.7) since $f(t)$ is not a bijective function and thus is not reversible. Instead, we resort to (3.2) and (3.5) of problem P1. We first prove the inequality part based on contradiction. Consider $G_s^c > \sum_{j=1}^{k} A_{h,j} + \sum_{l=1}^{h-1} \sum_{j=1}^{K_l} A_{l,j}$ in (3.7). Suppose $G_s < T_h^i + kT_F$, since $f(t)$ is a non-decreasing function of t, we have

$$G_s^c = f(G_s) \leq f\left(T_h^i + kT_F\right) = \sum_{j=1}^{k} A_{h,j} + \sum_{l=1}^{h-1} \sum_{j=1}^{K_l} A_{l,j}. \tag{6.14}$$

As (6.14) contradicts with $G_s^c > \sum_{j=1}^{k} A_{h,j} + \sum_{l=1}^{h-1} \sum_{j=1}^{K_l} A_{l,j}$, we have $G_s \geq T_h^i + kT_F$.

Next, consider $G_s^c = \sum_{j=1}^{k} A_{h,j} + \sum_{l=1}^{h-1} \sum_{j=1}^{K_l} A_{l,j}$ in (3.7). Suppose $G_s < T_h^i + kT_F$. Since the service request time is rounded to the beginning time of a frame, we have

$G_s \leq T_h^i + (k-1)T_F$. By applying function $f(t)$ on both sides of the inequality, we have

$$G_s^c = f(G_S) \leq f\left(T_h^i + (k-1)T_F\right) = \sum_{j=1}^{k-1} A_{h,j} + \sum_{l=1}^{h-1} \sum_{j=1}^{K_l} A_{l,j} \leq \sum_{j=1}^{k} A_{h,j} + \sum_{l=1}^{h-1} \sum_{j=1}^{K_l} A_{l,j}.$$

(6.15)

With $G_s^c = \sum_{j=1}^{k} A_{h,j} + \sum_{l=1}^{h-1} \sum_{j=1}^{K_l} A_{l,j}$, the first and second inequalities in (6.15) should take equal signs. Based on the second equality $\sum_{j=1}^{k-1} A_{h,j} + \sum_{l=1}^{h-1} \sum_{j=1}^{K_l} A_{l,j} = \sum_{j=1}^{k} A_{h,j} + \sum_{l=1}^{h-1} \sum_{j=1}^{K_l} A_{l,j}$, we have $A_{h,k} = 0$. According to (3.5), the summation of the resource allocation variables for the kth frame within the hth infostation coverage is upper-bounded by $A_{h,k}$, i.e., $\sum_{s \in S} x_{h,k,s} \leq A_{h,k}$. Moreover, since $x_{h,k,s}$ can take only non-negative values as stated by (3.2), we have $x_{h,k,s} = 0, s \in S$. This result indicates that for $G_s^c = \sum_{j=1}^{k} A_{h,j} + \sum_{l=1}^{h-1} \sum_{j=1}^{K_l} A_{l,j}$ in (3.7), we already have $x_{h,k,s} = 0$ for $G_s < T_h^i + kT_F$ in problem P1. The discussion on $D_s^c \leq \sum_{j=1}^{k-1} A_{h,j} + \sum_{l=1}^{h-1} \sum_{j=1}^{K_l} A_{l,j}$ is similar and omitted here. Since both sufficiency and necessity are satisfied, (3.4) is equivalent to (3.7) for problem P1.

Proof of Lemma 3: Define $c_{h,k}^p = \sum_{j=1}^{k-1} A_{h,j} + \sum_{l=1}^{h-1} \sum_{j=1}^{K} A_{l,j}$ as the cumulative capacity of all frames prior to the kth frame within the hth infostation coverage. Since $x_{h_1,k_1,s_1}, x_{h_2,k_2,s_2} \geq 1$, the two frames under consideration should have non-zero capacity, i.e., $A_{h_1,k_1}, A_{h_2,k_2} > 0$. Without loss of generality, we consider all blocks of the two frames belong to the nth virtual period, i.e.,

$$\left\{c_{h_1,k_1}^p + 1, c_{h_1,k_1}^p + 2, \cdots, c_{h_1,k_1}^p + A_{h_1,k_1}\right\} \subseteq [c_n + 1, c_{n+1}] \tag{6.16}$$

$$\left\{c_{h_2,k_2}^p + 1, c_{h_2,k_2}^p + 2, \cdots, c_{h_2,k_2}^p + A_{h_2,k_2}\right\} \subseteq [c_n + 1, c_{n+1}]. \tag{6.17}$$

The value of the objective function (3.1) is the same for X and X' since the the total numbers of blocks delivered for services s_1 and s_2 respectively are the same. For feasibility, (3.2) and (3.3) hold for X' straightforwardly. Constraint (3.5) holds for X'

149

since we have

$$x_{h_1,k_1,s_1} + x_{h_1,k_1,s_2} = (x_{h_1,k_1,s_1} - 1) + (x_{h_1,k_1,s_2} + 1) \tag{6.18}$$

$$x_{h_2,k_2,s_1} + x_{h_2,k_2,s_2} = (x_{h_2,k_2,s_1} + 1) + (x_{h_2,k_2,s_2} - 1). \tag{6.19}$$

Based on (3.7), for a feasible resource allocation variable X and $x_{h_1,k_1,s_1} \neq 0$, we have

$$G_{s_1}^c < \sum_{j=1}^{k_1} A_{h_1,j} + \sum_{l=1}^{h_1-1} \sum_{j=1}^{K} A_{l,j} = c_{h_1,k_1+1}^p. \tag{6.20}$$

Inequality (6.20) is equivalent to $G_{s_1}^c \leq c_{h_1,k_1}^p$ since the service request time is rounded to the beginning time of a frame. Similarly, $D_{s_1}^c \geq c_{h_1,k_1}^p + A_{h_1,k_1}$, $G_{s_2}^c \leq c_{h_2,k_2}^p$, and $D_{s_2}^c \geq c_{h_2,k_2}^p + A_{h_2,k_2}$. By (6.16) and (6.17), we have

$$G_{s_2}^c \leq \max\left\{G_{s_1}^c, G_{s_2}^c\right\} \leq c_n \leq c_{h_1,k_1}^p < c_{h_1,k_1}^p + A_{h_1,k_1} \leq c_{n+1} \leq \min\left\{D_{s_1}^c, D_{s_2}^c\right\} \leq D_{s_2}^c \tag{6.21}$$

$$G_{s_1}^c \leq \max\left\{G_{s_1}^c, G_{s_2}^c\right\} \leq c_n \leq c_{h_2,k_2}^p < c_{h_2,k_2}^p + A_{h_2,k_2} \leq c_{n+1} \leq \min\left\{D_{s_1}^c, D_{s_2}^c\right\} \leq D_{s_1}^c. \tag{6.22}$$

The second and sixth inequalities in (6.21) (and (6.22)) hold since no further partition (by G_s^c or D_s^c) exists within each virtual period according to definition (3.8). As a result, (3.7) holds for X'.

Proof of Lemma 4: The convexity follows since $H_n(x, u)$ is continuous and piecewise linear with respect to u, and the slope of the linear function for $u > x$ is greater than that for $u \leq x$. The convexity is preserved by restricting $H_n(x, u)$ to a convex set $u \in [0, x_{\max}]$ [89].

Proof of Lemma 5: Based on the convexity of $q(u)$, it is straightforward to show $q(u) = q^*$ for all $u \in [S, S']$. Moreover, $q(u)$ is non-increasing and non-decreasing on intervals $[0, S]$ and $[S', x_{\max}]$, respectively. By considering all five cases of x according to (4.12), we can easily verify $q(u) \geq q(u^*)$ for all $x \in [0, x_{\max}]$ and $u \in \left[\max\{0, x - u_{\max}^{dc}\}, \min\{x_{\max}, x + u_{\max}^{rc}\}\right]$.

Proof of Lemma 6: As shown in [85], function $Q(x)$ is convex with respect to x if $G_Q(x, a, b) \geq 0$ for any $a, b > 0$, where

$$G_Q(x, a, b) = Q(x + a) - Q(x) - a\frac{Q(x) - Q(x - b)}{b}. \tag{6.23}$$

We study the following ten cases: Case 1: $x - b < x < x + a < S - u^{rc}_{\max} < S' + u^{dc}_{\max}$; Case 2: $S - u^{rc}_{\max} < S' + u^{dc}_{\max} \leq x - b < x < x + a$; Case 3: $x - b < x < S - u^{rc}_{\max} \leq x + a < S' + u^{dc}_{\max}$; Case 4: $x - b < S - u^{rc}_{\max} \leq x < x + a < S' + u^{dc}_{\max}$; Case 5: $S - u^{rc}_{\max} \leq x - b < x < x + a < S' + u^{dc}_{\max}$; Case 6: $x - b < x < S - u^{rc}_{\max} < S' + u^{dc}_{\max} \leq x + a$; Case 7: $x - b < S - u^{rc}_{\max} \leq x < S' + u^{dc}_{\max} \leq x + a$; Case 8: $S - u^{rc}_{\max} \leq x - b < x < S' + u^{dc}_{\max} \leq x + a$; Case 9: $x - b < S - u^{rc}_{\max} < S' + u^{dc}_{\max} < x < x + a$; Case 10: $S - u^{rc}_{\max} \leq x - b < S' + u^{dc}_{\max} < x < x + a$.

The convexity of Case 1 and Case 2 follows since $q(x)$ is convex, while $x + u^{rc}_{\max}$ and $x - u^{dc}_{\max}$ are affine mappings with respect to x [89]. The proofs of Case 4, Case 5, and Cases 7-10 are straightforward. For Case 3, we have

$$G_Q(x, a, b) \geq \quad q^* - q^* - a\frac{q^* - q(x - b + u^{rc}_{\max})}{b} = a\frac{q(x - b + u^{rc}_{\max}) - q^*}{b} \geq 0 \tag{6.24}$$

where the first and second inequalities hold since $q(x + u^{rc}_{\max}) \geq q^*$ and $q(x - b + u^{rc}_{\max}) \geq q^*$, respectively. Similarly, we can prove $G_Q(x, a, b) \geq 0$ for Case 6.

Proof of Lemma 7: The proof is completed by induction. For $n = N$, we have $V_N(s, x + \epsilon) \geq V_N(s, x) - r'\epsilon$ since $r' \geq \left(\frac{r_n}{\eta} + \tilde{r}\right)$. Suppose Lemma 7 holds for $V_{n+1}(s, x)$. For $V_n(s, x)$, we first investigate the case $s = \mathcal{W}$. Note that for any $u \in \left[\max\{0, x + \epsilon - u^{dc}_{\max}\}, \min\{x_{\max}, x + \epsilon + u^{rc}_{\max}\}\right]$, there exists a $u' = \max\{0, u - \epsilon\}$, such that $u' \in \left[\max\{0, x - u^{dc}_{\max}\}, \min\{x_{\max}, x + u^{rc}_{\max}\}\right]$. Letting $\epsilon' = u - u'$ ($\epsilon' \in [0, \epsilon]$), we can easily verify $H_n(x + \epsilon, u) \geq H_n(x, u') - r'(\epsilon - \epsilon')$ based on the inequality $r' \geq \left(\frac{r_n}{\eta} + \tilde{r}\right) > r_n$. By applying Lemma 7 to $V_{n+1}(s, x)$ with respect to $\beta u - \beta u' \geq 0$, we

151

have $V_{n+1}(s_{n+1}, \beta u) \geq V_{n+1}(s_{n+1}, \beta u') - \gamma' \beta \epsilon' > V_{n+1}(s_{n+1}, \beta u') - \gamma' \epsilon'$. Then we have

$$
\begin{aligned}
V_n(\mathcal{W}, x + \epsilon) &= \min_u \{H_n(x + \epsilon, u) + E[V_{n+1}(s_{n+1}, \beta u)|s_n = \mathcal{W}]\} \\
&\geq \min_{u'} \{H_n(x, u') + E[V_{n+1}(s_{n+1}, \beta u')|s_n = \mathcal{W}]\} - r'\epsilon \\
&\geq V_n(\mathcal{W}, x) - r'\epsilon \qquad\qquad\qquad\qquad (6.25)
\end{aligned}
$$

where the first inequality holds by comparing the value of the objective function for any u with that for the corresponding u', while the second inequality holds since the values of u' always lie in a subset of $\left[\max\{0, x - u_{\max}^{dc}\}, \min\{x_{\max}, x + u_{\max}^{rc}\}\right]$. Similarly, $V_n(s, x + \epsilon) \geq V_n(s, x) - r'\epsilon$ holds for $s = \mathcal{H}$. Then we consider $s = \mathcal{C}$ and study the following function:

$$
V_{n+1}\big(s_{n+1}, \beta(x + \epsilon - \zeta_n)^+\big) + r'(\zeta_n - x - \epsilon)^+
$$

$$
\begin{aligned}
&\geq\; V_{n+1}\big(s_{n+1}, \beta(x - \zeta_n)^+\big) - r'[\beta(x + \epsilon - \zeta_n)^+ - \beta(x - \zeta_n)^+] \\
&\qquad + r'(\zeta_n - x)^+ + r'(\zeta_n - x - \epsilon)^+ - r'(\zeta_n - x)^+
\end{aligned}
$$

$$
=\; V_{n+1}\big(s_{n+1}, \beta(x - \zeta_n)^+\big) + r'(\zeta_n - x)^+ +
\begin{cases}
-r'\epsilon, & \text{if } x + \epsilon < \zeta_n \\
(1 - \beta)r'(x - \zeta_n) - \beta r'\epsilon, & \text{if } x < \zeta_n \leq x + \epsilon \\
-\beta r'\epsilon, & \text{if } \zeta_n \leq x
\end{cases}
$$

$$
\geq\; V_{n+1}\big(s_{n+1}, \beta(x - \zeta_n)^+\big) + r'_n(\zeta_n - x)^+ - r'\epsilon \qquad\qquad (6.26)
$$

where the first inequality holds by applying Lemma 7 to $V_{n+1}(s, x)$ with respect to $\beta(x + \epsilon - \zeta_n)^+ - \beta(x - \zeta_n)^+ \geq 0$, while the second inequality holds since for $x < \zeta_n \leq x + \epsilon$ and $\beta < 1$, we have $(1 - \beta)r'(x - \zeta_n) - \beta r'\epsilon \geq (1 - \beta)r'(x - x - \epsilon) - \beta r'\epsilon = -r'\epsilon$. By takeing expectation on both sides of (6.26), we have $V_n(s, x + \epsilon) \geq V_n(s, x) - r'\epsilon$ holds for $s = \mathcal{C}$. This completes the induction.

Proof of Theorem 3: The proof is completed by induction. For $n = N - 1$ and $s = \mathcal{H}$ or $\mathcal{W}$, we have

$$q_{N-1}(s, x, u) = H_{N-1}(x, u) + E\left[V_N(s_N, \beta u)|s_{N-1} = s\right]$$

$$= H_{N-1}(x, u) + \sum_{j \in \{\mathcal{H}, \mathcal{W}, \mathcal{C}\}} E\left[V_N(j, \beta u)\right] P_{N-1}(j|s). \tag{6.27}$$

By definition, $V_N(j, \beta u)$ is linear and thus convex with respect to u. Since the expectation can be considered as a nonnegative weighted sum, $E\left[V_N(j, \beta u)\right]$ is also convex [89]. Based on the convexity of $H_{N-1}(x, u)$ according to Lemma 4, $q_{N-1}(s, x, u)$ is also convex with respect to u. According to Lemma 5, the value of u to achieve the minimum of $q_{N-1}(s, x, u)$ is given by an $(S_{N-1}(s, x), S'_{N-1}(s, x))$ policy. Moreover, the minimum achieved by the $(S_{N-1}(s, x), S'_{N-1}(s, x))$ policy is convex with respect to x according to Lemma 6. Therefore, $V_{N-1}(s, x)$ is convex with respect to x for $s = \mathcal{H}$ or $\mathcal{W}$.

For $s = \mathcal{C}$, we first investigate the convexity of function $V_N(s_N, \beta(x)^+) + r'(-x)^+$ with respect to x. For the first term $V_N(s_N, \beta(x)^+)$, we have

$$\left.\frac{dV_N(s_N, \beta(x)^+)}{dx}\right|_{x=0^+} = \lim_{\epsilon \to 0^+} \left.\frac{V_N(s_N, \beta(x+\epsilon)) - V_N(s_N, \beta x)}{x + \epsilon - x}\right|_{x=0}$$

$$\geq \lim_{\epsilon \to 0^+} \frac{-\beta r'\epsilon}{\epsilon} = -\beta r' \tag{6.28}$$

where the last inequality holds according to Lemma 7. For the second term $r'(-x)^+$, we have $\left.\frac{dr'(-x)^+}{dx}\right|_{x=0^-} = -r'$. Based on Proposition 3.1 of [86], since both $V_N(s_N, \beta x)$ and $r'(-x)$ are convex and $\left.\frac{dV_N(d_N, s_N, \beta(x)^+)}{dx}\right|_{x=0^+} > \left.\frac{dr'(-x)^+}{dx}\right|_{x=0^-}$, we have $V_N(d_N, s_N, \beta(x)^+) + r'(-x)^+$ is convex with respect to x. Based on Proposition 4.1 of [85], since the convexity of a function is preserved by taking expectation with respect to $(x - \zeta_{N-1})$, we can conclude that $V_{N-1}(s, x)$ is also convex with respect to x for $s = \mathcal{C}$.

Suppose the theorem holds for $V_{n+1}(s, x)$, follow the same steps we can prove the optimality of the $(S_n(s, x), S'_n(s, x))$ policy and the convexity of $V_n(s, x)$. This completes the induction.

153

Proof of Proposition 1: The proof is completed by contradiction. Suppose $u_n^{r2}(s) > u_n^{d1}(s)$, we consider a small positive number $\delta > 0$ such that $u_n^{d1}(s) + \delta < u_n^{r2}(s)$. Then we have

$$
\begin{aligned}
& H_n^r(s, u_n^{d1}(s) + \delta) - H_n^r(s, u_n^{d1}(s)) \\
=\ & \left(\frac{r_n}{\eta} + \tilde{r}\right)\delta + E\left[V_{n+1}(s_{n+1}, \beta(u_n^{d1}(s) + \delta))|s_n = s\right] - E\left[V_{n+1}(s_{n+1}, \beta u_n^{d1}(s))|s_n = s\right] \\
>\ & r_n\delta + E\left[V_{n+1}(s_{n+1}, \beta(u_n^{d1}(s) + \delta))|s_n = s\right] - E\left[V_{n+1}(s_{n+1}, \beta u_n^{d1}(s))|s_n = s\right] \\
=\ & H_n^d(s, u_n^{d1}(s) + \delta) - H_n^d(s, u_n^{d1}(s)). \quad (6.29)
\end{aligned}
$$

In other words, the minimum of $H_n^r(s, u)$ and $H_n^d(s, u)$ cannot be achieved simultaneously at $u_n^{d1}(s) + \delta$ and $u_n^{d1}(s)$, which contradicts with the definition of the sets $[u_n^{r1}(s), u_n^{r2}(s)]$ and $[u_n^{d1}(s), u_n^{d2}(s)]$.

Proof of Theorem 4: Denote the economic dispatch policy given by (5.4) as $\mathbf{u}^* = \{u_{gv}^* | g \in \{1, 2, \cdots, G\}, v \in \mathcal{V}\}$. We consider two cases with respect to the relation between the cumulative generation and aggregated loads: Case 1): The aggregated loads cannot be satisfied based on the power generation of DG units, i.e., $\sum_{g \in \{1,2,\cdots,G\}} \bar{X}_g < \bar{Y}$ (or equivalently, $\sum_{g \in \{1,2,\cdots,G\}} X_g < Y$); Case 2): The aggregated loads can be satisfied based on the power generation of DG units, i.e., $\sum_{g \in \{1,2,\cdots,G\}} \bar{X}_g \geq \bar{Y}$ (or equivalently, $\sum_{g \in \{1,2,\cdots,G\}} X_g \geq Y$). The proofs of both cases are completed by contradiction.

Case 1): According to the first case of policy (5.4), all DG units should operate at the maximum output, i.e., $u_{gv}^* = x_{gv}$. Suppose another policy $\mathbf{u}' \neq \mathbf{u}^*$ is optimal. Then, there exists at least one pair (i, j) such that $u_{ij}' < x_{ij}$. Consider another policy $\mathbf{u}'' = \{u_{ij}'', u_{gv}' | g \in \{1, 2, \cdots, G\}, v \in \mathcal{V}, (g, v) \neq (i, j)\}$ with $u_{ij}'' \in (u_{ij}', x_{ij}]$. Then, the generation cost based on policy $\mathbf{u}''$ is given by

$$
\begin{aligned}
C_P(\mathbf{x}, \mathbf{y}, \mathbf{c}, \mathbf{u}'') &= c_A\left(Y - \sum_{g \in \{1,2,\cdots,G\}} \sum_{\substack{v \in \mathcal{V} \\ (g,v) \neq (i,j)}} u_{gv}' - u_{ij}''\right) + \sum_{g \in \{1,2,\cdots,G\}} \sum_{\substack{v \in \mathcal{V} \\ (g,v) \neq (i,j)}} c_g u_{gv}' + c_i u_{ij}'' \\
&= C_P(\mathbf{x}, \mathbf{y}, \mathbf{c}, \mathbf{u}') + (c_i - c_A)(u_{ij}'' - u_{ij}'). \quad (6.30)
\end{aligned}
$$

154

Since $c_i < c_A$ and $u''_{ij} > u'_{ij}$, we have $C_P(\mathbf{x}, \mathbf{y}, \mathbf{c}, \mathbf{u}'') < C_P(\mathbf{x}, \mathbf{y}, \mathbf{c}, \mathbf{u}')$, which contradicts with the assumption that $\mathbf{u}'$ is optimal.

Case 2): Based on Lemma 9, the aggregated power generation of the DG units and the aggregated loads should be balanced. In other words, a policy different from $\mathbf{u}^*$ should have at least two different elements with respect to the decisions on power generation. We consider a policy $\mathbf{u}'$ with exactly two different elements from $\mathbf{u}^*$, i.e., $\mathbf{u}' = \{u'_{ij}, u'_{mn}, u^*_{gv} | g \in \{1, 2, \cdots, G\}, v \in \mathcal{V}, (g, v) \notin \{(i, j), (m, n)\}\}$ with $u'_{ij} \neq u^*_{ij}$ and $u'_{mn} \neq u^*_{mn}$. An extension of the proof for a policy with more different elements is straightforward. Note that the two elements correspond to two different types of DG units with different generation costs. Otherwise, the total generation cost is the same based on the power balance equation. Suppose $1 \leq i < m \leq G$ and the policy $\mathbf{u}'$ is optimal. Since $\sum_{g \in \{1, 2, \cdots, G\}} X_g \geq Y$, we can define $g^* = \arg\max_{g \in \{1, 2, \cdots, G\}} \left\{ \sum_{i \in \{1, 2, \cdots, g\}} X_i \leq Y \right\}$. Then, we calculate the generation costs with respect to two different relations between i and g^*, i.e., $i \leq g^*$ and $i > g^*$, respectively. If $i \leq g^*$, we have $u'_{ij} < u^*_{ij}$ since $u^*_{ij} = x_{ij}$ according to (5.4). Moreover, we have $m > g^*$ and $u'_{mn} = u^*_{ij} + u^*_{mn} - u'_{ij}$ to balance the power generation and loads. Then, the generation cost based on the economic dispatch policy $\mathbf{u}'$ is given by

$$
\begin{aligned}
C_P(\mathbf{x}, \mathbf{y}, \mathbf{c}, \mathbf{u}') &= \sum_{g \in \{1, 2, \cdots, G\}} c_g \sum_{v \in \mathcal{V}} u^*_{gv} I_{(g,v) \notin \{(i,j),(m,n)\}} + c_i u'_{ij} + c_m (u^*_{ij} + u^*_{mn} - u'_{ij}) \\
&= C_P(\mathbf{x}, \mathbf{y}, \mathbf{c}, \mathbf{u}^*) + (c_i - c_m)(u'_{ij} - u^*_{ij}) \\
&> C_P(\mathbf{x}, \mathbf{y}, \mathbf{c}, \mathbf{u}^*)
\end{aligned}
\tag{6.31}
$$

where I_A is an indication function which equals 1 if A is true and 0 otherwise, while the inequality holds since $c_i < c_m$ and $u'_{ij} < u^*_{ij}$. The result in (6.31) contradicts with the assumption that $\mathbf{u}'$ is optimal. On the other hand, if $i > g^*$, we have $m > i > g^*$ and the proof follows similar steps. For other combinations of i and m, the generation and loads cannot be balanced. This completes the proof.

Proof of Lemma 11: According to the definitions of $W_{\mathcal{M}}^c$ and $W_{\mathcal{V}}^a$, we can easily verify that both matrices are symmetric. For the matrix $W_{\mathcal{M}}^c$, the states of the associated Markov chain can be partitioned into $|\mathcal{V}| - M + 1$ irreducible closed subsets, i.e., $|\mathcal{V}| - M$ subsets correspond to the nodes with only short-range communication devices and the dual-mode nodes with inactivated cellular communication devices, and one subset corresponds to $\mathcal{M}$. According to Lemma 10, the eigenvalues of $W_{\mathcal{M}}^c$ include $|\mathcal{V}| - M + 1$ ones. On the other hand, we can easily verify the rank of $W_{\mathcal{M}}^c$ is $|\mathcal{V}| - M + 1$ since the weights used by all nodes in $\mathcal{M}$ are the same. Therefore, the other $M - 1$ eigenvalues of $W_{\mathcal{M}}^c$ are equal to zero, which indicates that $W_{\mathcal{M}}^c$ is positive semidefinite.

For the matrix $W_{\mathcal{V}}^a$, the Laplacian of the associated graph is given by

$$L_{\mathcal{V}}^a = I - W_{\mathcal{V}}^a. \tag{6.32}$$

Since the Laplacian of the strongly connected graph is positive semidefinite [106], we have $\lambda_k(L_{\mathcal{V}}^a) \geq 0$ for all $k \in \{1, 2, \cdots, |\mathcal{V}|\}$. Moreover, we have

$$\sum_{j \in \mathcal{N}_i} \omega_{\mathcal{V}}^a(i,j) = \sum_{j \in \mathcal{N}_i} \frac{1}{2 \max\{|\mathcal{N}_i|, |\mathcal{N}_j|\}} \leq \frac{|\mathcal{N}_i|}{2|\mathcal{N}_i|} = \frac{1}{2} \tag{6.33}$$

where the inequality holds since $\max\{|\mathcal{N}_i|, |\mathcal{N}_j|\} \geq |\mathcal{N}_i|$. Therefore, the spectral radius of $L_{\mathcal{V}}^a$ is bounded as

$$\rho(L_{\mathcal{V}}^a) \leq \max_{i \in \mathcal{V}} \{|-\sum_{j \in \mathcal{N}_i} \omega_{\mathcal{V}}^a(i,j)| + \sum_{j \in \mathcal{N}_i} |\omega_{\mathcal{V}}^a(i,j)|\} = 2 \max_{i \in \mathcal{V}} \sum_{j \in \mathcal{N}_i} \omega_{\mathcal{V}}^a(i,j) \leq 1. \tag{6.34}$$

That is, all eigenvalues of $L_{\mathcal{V}}^a$ are within $[0, 1]$. According to (6.32), $L_{\mathcal{V}}^a$ and $W_{\mathcal{V}}^a$ have the same eigenvectors, and thus the kth largest eigenvalue of $W_{\mathcal{V}}^a$ is given by

$$\lambda_k(W_{\mathcal{V}}^a) = 1 - \lambda_{|\mathcal{V}|-k}(L_{\mathcal{V}}^a). \tag{6.35}$$

Therefore, all eigenvalues of $W_{\mathcal{V}}^a$ are bounded by $[0, 1]$, which implies that $W_{\mathcal{V}}^a$ is also positive semidefinite.

Proof of Theorem 5: Since both $W_{\mathcal{M}}^c$ and $W_{\mathcal{V}}^a$ are symmetric and positive semidefinite, we have

$\sum_{i=1}^{k} \lambda_i(W_{\mathcal{M}}^c W_{\mathcal{V}}^a) \leq \sum_{i=1}^{k} \lambda_i(W_{\mathcal{V}}^a)\lambda_i(W_{\mathcal{M}}^c)$ for any $k \in \{1, 2, \cdots, |\mathcal{V}|\}$ [122]. Letting $k = 2$, we have

$$\lambda_2(W_{\mathcal{M}}^c W_{\mathcal{V}}^a) \leq \sum_{i=1,2} \lambda_i(W_{\mathcal{V}}^a)\lambda_i(W_{\mathcal{M}}^c) - \lambda_1(W_{\mathcal{M}}^c W_{\mathcal{V}}^a). \tag{6.36}$$

According to the Perron-Frobenius theory [123], since the graph associated with matrix $W_{\mathcal{V}}^a$ is strongly connected, the Markov chain associated with $W_{\mathcal{V}}^a$ is irreducible. Based on Lemma 10, the multiplicity is 1 for eigenvalue 1 with respect to $W_{\mathcal{V}}^a$, i.e., $\lambda_1(W_{\mathcal{V}}^a) = 1$ and $\lambda_k(W_{\mathcal{V}}^a) < 1$ for $1 < k \leq |\mathcal{V}|$. Suppose $W_{\mathcal{M}}^c W_{\mathcal{V}}^a = [\omega_{\mathcal{M}\mathcal{V}}^{ca}(i,j)]_{|\mathcal{V}| \times |\mathcal{V}|}$, and consider an arbitrary element $\omega_{\mathcal{M}\mathcal{V}}^{ca}(i,j)$ such that the corresponding element in $W_{\mathcal{V}}^a$ satisfies $\omega_{\mathcal{V}}^a(i,j) > 0$. Then, we have

$$\omega_{AR}^{ac}(i,j) = \sum_{m \in \mathcal{V}} \omega_{\mathcal{M}}^c(i,m)\omega_{\mathcal{V}}^a(m,j) \geq \omega_{\mathcal{M}}^c(i,i)\omega_{\mathcal{V}}^a(i,j) > 0 \tag{6.37}$$

where the first inequality holds since all elements in $W_{\mathcal{M}}^c$ and $W_{\mathcal{V}}^a$ are non-negative, and the second inequality holds since $\omega_{\mathcal{M}}^c(i,i) > 0$ for all $i \in \mathcal{V}$ according to (5.12). Therefore, we can conclude that the Markov chain associated with $W_{\mathcal{M}}^c W_{\mathcal{V}}^a$ is irreducible, given that the Markov chain associated with $W_{\mathcal{V}}^a$ is irreducible. Based on Lemma 10, we have $\lambda_1(W_{\mathcal{M}}^c W_{\mathcal{V}}^a) = 1$ while $\lambda_k(W_{\mathcal{M}}^c W_{\mathcal{V}}^a) < 1$ for $1 < k \leq |\mathcal{V}|$. Taking into account (6.36), we have

$$\lambda_2(W_{\mathcal{M}}^c W_{\mathcal{V}}^a) \leq \lambda_2(W_{\mathcal{V}}^a)\lambda_2(W_{\mathcal{M}}^c) + \lambda_1(W_{\mathcal{V}}^a)\lambda_1(W_{\mathcal{M}}^c) - \lambda_1(W_{\mathcal{M}}^c W_{\mathcal{V}}^a)$$
$$= \lambda_2(W_{\mathcal{V}}^a)\lambda_2(W_{\mathcal{M}}^c) + 1 - 1 = \lambda_2(W_{\mathcal{V}}^a)\lambda_2(W_{\mathcal{M}}^c) \tag{6.38}$$

where the first equality holds since the largest eigenvalues of $W_{\mathcal{V}}^a$, $W_{\mathcal{M}}^c$, and $W_{\mathcal{M}}^c W_{\mathcal{V}}^a$ are equal to 1. On the other hand, since all eigenvalues of $W_{\mathcal{M}}^c$ are less than or equal to 1, we have $\lambda_2(W_{\mathcal{M}}^c W_{\mathcal{V}}^a) \leq \lambda_2(W_{\mathcal{V}}^a)$ based on (6.38).

Proof of Proposition 2: According to the proof of Lemma 11, the eigenvalues of $W^{\mathrm{c}}_{\mathcal{M}'}$ include $|\mathcal{M}'| - 1$ zeros and $|\mathcal{V}| - |\mathcal{M}'| + 1$ ones. Therefore, we have $\lambda_k(W^{\mathrm{c}}_{\mathcal{M}'}) \leq \lambda_k(W^{\mathrm{c}}_{\mathcal{M}})$ for any $1 \leq k \leq |\mathcal{V}|$. Substituting this result in (5.16) and (5.17), we can easily verify $\theta(\mathcal{M}') \leq \theta(\mathcal{M})$ and $\varphi(\mathcal{M}') \leq \varphi(\mathcal{M})$.